Technische Universität München
Fakultät für Physik

Influence of thin surface oxide films on deuterium uptake, retention and release from tungsten

Kristof Jonny Kremer

Vollständiger Abdruck der von der Fakultät für Physik der Technischen Universität München zur Erlangung eines

Doktors der Naturwissenschaften (Dr. rer. nat.)

genehmigten Dissertation.

Vorsitz: Prof. Dr. Nora Brambilla

Prüfer*innen der Dissertation:

1. Prof. Dr. Ulrich Stroth
2. Prof. Dr. Christoph P. Hugenschmidt

Die Dissertation wurde am 03.08.2022 bei der Technischen Universität München eingereicht und durch die Fakultät für Physik am 13.09.2022 angenommen.

Abstract

For future fusion power plants, the uptake, retention and release of fuel elements (deuterium and radioactive tritium) in plasma-facing components (PFCs) is essential for the fuel self-sufficiency and the radioactive inventory of the reactor. Tungsten (W) is envisaged as the most likely candidate material for the PFCs and its interaction with deuterium (D) has been extensively studied in well-defined laboratory experiments. However, the possible influence of thin (1–2 nm) naturally occurring surface oxide films on W has so far been neglected. Since natural oxide films occur in all ex-situ studies, but will most likely not be present in a future fusion reactor, they represent a possible discrepancy between the laboratory results and the real-world application as PFCs. Therefore, this work investigates the influence of oxide films on D uptake, retention and release from W.

To study these effects quantitatively, a novel approach was used. W samples were bombarded with 20 MeV W ions to create a defect-rich "self-damaged" zone underneath the oxide, which strongly increases D retention. The self-damaged zone acts either as a D "getter-layer" (uptake) or as a D reservoir (release). Oxide films with thicknesses of 5 to 100 nm were grown thermally or electro-chemically and consisted mainly of tungsten-tri-oxide (WO_3). To investigate D uptake, the samples were exposed to a D plasma with well-defined D energy and flux at 370 or 500 K. Several fluence series in the range of 5.9×10^{23} to 2.3×10^{25} D/m^2 were conducted at D energies of <5 eV/D, 15 eV/D and 38 eV/D, respectively. For D release, the self-damaged zone was filled with D by plasma exposure prior to oxidation and the release behavior through the oxide was investigated with thermal desorption spectroscopy (TDS). The depth-resolved D and O concentrations in the sample were determined with ion beam analysis. Top-view images and cross sections though the oxide film were investigated with scanning electron microscopy (SEM).

It was found that WO_3 completely blocks D uptake from a plasma into metallic W at 370 K as long as the interface between oxide and metal consists of intact, not-reduced WO_3. However, the oxide film itself retains significant quantities of D up to a concentration of 1.5 atomic %. To explain this behavior a physical picture of the energy landscape of D in WO_3 and W was conceived: D is implanted into W oxide and diffuses through the thin film within minutes. However, it cannot pass through the interface to the metallic W due to the large difference in the enthalpy of solution between the two materials (~1.4 eV). It is thus not the transport in the oxide that prevents the D uptake into W but the potential energy barrier at the interface. During plasma exposure the oxide film is (partially) reduced depending on D energy, sample temperature and total D fluence. For "gentle" plasma conditions (<5 eV/D, 370 K), a W-enriched layer forms on the surface and protects the underlying oxide from reduction. At higher D energies or higher temperatures, the oxide reduction progresses significantly faster and eventually reaches the metallic W. Once this happens, D uptake increases proportionally to the fraction of surface area with reduced oxide at the interface. It can be estimated that thin (1–2 nm) natural oxide films on W will be fully reduced and become permeable for D after a fluence of about 1.6×10^{23} D/m^2 already at gentle exposure conditions and even earlier for higher D energies or sample temperatures. It was concluded that natural oxide will affect D uptake studies only at low D fluence or during fluence series with multiple air exposure.

The TDS studies on D release showed that 5–100 nm thick oxide films significantly influence the release behavior of D from W. The oxide film acts as both a D reservoir and a transport barrier that delays D release depending on the oxide thickness. Above 475 K, D starts to interact chemically with the oxide film and is released not only as HD or D_2 but also in the form of heavy water (HDO and D_2O). Above 700 K, D is released exclusively in form of heavy water as

long as enough oxide is available. For oxide thicknesses $\geq$15 nm some heavily modified oxide remains after TDS. The release spectra are then dominated by the oxide in the sense that the high temperature release peak consists exclusively of heavy water. Heavy water is difficult to quantify in TDS and thus normally neglected, which would lead to an under-estimation of the total D release and a misinterpretation of the binding energies of D in defects in such cases. But even for films of 5–10 nm, the spectra are affected by the oxide until it is fully removed by the outgassing D. It was concluded that oxide films become relevant for the D release during TDS, if the ratio of O atoms on the surface to D atoms in the sample is larger than 5–10 %. For D release studies with (self-)damaged W and high D retention (2×10^{21} D/m^{2}here), the effect of the natural oxide is small. However, for studies with lower D retention even natural oxide films (1–2 nm) may significantly influence the release behavior of D during TDS.

Lastly, a first estimate was made whether natural oxidation of W might affect the D uptake and release from PFCs in a fusion reactor. It suggests that oxide films in a fusion reactor would be quickly reduced during plasma operation and would not have a significant effect. A comprehensive investigation of the interaction of D with W oxide is nevertheless necessary to correctly extrapolate the results of laboratory studies to PFCs in a reactor.

Contents

Chapter 1

Motivation: Why are surface oxide films on W relevant for nuclear fusion?

The currently highest developed and most researched concepts for future fusion power plants rely on magnetic confinement of a hot plasma. They use the hydrogen isotopes deuterium (D) and tritium (T) as fuel for the nuclear fusion reaction:

$$^{2}_{1}\mathrm{D} + ^{3}_{1}\mathrm{T} \rightarrow ^{4}_{2}\mathrm{He}\,(3.5\,\mathrm{MeV}) + ^{1}_{0}\mathrm{n}\,(14.1\,\mathrm{MeV}).$$

Compared with other possible fusion reactions, D-T fusion has a significantly higher cross sections (reaction probability) at achievable plasma core temperatures (above $\approx 10^8$ K) and is thus the best (and many would say only) candidate to achieve a net energy production via nuclear fusion with currently conceivable technology. A typical reactor consists of a torus (donut shape) of confined plasma surrounded by a vacuum vessel (first wall) which absorbs the heat generated by the fusion reaction. A reinforced section of the wall - the so called divertor - has direct contact to open field lines of the plasma edge and allows the removal of impurity particles and helium ash during operation. However, D-T fusion imposes a set of challenges for the design and material choices of a power producing fusion reactor. Firstly, the tritium fuel is radioactive which complicates handling of the machine. Furthermore, tritium has a relatively short half-life of 12.3 years, which means that it is not naturally abundant and has to be constantly produced in breading blankets in the reactor walls to allow self-sufficient refueling. Secondly, the highly energetic neutrons (14.1 MeV) from the fusion reaction are not confined by the magnetic fields and can directly reach the plasma-facing components (PFCs) and structural elements of a reactor. There they can collide with nuclei of the wall material and create displacement damage (material defects) that can bind hydrogen isotopes (HIs) [1], which further complicates the aspects of radioactive inventory and fuel self-sufficiency. In addition to these effects, the plasma-facing material in a fusion power plant has to withstand high cyclic thermal loads (e.g. during plasma disruptions or instabilities at the plasma edge) and high heat and particle fluxes from charge exchange neutrals or ions that are accelerated in the sheath region of the plasma.

To address all these requirements, extensive research on the fundamental properties and the component design of plasma-facing materials has been conducted over the last decades and tungsten (W) has emerged as the material of choice for the divertor of the future experimental fusion reactor ITER [2] and as a candidate material for the divertor and main wall armor of the planned demonstration fusion reactor DEMO [3]. The main advantages of W are its high threshold for physical sputtering, high melting point and low intrinsic HI retention [4]. The low retention of HIs and especially of the radioactive tritium fuel is vital for fusion reactors to keep the tritium inventory of the reactor wall low and to conserve the valuable tritium fuel.

However, the above-mentioned degrading effects dynamically change the properties of the wall materials and increase HI retention over the life time of a reactor. The material defects that are created by irradiation act as traps for HIs and can increase the total HI retention in W by several orders of magnitude compared with not-irradiated W [5]. In addition, the presence of HIs in the material also increases the maximum concentration of stable defects that can be created in W by ion or neutron irradiation and thus further increases HI retention [6]. These effects make HI uptake, retention and release from W in reactor conditions an active area of research [7] with high relevance for the design and economic feasibility of a future fusion power plant.

In recent years, dedicated laboratory studies have been conducted to isolate individual aspects of HI uptake, retention and release from W in well-defined model systems [6, 8–11]. As no neutron source in the 14 MeV energy range is available, these experiments use high-energy ions as a substitute to create displacement damage. In most cases, MeV-energy tungsten ions are used as such self-ion implantation avoids inserting foreign elements into the material that may influence retention due to additional chemical effects [12]. Commonly, D is used in these experiments, as it is well quantifiable and not radioactive. The D retention in the near surface area can then be determined by ion-beam analysis. Complementary to this, the total D retention in the sample and also the D release can be investigated by thermal desorption spectroscopy (TDS). By repeating such experiments for different exposure conditions, the binding energies of HIs in material defects in W can be derived [6, 8, 13–15].

For practical reasons the overwhelming majority of these experiments is carried out “ex-situ” meaning that the W samples have contact with ambient air before and in between experimental steps, e.g., between D plasma loading and ion beam analysis. Due to its affinity for oxygen, W readily forms a thin natural oxide film on the surface upon contact with ambient atmosphere [16]. Because, this natural oxide film is very thin (only 1–2 nm) it was commonly neglected in HI uptake, retention and release studies; see, e.g., [17, 18].

Recently, however, a study by Hodille et al. [9] has indicated that even thin natural surface oxides on W may influence the D retention and release. Such natural oxide films are always present on W in ex-situ laboratory studies (and also in in-situ studies, if not great care is taken to remove them) [9, 19], but they may not be present in the divertor or first wall of a fusion reactor, where they could be quickly reduced by the plasma [20], at least for directly plasma-exposed surfaces. In this case, effects of natural oxide films might represent an unaccounted discrepancy between laboratory studies and reactor-relevant conditions. Clearly, a detailed understanding of the effects that oxide films have on the interaction of HIs with W is necessary to interpret ex-situ experiments correctly and to enable the extrapolation of these results to reactor-relevant conditions.

This thesis addresses this questions in two main parts. The first part (chapter 4) is concerned with the uptake of D through surface oxide films into metallic W and the second part (chapter 5) is dedicated to the release of D from W through thin surface oxide films.

The effects on D uptake are approached by deliberately oxidizing W samples to surface film thicknesses of 33 and 55 nm. These oxides are thick enough to yield a measurable effect, but still thin enough not to develop cracks during thermal oxidation. Thick oxide films (µm scale) are known to crack due to their volume difference compared with metallic W and data interpretation is then ambiguous [21]. The interaction of hydrogen with tungsten oxide (especially WO_3) has been extensively studied in the context of W-oxide-based gas sensors or electro-chromic devices [22, 23]. However, up to date there are only very few studies which are concerned with the effects of surface oxide films on D uptake, retention and release from W, i.e., aspects relevant for the application of W as a first-wall and divertor material for nuclear fusion reactors. There are studies by Alimov et al. [21], Ogorodnikova et al. [24] or Addab et al. [25] who

found increased deuterium (D) uptake and retention in the oxide films themselves, but these studies do not allow to draw any conclusion on the uptake, retention and release of HIs from bulk tungsten through the surface oxide films.

The goal of the present study is to a) investigate to what extent oxide films with a thickness of a few tens of nm, affect D uptake into the underlying W and b) be able to draw conclusions about the effects of the thinner, natural oxide film that is almost always present in laboratory experiments. To this end, a novel approach was used: Thin oxide films were thermally grown on top of MeV-ion-irradiated, defect-rich W. The defect-rich W acts as a getter-layer for any HIs that possibly penetrate the oxide film into the metallic tungsten. The samples were then exposed to D plasma at various D energies, D fluence and sample temperatures. Afterwards, the depth-resolved concentration of D and O was evaluated with ion beam analysis and scanning electron microscopy to determine the D uptake into metallic W and to investigate the reduction of the oxide.

After this, the release of D from metallic W through thin oxide films was studied. D retention in tungsten is typically lower than in tungsten oxide [21]. Consequently, D desorption would be dominated by the D retained in the oxide itself rather than by the D retained in the underlying bulk W. Thermal oxidation of deuterium-containing tungsten is also not a viable option, as most of the retained deuterium would be released at the necessary oxidizing temperatures. In order to overcome this difficulties, a novel approach has been devised: First, a defect-rich self-ion-damaged layer of W was used as a D reservoir. Next the traps in this self-damaged layer were filled with D by exposure to a D plasma. After this, the samples were electro-chemically oxidized to oxide film thicknesses of 5–100 nm. This oxidation method works at room temperature and avoids D release during the oxidation process. Finally, the release of D through the oxide films was monitored by thermal desorption spectroscopy by analyzing the outgassing D-containing species (HD, D_2, HDO, D_2O) and their quantity with a quadrupole mass spectrometer.

This thesis is structured in the following way: Chapter 2 presents some background information on the interaction of D with W and gives a brief overview over the W oxide system and its interaction with D. Chapter 3 presents a detailed description of the experimental approach, the experimental setups and the main analysis techniques. Chapter 4 discuses the results on D uptake through 33 and 55 nm thick surface oxide films and the reduction of the oxide for various exposure conditions with different D fluence, D energy and sample temperature. Chapter 5 presents the results on the effects of 5–100 nm thick surface oxide films on thermal D release from W during TDS up to 1000 K. Finally, Chapter 6 gives a summary of the results and presents the conclusions. It also gives an outlook on remaining open questions and a motivation on why and how to approach them.

Chapter 2

W oxides and their interaction with hydrogen isotopes

This chapter will first present an overview over the basic interaction of HIs with pristine and ion-damaged W and then summarize some fundamental information on the W oxide system and its interaction with hydrogen isotopes. The aim of this chapter is to set up a common frame of reference and provide the necessary background for interpretation of the results of this work, which are discussed in chapter 4 and 5.

2.1 Interaction of hydrogen isotopes with tungsten

The main goal of this PhD thesis is to asses the influence of thin surface oxide films on HI retention and release from W. However, since displacement-damaged W is used as a getter-layer or reservoir for HIs, it is helpful to recapitulate the mechanism of HI interaction with not-oxidized, metallic W in order to correctly interpret the role of the oxide films.

2.1.1 Uptake and release of hydrogen isotopes in W

Fig. 2.1 shows a schematic representation of the potential energy of HIs on the surface and in the bulk of metallic W. The uptake of HIs from the molecular gas phase into metallic W is a multi-step process. First the HIs adsorb at the surface of the metallic W as a molecule (physisorption) with the binding energy Q_p. After that they can dissociate into atoms which are then chemisorbed at the surface. The binding energy for this state (enthalpy of chemisorption) is given as Q_c. For the dissociation at the metallic surface, an activation energy E_c has to be overcome. This energy is much smaller than the dissociation energy of molecular hydrogen in vacuum (2.25 eV), and for W at room temperature it is close to zero. From the chemisorbed state the HIs can enter the metal (absorption) by overcoming the absorption energy E_{sb} and reaching a solute site. For W, E_{sb} is relatively high (in the range of 1.4 eV as will be discussed below), which means that HI uptake into the metal is energetically not favored. The ad- and absorption process is reversible and governs not only the uptake but also the release of HIs from W. Atomic HIs leave the metal by first entering a chemisorbed state at the surface, then, in order to leave the sample, they have to recombine to a physiosorbed molecule which can eventually desorbes into the vacuum. Since the energy of atomic hydrogen in vacuum is comparatively high, hydrogen is not released in atomic form from W for temperatures below 1200 K, which is above the highest temperatures used in this work [26].

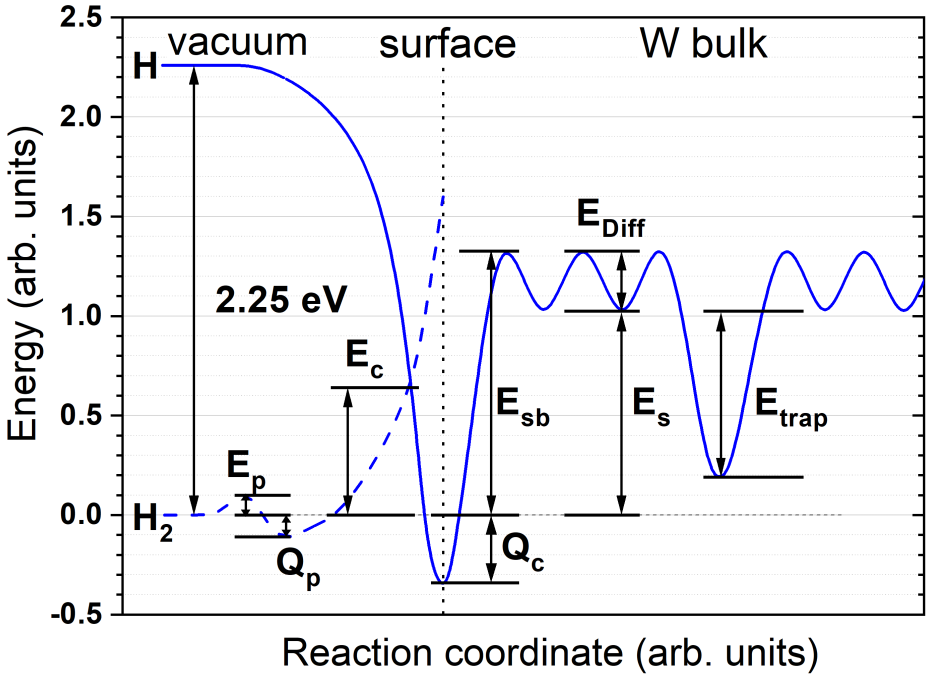

Figure 2.1 – Schematic representation of the potential energy of HIs in W and at the surface. The solid blue line depicts the potential of atomic hydrogen; the dashed blue line the potential of molecular hydrogen. At the intersection point of the two lines the molecules dissociate.

Apart from this process, HIs can also be directly implanted into W if their kinetic energy E_{HI} is larger than E_{sb}. This process bypasses the adsorption stages and is possible with ions, atoms or even molecules (which dissociate on impact), e.g., from an ion beam or from a plasma.

2.1.2 Hydrogen isotopes in pristine W

The hydrogen retention in undamaged, pristine and annealed W is very small (in the range of 5×10^{-3} at. % at 300 to 450 K [24, 27, 28]), which — together with other favorable properties — makes W a good candidate material for the divertor and first wall of a fusion reactor. In ideal (defect-free) W, HIs are only retained as solute at interstitial sites of the W lattice. These interstitial sites correspond to the shallow potential minima in the W bulk part of Fig. 2.1. The enthalpy of solution (E_s) of HIs in pristine W was recently remeasured with high precision and is given as 1.13±0.04 eV for H and 1.14±0.04 eV for D [29]. The activation energy for diffusion of D in W from one interstitial site to the next (E_{Diff}) was also remeasured and is given as 0.28±0.06 eV [30]. A qualitative interpretation of this data is that, while it is difficult for thermalized HIs to enter W (at moderate temperatures below 1000 K), diffusion of solute HIs between interstitial sites in W is relatively easy and fast already at temperatures of around 370 K (100°C) [31]. Even if significant quantities of HIs are inserted into metallic W (either exposing it to HI containing atmosphere at elevated temperatures (> 1500 K) or by directly implanting energetic HIs from an ion beam or plasma), most inserted HIs will diffuse towards the surface where they will exothermally leave the W lattice to be adsorbed on the surface before they recombine to a molecular gas and desorb. The maximum deuterium concentration in pristine W (i.e., a W sample fully recrystallized at 2000 K) after D plasma exposure at 370 K with an energy of 38 eV/D, is reported to be in the range of 10^{-1} at.% for a D fluence of up to 5×10^{25} D/m^2 according to [32].

2.1.3 Hydrogen isotopes in (displacement)-damaged W

In reality the W lattice is never ideal and always contains material defects. Furthermore, when used as a first wall and divertor material in fusion reactors, W will suffer additional damage by bombardment with highly energetic particles from the plasma (e.g. charge exchange neutrals) and 14.1 MeV neutrons from the fusion reaction, which creates additional material defects. It has been shown that material defects act as trapping sites for HIs and strongly increase the HI retention in W [1]. An example for the potential energy well of such a trap is also represented in Fig. 2.1. According to a review from Causey [18], there are different trapping sites with different binding energies for HIs ranging from 0.5 eV to 2.5 eV. The relative importance of different defect types (e.g. interstitials, vacancies, dislocation loops or vacancy clusters) for HI retention is still actively discussed in literature. It is also not fully clear if the different binding energies stem from different trap types or if they can be explained by a single type of defect that can bind multiple HIs and has different binding energies depending on the fill level.

In any case, if the defect concentration in W is high, the HI retention increases by more than two orders of magnitude compared with undamaged W [5]. In such cases, the overall HI retention is governed by the material defects, but the diffusion of HIs in W is still governed by solute diffusion. It should be noted, however, that HIs in displacement-damaged W cannot diffuse unhindered through the material at room temperature as they will eventually reach a trapping site and be bound there [12, 33]. Thus, if HIs are inserted into the surface near region, a diffusion front will form and gradually progress into depth when the surface near traps are filled.

2.2 W oxides

The tungsten oxide system is rather complex and while the existing literature is vast, the results and statements are sometimes ambiguous or even contradictory. Therefore, a comprehensive treatment of this subject would be far beyond the scope of this thesis and here only a compact overview shall be given with focus on the aspects that are relevant for the current work. The information in this section is based on the book of Lassner and Schubert [34] on tungsten and on two books dedicated to W oxides by Best et al. [35] and Jehn at al. [16], which themselves are based on numerous publications.

2.2.1 W oxide stoichiometry and phases

W oxides exist in a variety of different stoichiometries such as tungsten (II) oxide (WO), tungsten (IV) oxide (WO_2), tungsten (VI) oxide (WO_3 – also called α-tungsten oxide) and oxides with more complex stoichiometry such as β-tungsten oxide $WO_{2.9}$ ($W_{20}O_{58}$), γ-tungsten oxide $WO_{2.72}$ ($W_{18}O_{49}$) and others. Which oxide is formed depends on the oxidation method, the W grain orientation and surface condition and, in case of thermal oxidation, on the temperature and the oxygen partial pressure. In addition, most of these oxide types can exist in different allotropic modifications, depending on temperature. Please note that the allotropic modifications of WO_3 are also denoted by the Greek letters (α, β and γ), where α-WO_3 stands for the orthorombic, β-WO_3 for the triclinic and γ-WO_3 for the monoclinic configuration of the corner sharing metal-oxygen octahedral structure of WO_3. Care should be taken not to confuse the allotropic modification with the stoichiometry of the oxide when researching literature about W oxides.

In the present work, the oxide films are very thin (≤ 100 nm) and are created either via thermal oxidation at 600 K in synthetic air or by electro-chemical oxidation. Both methods are described in detail in section 3.5. For the thermally grown oxide films, Lassner and Schubert [34] predict the formation of monoclinic γ-WO_3, which is allotropically stable in the temperature range of 290 to 600 K, i.e., over the full temperature spectrum that is used for D uptake studies in this work. The predicted stoichiometry (WO_3) matches with the characterization of the thermally grown oxide films that has been done in this work (compare section 3.5 and 4.1), although small contributions of β-tungsten oxide $WO_{2.9}$ or γ-tungsten oxide $WO_{2.72}$ cannot be fully excluded. For the electro-chemical oxidation [35] (p. 83) predicts the creation of an amorphous WO_3 film, which also matches the oxide characterization done in this work (section 3.5).

WO_3 is reported to be chemically stable in acids (except HF) but easily dissolved in aqueous alkali hydroxide solutions, which is confirmed for the oxides in this work by solution in NaOH.

2.2.2 W oxide color: "natural" color vs. interference color of thin oxide films

Different stoichiometries of W oxides have different colors. WO_3 is colored yellow (and is also used as a color pigment in yellow paints) and WO_2 is colored brown. There is also tungsten blue oxide (which is a mixture of different constituents with different stoichiometries) [34]. However, the oxide films used in this work (5–100 nm) are too thin to see the natural color and it is reported in literature that oxide films of these thicknesses are not yet visible [36]. Nevertheless, on the mirror-polished W samples used in the present work, a coloring of the oxide arises from light interference in the (at these thicknesses) transparent WO_3 films when the light is reflected from the underlying polished W surface. This interference color is determined by the optical properties of the oxide (and thus its stoichiometry) but also by the film thickness. In the present case, WO_3 films of 33 nm appear yellow, films of 55 nm appear blue and films of 100 nm appear light green. A picture of such a (thermally grown) 55 nm thick oxide film and two 33 nm thick oxide films is shown in Fig. 2.2 together with a W sample with only natural oxide. The electro-chemically prepared oxide films show identical colors for identical oxide thickness, which indicates that they have the same stoichiometry as the thermally grown oxides. This interference colors should, however, not be confused with the "natural" color of the oxide films.

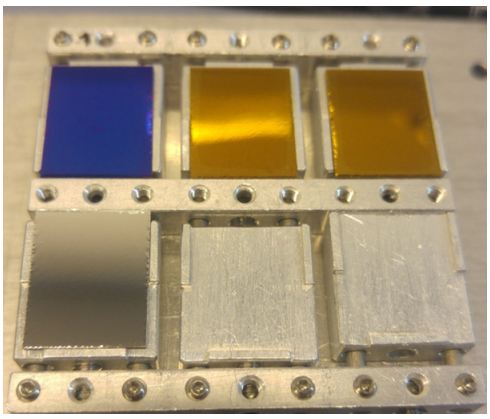

Figure 2.2 – Interference colors of W oxide films on W polished to a mirror finish; blue: 55 nm, yellow: 33 nm, gray: natural oxide (1–2 nm)

2.3 Interaction of HIs with W oxides (hydrogen W bronzes)

WO_3 can form a so-called hydrogen tungsten bronze (H_xWO_3) upon uptake of hydrogen isotopes. Here x denotes the fraction of H atoms in the compound and is typically smaller than 0.5. The term "bronze" is assigned to this compounds due to their metallic shine. Appart from hydrogen, tungsten-bronzes can also form with many other (light) elements (M_xWO_3), were M denotes an element [34].

The intercalation of H (or D) atoms into WO_3 leads to a change of the optical properties of the bronze, depending on the fraction x of HIs in the compound. In case of the thin WO_3 films studied in this work, this leads to a color change of the film when D is intercalated in the oxide. The electrical properties of H_xWO_3 also change with the fraction of H. For $x \leq 0.3$ the bronze behaves as a semiconductor and for $x > 0.3$ it behaves as a conductor.

Literature on the heat of solution of HIs in WO_3 is scarce, but there is one study by Dickens et al. [37], which reports a slightly negative enthalpy of formation of -0.28 ± 0.04 eV for H_xWO_3. This indicates that HI uptake in WO_3 is energetically favored (in contrast to metallic W). The activation energy for hydrogen diffusion in WO_3 is stated as 0.35 eV from DFT calculations in [38] and as 0.4 eV from experiments in [39]. This is larger than in metallic W, but still allows fast diffusion of HIs in the oxide. The diffusivity of HIs in WO_3 is reported to be quite high [40] for both crystalline and amorphous oxides and HIs are expected to diffuse through the full extent of thin WO_3 films used in this work within minutes even at room temperature.

Formation: Hydrogen-W-bronze does not directly form by contact of H_2 containing atmosphere with WO_3 but a thin cover layer of platinum or palladium is necessary to assist the dissociation of H_2 molecules before the atomic H can enter the WO_3. Even then, a significant formation of bronze occurs only at elevated temperatures of about 100 °C (≈370 K). However, if atomic H is present in the surrounding atmosphere, tungsten bronze can form without catalysts. Of course the bronze can also form if HIs with sufficient kinetic energy are directly implanted into the oxide via ion beam or plasma exposure. Appart from this, it is also possible to insert (or extract) H either electro-chemically in wet cells or electrically in solid state devices (see e.g. [22] for details).

Applications: The possibility of reversible H insertion in H_xWO_3 and the resulting controllable changes in its electrical and optical properties leads to a wide range of possible applications. This stimulated extensive studies of this compound in the past. According to a review by S. Deb [22] those include: Smart windows with adjustable light transmittance (electrochromism), sensors for hydrogen or other gases (with catalyst layer) based on the change of optical properties or electrical conductivity of WO_3, prototypes of photo-electro-chromic solar cells and early electro-chromic displays. There are also reports on high temperature superconductivity (above 91 K) of Na-doped WO_3.

W oxides and HI plasma: There are only very few studies on the interaction of HIs from a plasma with W oxides or the possible effects that surface oxide films could have on HI uptake, retention and release from W. There are studies by Alimov et al. [21], Ogorodnikova et al. [24] or Addab et al. [25] who found increased deuterium (D) uptake and retention in the oxide films themselves. The study by Alimov et al. [21] investigated WO_3 films of several μm thickness

and found D retention values of up to 2.5 at.% (with respect to the total number of atoms, i.e., W and O atoms), which is significantly higher than in displacement-damaged W. However, these studies do not allow to draw any conclusion on the uptake, retention and release of HIs from bulk tungsten through surface oxide films. These questions, are addressed in the present work.

Chapter 3

Experimental Setup and analysis techniques

This chapter will introduce the experimental approach to study HI uptake and release from W through thin oxide films. In all experiments the HI deuterium (D) is used. The main experimental steps are: The so-called "self-damaging" (to enhance D retention), oxidation (thermally or electro-chemically), D plasma exposure and thermal D release. The main analysis techniques are: Ion Beam Analysis (IBA), Scanning Electron Microscopy (SEM) and Thermal Desorption Spectroscopy (TDS). As large parts of the methodology are applied to D uptake as well as to D release, the similarities and differences between these two cases will also be elaborated here.

3.1 Experimental approach

Fig. 3.1 illustrates the experimental approach to study D uptake and release. The distinguishing feature, is the use of a "self-damaged" zone in the metallic W (dark gray in Fig. 3.1), which is created by bombardment with high-energy W ions (see section 3.3). This introduces a well-controlled amount of defects in the material without changing the elemental composition. As described in section 2.1.3, the defects significantly increases the retention of D by binding it in "traps". This is a vital point as otherwise the D retention in the sample would be dominated by the oxide film itself and it would not be possible to reliably measure D uptake or release through the oxide film. In addition, D that is bound in these traps can no longer diffuse at room temperature [12, 33]. Thus, for the D uptake experiments, the self-damaged zone serves as a "getter-layer" that retains any D that penetrates through the oxide film for later ex-situ measurements. For the D release experiments, on the other hand, the self-damaged zone is filled with D (by plasma exposure) prior to oxidation and then serves as a large reservoir for D release through the oxide film during TDS.

Both experiments use D as it is readily available but far less abundant than protium (H) and thus avoids strong background signals from ambient hydrogen. D is also detectable with ion beam analysis via the nuclear reaction with ^{3}He and can be precisely measured and quantified in W. In contrast to Tritium (T), D is not radioactive and can be handled in the laboratory without nuclear safety issues. As the nuclear mass of HIs does only play a minor role for their uptake, retention or release from W (oxides)[1], the results for D can be easily extrapolated to other hydrogen isotopes.

[1] The solute diffusion of HIs is proportional to $1/\sqrt{m}$, but diffusion length in the oxide and the self-damaged W is determined by material defects (see section 2.1.3). The nuclear mass does, however, affect the sputter yield of W (oxides) by HIs, which of course depends on the nuclear mass of the involved particles.

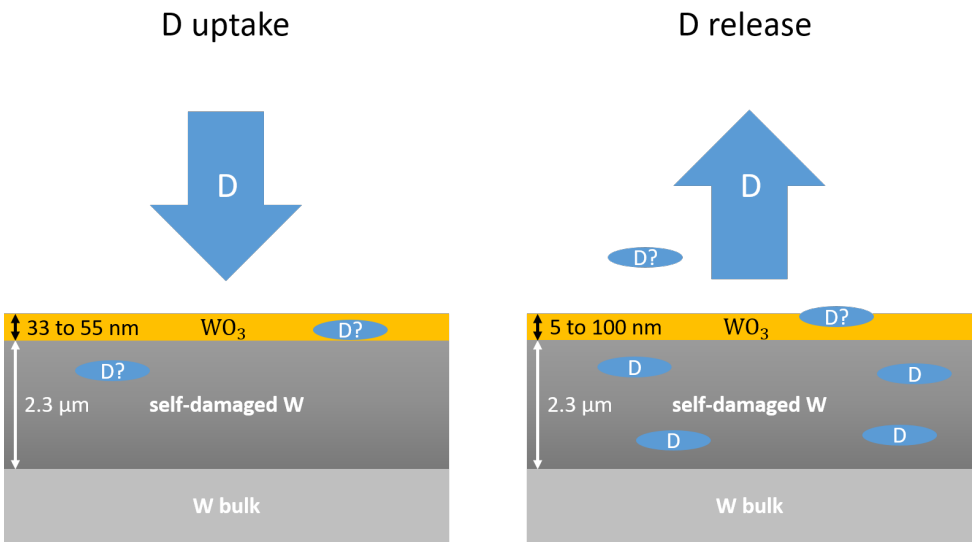

Figure 3.1 – Schematic of self-damaged and oxidized sample for D uptake (left) and D release (right). D uptake: The self-damaged zone (dark gray) acts as getter-layer for D atoms permeating the surface oxygen film (yellow). D release: The self-damaged zone is filled with D prior to oxidation and serves as a quantified D reservoir for D release during TDS.

Furthermore, for all experiments on D uptake and D release, identical W samples were used. In a first step they were polished, annealed and then self-damaged. After this the process differs for D uptake and D release, which is illustrated in Fig. 3.2.

For the D uptake experiments the samples are first thermally oxidized and then exposed to D plasma. After that the depth-resolved D concentration in the sample and the depth-resolved oxygen (O) concentration in the oxide film are measured ex-situ by IBA. Additionally, the changes of the oxide film is investigated with SEM imaging of the surface and of cross sections through the oxide. For D release the samples are first filled with D and then electro-chemically oxidized. The electro-chemical oxidation is carried out at room temperature and thus prevents thermal release of D during the oxidation process. After that the D release through the oxide is investigated with TDS.

In the following the individual experimental steps and setups will be introduced and discussed in detail. Section 3.5 (oxidation) also contains the characterization and comparison of the oxide films created by the two different oxidation methods. In addition, analysis methods such as IBA and SEM (sections 3.6 and 3.7) are applied after each relevant experimental step (i.e., oxidation, plasma exposure and TDS).

Please note that the samples and procedures described here are applicable to the two main studies in this work (D uptake and release through oxide). Apart from that, there are additional experiments such as the D release directly from W oxide (section 4.2.3) or the determination of the sputter yield of W from W oxide by D (section 4.5), which use different kinds of samples or methods. In those cases, the experimental details are described directly in the according section.

3.2 Polishing and annealing

All samples are cut from a single sheet of hot-rolled W with a purity of 99.97 weight % supplied by the company Plansee [41] and are $15 \times 11.8 \times 0.8$ mm^3 in size.

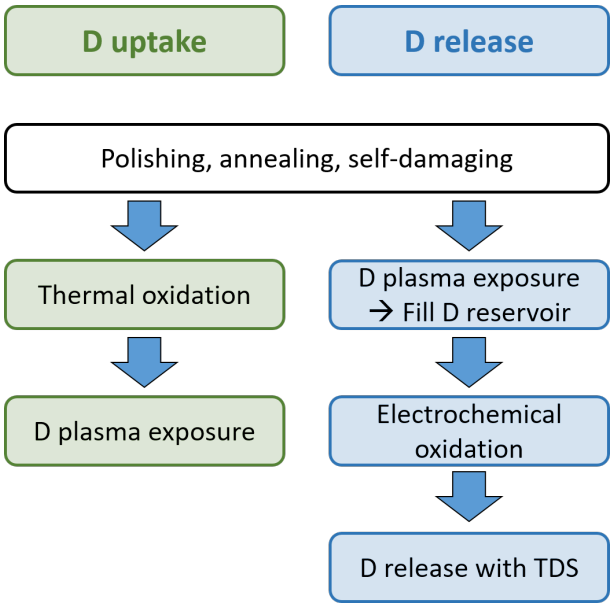

Figure 3.2 – Schematic of the order of experimental steps for D uptake (green) and D release (blue).

First, the sample surface is mechanically grinded and then electro-polished in 1.5 % NaOH to achieve a mirror-like finish. Details on this technique can be found in [42]. The samples are then cleaned in an ultrasonic bath first with acetone then with isopropanol for 20 minutes each and then rinsed in distilled water.

Next, the samples are annealed by electron-beam heating in ultra-high vacuum (base pressure $<5\times10^{-7}$ Pa, rising to $<3\times10^{-5}$ Pa during annealing). They are first outgassed and stress relieved at ≈1400 K for 20 minutes and then annealed at 2000 K for 5 minutes. This reduces the defect density in the bulk and thus minimizes its contribution to the total HI retention in the sample. Additionally, the heating induces grain growth to a diameter of ≈ 10 to 50 µm (see Fig. 3.4 and 3.5), which minimizes possible effects of grain boundaries on HI retention.

3.3 Self-damaging

Afterwards, the samples are irradiated with 20.3 MeV W^{6+} ions at 300 K on a water-cooled sample holder. The ion beam is scanned across the sample surface to achieve a laterally homogeneous irradiation. The absolute W flux was measured by Faraday cups in the scanning area of the beam and the samples were exposed to a total W fluence of 7.87×10^{17} W ions/m^2. In the first 2.3 µm of the W sample this creates an irradiation damage of 0.23 displacements per atom (dpa). This value was calculated with the program "SRIM" (Stopping Range of Ions in Matter) [43] according to the procedure described in [44]. Due to the use of self-ion bombardment for its creation, this zone is called "self-damaged zone". During implantation, a molybdenum mask with an opening of 10×14 mm^2 is used to hold the samples in place. It shields the edges of the sample from the W-ion bombardment and leaves an un-damaged rim along the sample edges.

It should be mentioned that in the more general scope of material research for future fusion reactors, self-damaging is a technique to simulate the displacement damage that is expected in W by bombardment with fast 14.1 MeV neutrons [1, 6]. As neutron sources in this energy spectrum are not available at present, this technique allows to study the effects these defects have on HI retention and any synergistic effects of HI or He retention and defect creation in

W in a laboratory frame. However, in the present work the self-damaged zone is used either as a "getter-layer" that accumulates HIs that permeate through the oxide film during D plasma exposure (D uptake) or as a D reservoir that is filled with D prior to oxidation and can store large amounts of D (200×10^{19} D/m^2) underneath the oxide (D release).

3.4 Plasma exposure in "PlaQ"

D plasma exposure of the W samples was carried out in the electron cyclotron resonance (ECR) plasma device "PlaQ". A detailed description of the setup is given in [45] and [46]. Here only a short description of the key features is provided. Fig. 3.3 shows a schematic of the setup.

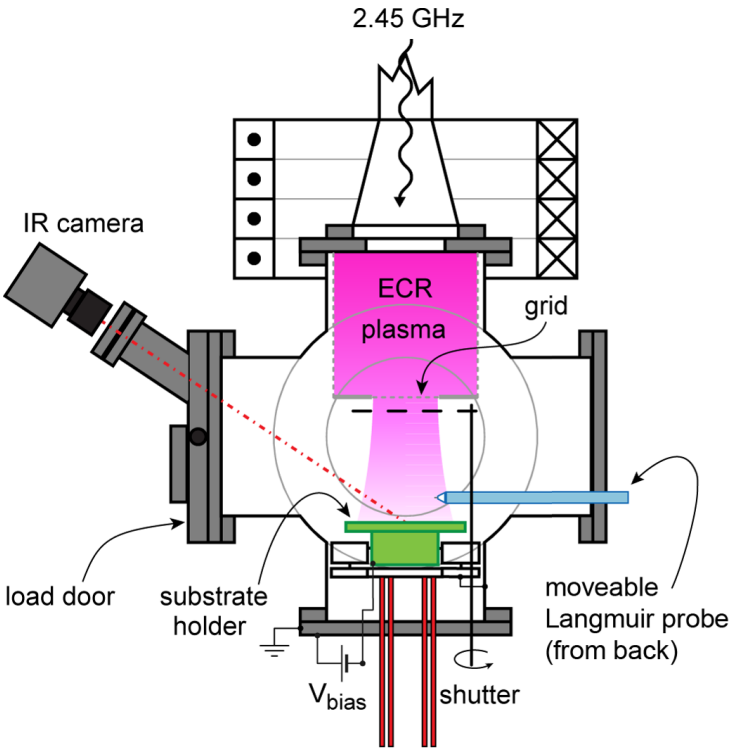

Figure 3.3 – Schematic of the "PlaQ" plasma exposure device. Picture adopted from [45] and [46] with kind permission of Armin Manhard.

PlaQ permits highly reproducible D plasma exposure with adjustable D energy. Up to six samples can be exposed radially symmetric on a single sample holder to ensure identical plasma-loading conditions. The sample holder has a feedback-controlled temperature regulation that maintains a constant exposure temperature independent from the particle flux. For most cases (except the high temperature plasma exposure in section 4.4.2), the sample temperature is kept at 370 K during plasma exposure. This is high enough to allow for D mobility in W and low enough to avoid significant annealing of the displacement damage that was introduced during the self-damaging [31].

The majority of the ion flux in PlaQ consists of D_3^+ (94 %) with a minority of D_2^+ and D^+ (3 % each). The energy of the D (molecular) ions impinging on the sample can be adjusted by a sample bias voltage. For the molecular ions (D_3^+, D_2^+) the energy is shared evenly between the D atoms upon contact with the sample surface. Thus, the total energy of the impinging molecular ions is given by the plasma sheath potential (-15 eV) plus the negative DC bias

voltage divided by the number of D atoms per molecular ion. For floating potential (no bias) this results in an energy of <5 eV/D for the D_3^+ majority species and an energy of <15 eV/D for the D^+ minority species. This setting is called "gentle" plasma and many ex-situ D uptake and retention studies in (self-)damaged W have been performed under similar conditions, e.g., [6, 12, 44]. The low D energy is below the damage threshold of W and prevents the creation of additional defects in the material [31]. Restrictively, it should be mentioned that it is not a priori clear if this assumption also holds for W oxides. This gentle exposure is used for the first D uptake experiments (section 4.1 to 4.3) and for all D release experiments. For higher bias voltages, e.g. -100 V sample bias, the resulting D energies would be 38 eV/D for the majority and 115 eV/D for the D^+ minority.

A typical PlaQ plasma exposure begins with a 15 minutes "burn in" phase in which a shutter prevents the plasma from interacting directly with the samples. This procedure cleans the vacuum chamber by removing remaining adsorbates from the walls. During this phase only atomic D can reach the samples via gas phase collisions or by collisions with the chamber walls. Then, the shutter is opened and the samples are exposed to a charged D flux of about 5.6 to 10×10^{19} D/m^{2}s (the exact flux is depending on the applied bias voltage, as has been determined in [45]). Plasma exposures in this work range from 2 to 96 h, which translates to a D fluence of about 6×10^{23} to 2×10^{25} D/m^2.

D uptake: For the D uptake experiments the sample is first thermally oxidized and then exposed to plasma in PlaQ. Different bias energies (0 to -100 V) and temperatures (370 and 500 K) are used and several fluence series are conducted. For the initial campaign with gentle (<5 eV/D) plasma (section 4.1 to 4.3) two samples with different oxide thicknesses (33 and 55 nm) and an additional, self-damaged reference sample with only a natural oxide film (1–2 nm) were exposed simultaneously. For later exposures at higher bias voltage or temperature (section 4.4) only samples with 55 nm thick oxide films were used.

D release: For D release the plasma exposure is conducted prior to oxidation in order to decorate (fill) the defects in the self-damaged zone as a reservoir for later D release during TDS. To assure a homogeneous D filling level across the samples, the existing defects in the self-damaged zone have to be saturated with D. In addition, the loading has to be "gentle" enough to avoid the creation of new defects during plasma exposure which would lead to dynamic release during storage (see [10, 47]). Therefore, the samples were exposed to a high D fluence at a low D energy of $<$ 5eV/D and a substrate temperature of 370 K.

The samples were exposed in two different batches (a third batch was not exposed and serves as reference for purely thermally introduced changes in the oxide during TDS; see section 5.1). The first batch contained the samples that were later oxidized to thicknesses of 25, 50 and 100 nm and an additional reference sample with only natural oxide (1–2 nm), that was also self-damaged prior to D loading. The second batch contained samples that were later oxidized to 5, 10 and 15 nm. The first batch was exposed to the plasma for 72 h accumulating a total fluence of 1.4×10^{25} D/m^2. After the exposure, when the D content was measured with NRA, it became clear that the samples from the first batch exhibit a gradient of 10 % in the D content from sample top to bottom, i.e., in radial direction on the sample holder. This indicates that these samples were not filled with D up to the maximum possible retention everywhere on the sample surface, which has to be taken into account for the D release by TDS. The total (average) retention in the first batch was 2.0×10^{21} D/m^2. For the second batch, the exposure time was increased to 96 h and a total D fluence of 1.9×10^{25} D/m^2. These samples exhibited a uniform D

content across the sample with a total D retention of 2.3×10^{21} D/m^2 in the self-damaged zone. For the D release experiments (chapter 5) all measurements concerning the D content or change thereof in the first batch have been normalized with the D content at each given measurement position, so that the D gradient is accounted for and does not further influence any statements or conclusions drawn in this work.

3.5 Oxidation

This section contains information about the two different oxidation methods (thermally and electro-chemically) and also details the characterization of the oxides.

3.5.1 Thermal oxidation

This method was used to create the oxide films for the D uptake experiments. After self-damaging, the W samples were oxidized thermally at 600 K in "synthetic air" (80 % argon, 20 % oxygen) in a vacuum thermo-gauge. Two pairs with different oxide film thicknesses were prepared: 33 nm (12 h of oxidation time) and 55 nm (36 hours). In the following these samples will be referred to as thin and thick oxide. A relatively low temperature of only 600 K was chosen for oxidation in order to minimize thermal annealing of the defects in the self-damaged zone [48, 49].

As pointed out e.g. in [34], the tungsten-oxygen system is rather complex. Besides the stable oxides WO_3, $WO_{2.9}$, $WO_{2.72}$, and WO_2 a variety of non-stoichiometric compounds exist. However, at temperatures between 290 and 600 K monoclinic γ-WO_3 is expected to grow [34]. The thermally grown oxide films were investigated with NRA which yields the total areal density[2] of oxygen in the surface oxide film (see section 3.6.1) and with RBS, from which a depth-resolved oxygen concentration profile in the oxide film can be determined (see section 3.6.2 for details on the technique). The resulting concentration profiles from RBS are discussed in detail in section 4.1.4 and are in good agreement with stoichiometric WO_3. In addition, the films were investigated with laser ellipsometry, which is briefly described in section 3.8. The results of the ellipsometry measurements are discussed in detail in section 4.1.2 and are also in good agreement with WO_3. Finally, the films were characterized with sputter X-ray photoelectron spectroscopy (XPS). The measured XPS peak positions as well as the stoichiometry (determined from the relative intensities of the W_{4f} and O_{1s} peak integrals) match WO_3 (compare [50]). The possible contribution of sub-oxides to the XPS signal is estimated to be below 10 at.%. No hints of other impurities were found in the XPS analysis, after the topmost surface layer of adsorbates was removed by argon sputtering. The sensitivity for detection of other species is estimated to be < 1 at.%. However, even with all these different methods it is not possible to exclude the presence of small amounts of non-stoichiometric oxides that are very close to WO_3 with certainty.

An additional reference sample was subjected to the same temperature profile (i.e., exposure to 600 K) in the same thermo-gauge, but without oxygen (100 % Argon atmosphere). Thus, it experienced the same amount of defect annealing as the thermally oxidized samples, but did not grow an additional oxide. Of course, the natural oxide present before annealing remains on the sample since the annealing temperatures are not high enough to desorb tungsten oxide [34].

[2] The areal density is a measure for the amount of D (or other elements) that are retained in the sample per unit area of surface. This does not mean that D is located only at the surface, but gives the integral of the D content in the measured depth.

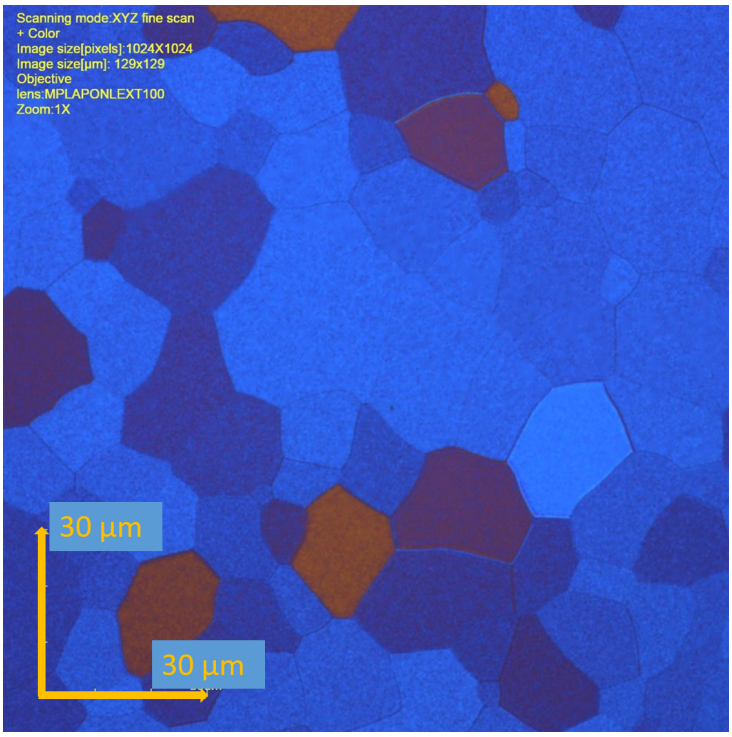

Figure 3.4 – Optical microscopy image of a W sample with thick, thermally grown oxide. The different grain heights are illustrated by the color difference that stems from light interference in the transparent oxide film. Most grains are very close to the maximum oxide thickness of 55 nm (blue). Only a few grains are less thick (orange). The thickness distribution ranges from 30 to 55 nm.

Note, however, that the growth rate of thermally grown WO_3 depends on the crystal orientation of the W substrate [51, 52]. The oxide thickness is, therefore, varying between different W grains. The diameter range of the W grains in the used samples is approximately 10–50 µm, as is shown in the microscopy image (taken with a LEXT OSL4000 by Olympus) in Fig. 3.4. The grain-dependent thickness of the oxide is visualized by the different colors in Fig. 3.4, which are created by light interference in the transparent oxide film. Most grains are close to the maximum thickness of 55 nm (blue) and only a few show a lower thickness (orange).

According to electron backscatter diffraction (EBSD) mapping and FIB cross sections by K. Schlüter [53] of thermally oxidized W samples at different oxide thicknesses using the same W grade that is used here, most W grain orientations grow a very similar oxide thickness close to maximum thickness and only a few W grain orientations grow up to 40% thinner oxides. This is in good agreement with the relative thickness distribution observed in Fig. 3.4. The relative grain-dependent thickness distribution is independent from the overall oxide film thickness in the here used range and it is assumed for both the thin and the thick oxide. This distribution does affect certain parts of the oxygen depth profiles taken with Rutherford Backscattering Sspectroscopy (RBS) but the effect can be compensated when the distribution is known (see section 3.6.2 for details).

Furthermore, Fig. 3.5 shows a top-view scanning electron microscope (SEM) image of the sample surface using backscattered electrons (Z contrast; see section 3.7 for details on SEM imaging). Parts of three different W grains (typical grain size 10–50 µm) are visible underneath the oxide film. Distinct grooves at the grain boundaries (dark lines) are formed during the annealing at 2000 K before oxidation. The oxide film itself is visible on top of the W grains. It has a much smaller, nano-crystalline structure, with a grain size ranging from 10 to 30 nm.

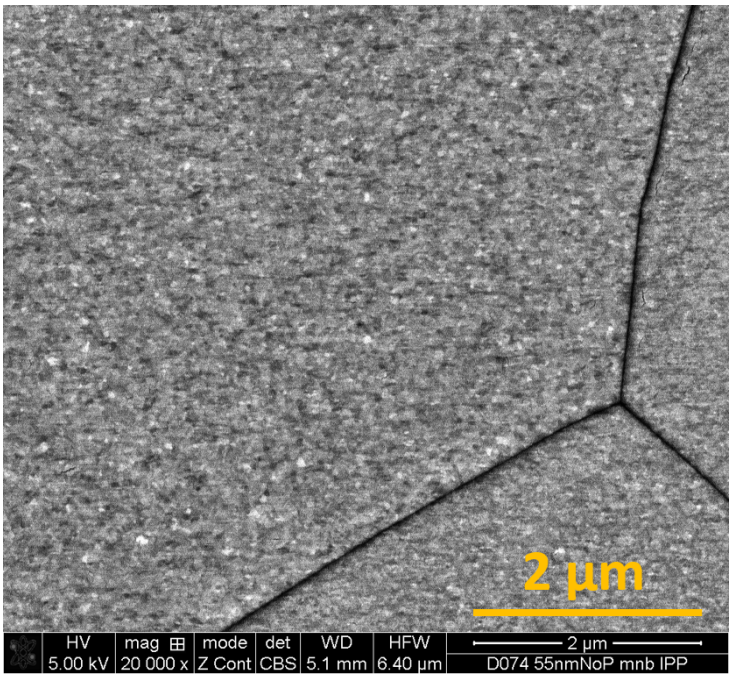

Figure 3.5 – SEM image of the thick (55 nm) thermally grown oxide film on W sample from backscattered electrons in Z-contrast. Three different W grains are shown. The nano-crystalline structure of the oxide film is visible.

3.5.2 Electro-chemical oxidation

This method is used to create oxide films for the D release experiments. After the D "reservoir" (the self-damaged zone) was filled, the samples were electro-chemically oxidized to film thicknesses of 5, 10, 15, 25, 50 and 100 nm. The electro-chemical oxidation method was originally devised by McCargo et al. [54] for precise removal of thin films of tungsten via oxidation and subsequent oxide dissolution in NaOH. To the best knowledge of the author, this method is used for the first time to deliberately create W oxide films to study D release from W.

For the oxidation process, the W sample was used as anode and immersed in an aqueous solution of 0.4 mol/l KNO_3 and 0.04 mol/l HNO_3. Two W sheets were also immersed and used as cathodes. The desired oxide thickness can be adjusted by the applied voltage (see [54]). To ensure a homogeneous oxidation, the constant current density through the sample (and W holding clamps) was limited to 2 mA/cm^2. During oxidation, the voltage drop across the oxide film grows with the oxide thickness. After reaching the maximum voltage, the voltage was kept constant for one minute (during which the sample current decreased further). After that, the voltage was switched-off and the sample was removed and rinsed in distilled water before immediately drying it.

The main benefit of this method, compared with thermal oxidation, is that it works at room temperature. This makes it possible to oxidize the surface of the tungsten sample without causing a thermal release of the trapped D in the self-damaged zone. Furthermore, the method works on a timescale of minutes rather than of hours or days as it would be the case for thermal oxidation. Another advantage of these films is their smoothness. This can be seen in Fig. 3.6, which compares SEM images of a electro-chemically grown oxide with a thermally grown one. While the electro-chemically grown oxide film (Fig. 3.6 a) is very smooth and does not show a crystalline structure in itself, the thermally grown oxide (Fig. 3.6 b) shows a nano-crystalline microstructure. A further advantage is that the oxide thickness does not depend on the orientation of the underlying W grain as is the case for thermally grown oxide films [52]. This is because the

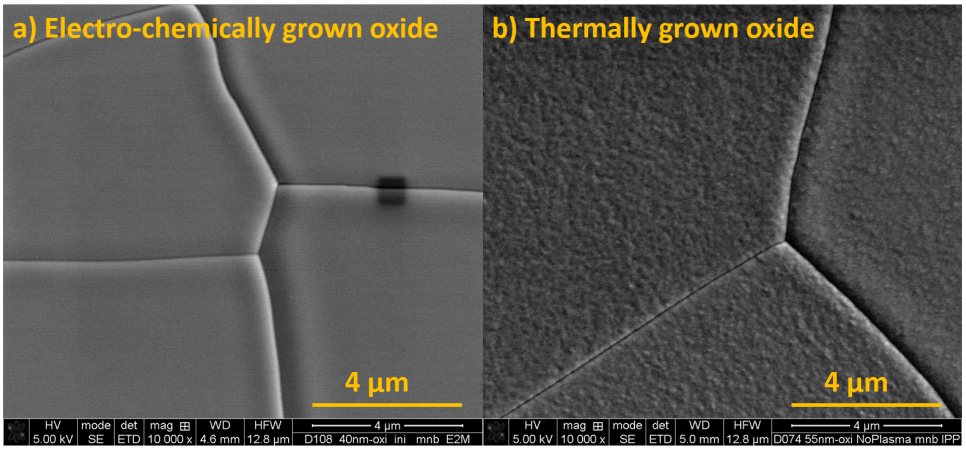

Figure 3.6 – W oxide films by top-view SEM images in secondary electron mode: a) electro-chemical grown oxide (40 nm). Parts of five W grains and their grain boundaries are visible underneath the oxide film. The black square is an artifact. b) thermally grown oxide (55 nm) prepared at 600 K at atmospheric pressure in a dry mixture of 80 % argon and 20 % oxygen. Parts of threes W grains are visible and the oxide shows a nano-crystalline microstructure.

oxide film thickness is determined by the applied voltage and not by different growth rates on different crystal orientations.

It should, however, be noted that the electro-chemically grown W oxide has an amorphous structure (as observed by Raman and infrared spectroscopy [55, 56]) and thus differs from the nano-crystalline thermally grown W oxide. A more detailed characterization of the electro-chemically grown oxides with these techniques is presently under way and will be the content of an upcoming publication.

The oxygen areal density of the electro-chemically grown oxide film was determined ex-situ by NRA after each experimental step. This method is applicable, before and after TDS and is described in detail in section 3.6.1. The results of these measurements are presented in the results section in chapter 5.

In addition, laser ellipsometry was applied to the electro-chemically grown films and their results match with stoichiometric WO_3 for all film thicknesses. Finally, the oxygen areal density and stoichiometry of the oxide film was determined by RBS, which is described in detail in section 3.6.2. The RBS results for the electro-chemically grown oxide also match with stoichiometric WO_3. However, oxide films with an thickness of 15 nm or below cannot be reliably quantified by this method. Furthermore, after D release during TDS, the roughness of the oxide film increases strongly, so that a quantification of the oxygen depth profile with RBS is no longer possible. Therefore, RBS oxygen depth profiles of the electro-chemically grown oxide films are only available for the thicker oxide films (25, 50 and 100 nm) prior to D release.

3.6 Ion beam analysis

Ion beam analysis (IBA) describes a wealth of different methods that use beams of highly energetic ions to probe different material properties with minimal invasiveness. Here especially Nuclear Reaction Analysis (NRA) and Rutherford Backscattering Spectroscopy (RBS) are employed as they are capable of determining not only areal densities but also depth-resolved concentration profiles of deuterium and oxygen in the surface near region of the samples. The

limitation of IBA to the surface near region (several μm) is due to energy loss of the ion beam in the sample. However, the interesting regions of the W samples in this work are the oxide film (< 100 nm) and the self-damaged zone (2.3 μm). Thus, IBA techniques are ideally suited for the present study and are the main source of information on D uptake/release and also on oxygen concentration. All IBA measurements were carried out ex-situ, meaning that the samples have been carried through ambient air in-between the experimental steps (oxidation, plasma exposure, TDS) and the ion beam analysis.

3.6.1 Nuclear reaction analysis

NRA can be used to determine the areal density of D and O in the surface near region (7.4 μm in the present case) of the W samples by detecting highly energetic particles that are created in nuclear reactions with specific target atoms. Quantitative information on the abundance of these target atoms can be acquired when the cross section of the reaction and solid angle of the detector setup are known. D is detected via the D(^{3}He, p)α nuclear reaction[3] and oxygen via ^{16}O(^{3}He, p_0)^{18}F. Conveniently, both reactions occur during irradiation with a ^{3}He beam at 4 MeV and thus the D and O areal density can be measured simultaneously. In addition, for D also depth-resolved concentrations profiles can be measured with NRA by varying the energy of the incident ^{3}He beam. For oxygen this is not possible due to the broader form of the energy-dependent cross section of this reaction. Both D and oxygen measurements with NRA are described in more detail in the following two paragraphs. In the last paragraph in this section the uncertainty quantification of NRA is discussed.

D areal density and depth profiles: By varying the energy of the incident ^{3}He beam it is possible to obtain a depth-resolved concentration profile of D atoms in the sample – the so-called "D depth profile". A detailed description of this technique can be found in [57]. It exploits that the cross section of the D(^{3}He, p)α reaction has a sharp peak at 690 keV and is significantly lower at higher energies. For incident ^{3}He particles with 690 keV, the nuclear reaction takes place very near the surface and thus probes predominantly small depths. For higher beam energies the cross section at the surface is significantly lower but peaks at a certain depth in the sample, when the incident particles have lost sufficient energy in the material. This principle is illustrated in Fig. 3.7 for incident energies of 500 to 6000 keV. In the present studies 10 different energies were used (500, 690. 800, 1000, 1200, 1800, 2400, 3200, 4000, 4500 keV).

The protons resulting from the nuclear reaction were detected by a Si(Li) annular detector with a solid angle of 19.5±0.5 msr (Millisteradian). The detector circularly encloses the ion beam at a laboratory scattering angle of 175°. This allows for a depth resolution at the surface of 54 nm for pure W or 80 nm in WO_3. Note that the depth resolution of NRA measurements depends on the stopping power of the material on the incident particles. Due to the lower W density, the stopping power and thus the depth resolution in the WO_3 film is lower than in pure W. All depth resolutions were calculated with the program "ResolNRA" [58] using SRIM stopping powers [43].

For ^{3}He energies below 1200 keV the α particles from the D(^{3}He, p)α nuclear reaction can contribute information about the D concentration in the near surface region. The α particles were measured with a passivated implanted planar silicon (PIPS) detector with a solid angle of

[3] In this notation the two particles inside the brackets mark the incoming particle (in this case ^{3}He) and the measured particle (in this case the proton p). The particle before the brackets denotes the quantity to be measured and the particle behind the brackets is a byproduct that is not analyzed in this context

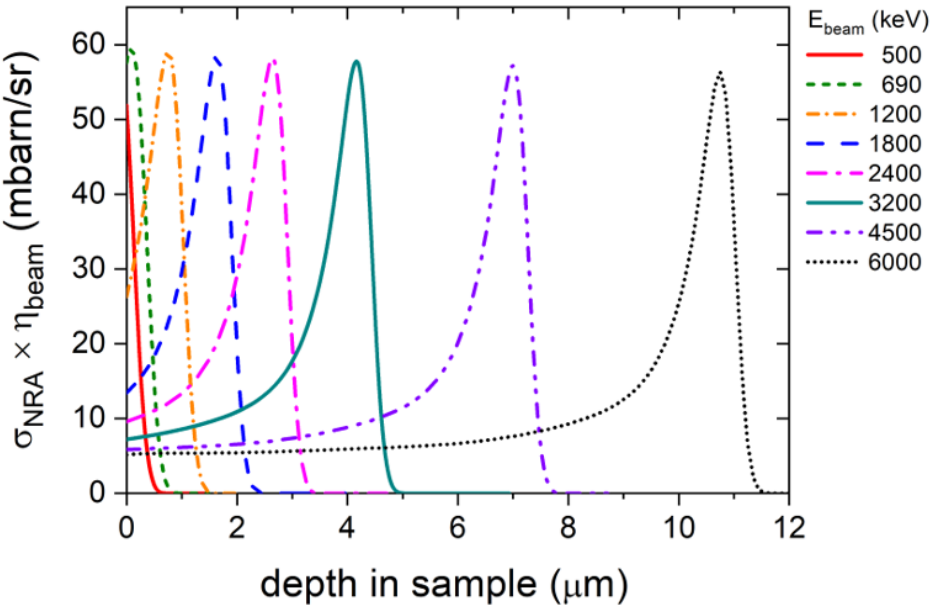

Figure 3.7 – Schematic of the effective, differential cross section of the D(^{3}He, p)α reaction in W depending on the energy of the incident ^{3}He ions and the depth in the W sample (i.e., on the remaining energy of the ^{3}He ions in a certain depth after attenuation by the material). The cross section data for the reaction was convoluted with stopping simulations for different incident He energies and includes range straggling. Taken with kind permission from Armin Manhard (IPP).

7.65±0.26 msr at a laboratory scattering angle of 102°. As the stopping power of α particles in W or WO_3 is higher than that of protons, they provide a better depth resolution of 27.5 nm (pure W) or 50 nm (WO_3). The drawback of this method is that it yields information on the D content only to a depth of approximately 0.3 µm. Thus, the information from the α particles is combined with the information from the protons to enhance the depth resolution of the D depth profile near the surface. This is a pivotal point as it allows to separate D content in the oxide film from D content in the underlying (self-damaged) W, when the oxide film is thicker than 50 nm.

However, the D depth profiles cannot be directly drawn from the NRA spectra, as the (depth-dependent) cross section of ^{3}He ions with different initial energy overlaps at certain depths (see Fig. 3.7). Therefore, the measured signal intensity at a given incident beam energy does not only depend on the D concentration at one given depth but also (to a minor degree) on the D concentration at smaller depths. To obtain a D depth profile it is thus necessary to perform a deconvolution of the measured NRA spectra and the depth-dependent cross sections. This is possible with the program "NRADC" [59] which uses the proton and α spectra at all measured energies as input to construct the most likely distribution of D across the sample depth. A detailed description can be found in [59].

Please note that in the following, when D areal densities are stated, these values are always obtained from integrating over D depth profiles. It is also possible to obtain the D areal density from a single measurement at high incident ion energy (similar to the approach for the oxygen areal density discussed in the next paragraph), but the depth profiles contain multiple measurements at different energies and thus have a lower statistical uncertainty.

Oxygen areal density: The $^{16}O(^3He, p_0)^{18}F$ nuclear reaction allows to directly measure and quantify the areal density of oxygen in the surface oxide film. The cross section of this reaction was recently measured [60] and has an absolute accuracy of 4.7 % at an ^{3}He ion energy of 4000 keV. This energy was used for all NRA oxygen measurements here, since the cross section of the reaction is flat in this energy range. Therefore, uncertainties in the incident ion beam energy cause only a small change of the cross section. The energy loss of the ^{3}He ions due to stopping in the oxide is small and can be neglected. The maximum probing depth in the WO_3/W material is in the range of several µm, i.e., much larger than the oxide film thickness. Thus, the areal density of oxygen in the oxide film is reliably measured by this method for all samples in this study.

On the other hand, this high penetration depth is associated with a low depth resolution at the surface. Therefore, this method cannot yield a depth-resolved concentration profile of the oxygen in the oxide film. From the areal density of O atoms the corresponding thickness of the oxide film in nm can be derived via the density of the oxide, which is assumed to be stoichiometric WO_3 (see section 3.5). The literature values for the density of WO_3 vary between 6.87 [61] and 7.3 g/cm^3 [34]. Here we assume a density of 7.16 /cm^3 according to [62].

The protons from the nuclear reaction with oxygen are measured with a Si(Li) detector with a solid angle of 78.7±0.5 msr at a scattering angle of 135°. To determine the areal density of oxygen in the sample, the background-subtracted integral of the proton peak is taken, and compared with SIMNRA [63, 64] simulations.

Uncertainty quantification: In order to assure that the conclusions drawn from NRA deuterium depth profiles are backed by the data, a thorough understanding and quantification of the uncertainty of the method is necessary. There are two classes of uncertainty involved: The first one is the systematic uncertainty that is given by the uncertainty of the cross sections of the reaction D(^{3}He,p)α measured by [65] and the reaction D(^{3}He,α)p measured by [66]. Both cross sections have a total uncertainty of $< \pm 5$ %. This systematic uncertainty applies only to the absolute amount (or concentration) of D that is measured but does not affect the comparison of different D depth profiles with each other. Also, the relative comparison of D concentrations at different depths in the sample is not affected by this uncertainty. Therefore, it is not shown in the graphs depicting D depth profiles in this work and is also not used when D amounts are compared relative to each other. It is, however, included when absolute values of the D areal densities are stated in text or tables.

The second kind of uncertainty is the statistical uncertainty that affects the relative comparability and reproducibility of different D depth profiles and also of D concentrations at different depths in the same depth profile. This statistical uncertainty comprises the uncertainty of the ion dose measurement which is determined via the beam current and the uncertainty of the deconvolution via NRADC which includes the counting statistics of the spectrum. The beam current measurement is influenced by the secondary electron emission coefficient of the sample surface and its uncertainty is estimated to lie below 3 %. The uncertainty of the deconvolution is determined via Markov-Chain Monte Carlo post processing as described in [67] and gives an asymmetric 1-σ confidence interval of the D concentration around the median concentration for each sub-layer of the target. The resulting total statistical uncertainty of the total D amount is calculated with Gaussian error propagation and stated for all D concentrations given in text or tables in this work that describe relative comparison of D areal densities.

However, due to the convolution of the D concentration and the depth-dependent cross section at different energies, the uncertainties in the ion dose measurement (for each incident beam

energy) do not directly translate to the uncertainty of the D concentrations or the depth sampling in the final depth profiles. Thus, they are not included in the graphical representation of the D depth profiles in this thesis and only the uncertainty of the deconvolution process is shown. An incorporation of the uncertainty of the ion dose measurement into the NRADC post processing is currently envisaged, but not yet implemented.

Lastly it should be mentioned that NRADC assumes a perfect energy calibration of the measured data, as a quantification of the resulting uncertainties for the D depth profile is not possible within practical boundaries with the current version of NRADC. It can, however, be assumed that the contribution of this uncertainty is small, since a) the energy uncertainty of the accelerator is small (< 15 keV) and b) a significant mismatch of the energy calibration for a certain energy is obvious in the raw data and can be manually corrected by adjusting the energy offset of individual spectra.

3.6.2 Rutherford backscattering spectroscopy

Rutherford backscattering spectroscopy (RBS) uses an incident beam of light ions (e.g. He) to gain information on the elemental composition of a target by analyzing the energy spectrum of backscattered particles. In contrast to NRA, no nuclear reaction is involved and the backscattering process is purely determined by the coulomb potential. The energy of the backscattered particle depends on the scattering angle, the energy of the incident particle directly before the collision and on the masses of the target atom and the incident particle. RBS is thus well suited to detect different elemental compositions in a target and provides another independent method to quantify the areal density of oxygen in the sample. Furthermore, the energy of backscattered particles decreases due to energy loss in the material, when the scattering process takes place deeper in the sample. Thus, RBS can yield depth-resolved information on elemental composition. Consequently, the strength of this method in the current context is its ability to determine the oxygen depth profile of the surface oxide film, i.e., the oxygen concentration at different depths within the oxide film.

Note, however, that RBS is best suited to detect heavy ions in a light matrix and it is thus not straight forward to detect (light) oxygen on a (heavy) W substrate. Incident ions that are scattered from (light) oxygen have far less energy than He ions scattered from (heavy) W atoms. As, additionally, the RBS cross section is proportional to Z^2, the oxygen signal is much lower than the W signal. Consequently, the low intensity O signal at low energy is superimposed by a huge W background and cannot be reliably quantified.

However, the information of the oxygen depth profile appears indirectly in the RBS spectrum as a "lack of W signal intensity" at high recoil energies. This is illustrated in Fig. 3.8, where the RBS spectrum (^{4}He ions at 800 keV) of a 55 nm thick oxide film on W (red) is compared with the spectrum of a W reference sample with only natural oxide (blue). The RBS spectrum of the bulk W of the reference sample exhibits a single step at about 730 keV followed by a continuum towards lower energies. This is the typical picture for a bulk sample of a single element. In this case, the energy scale can be interpreted as a depth scale, where lower backscattering energies correspond to larger distances from the sample surface. The RBS spectrum of the thick oxidized sample, on the other hand, exhibits two steps; a first step of lower intensity ranging from 730 to about 600 keV that marks the oxide film and a second one at about 575 keV that marks the transition to metallic W. From the width of the "first step", one can deduce the W and O areal densities and thus (indirectly) the areal density of the oxide film. In addition, one can infer the oxygen concentration at a certain depth, from the height difference of the two spectra at the corresponding energy.

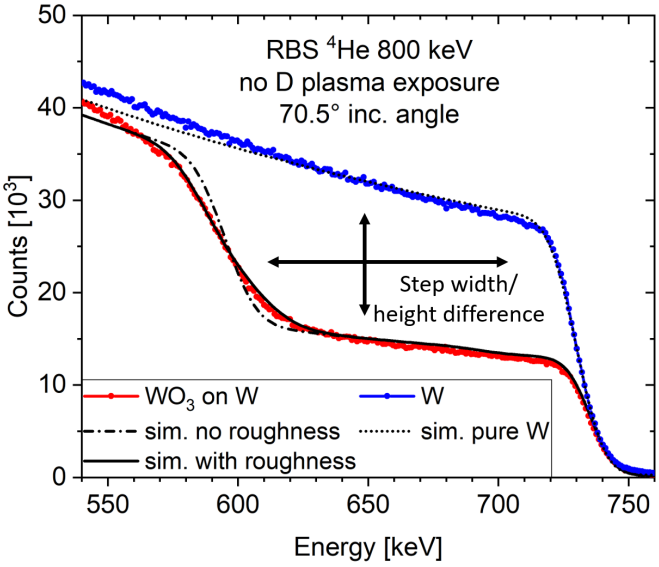

Figure 3.8 – Measured RBS spectra of W with natural oxide (blue) and with a 55 nm thick oxide film (red) together with SIMNRA simulations of pure W (dotted black line) and WO_3 on W with and without roughness (solid and dashed black line, respectively).

It is worth mentioning that backscattering of incident He atoms from O atoms is not the main reason for the reduced W intensity within the oxide. The dominant cause for the lower intensity in the surface oxide (above about 600 keV in Fig. 3.8) is the additional electronic stopping from the O atoms. This additional, statistical energy loss in between W atoms "stretches" the number of recoiled He atoms over a wider energy region. Thus, the number of detected recoils per energy interval is decreased within the oxide film. An instructive example of this phenomenon can be found in the appendix A.1.

Please note that the absolute height (counts per energy interval) of the spectrum does not only depend on the composition of the sample at this depth but also on the composition closer to the surface (where the ions have to go through to be detected). Thus, absolute heights of different spectra are not directly comparable and a simulation with, e.g., SIMNRA [63, 64] is necessary for quantitative interpretation of the sample composition. It is also important to note that the corresponding concentration of O atoms at a given depth can only be deduced in this way when assuming that there are no other impurities present in the material. This assumption is valid here, as only negligible amounts of other light elements (e.g., carbon < 1 at.%) have been found on the sample with NRA, XPS and energy dispersive X-ray (EDX) measurements.

All RBS spectra were measured by a PIPS detector with a solid angle of 1.108 ± 0.038 msr at a scattering angle of 165° in Cornell geometry. To obtain the RBS spectrum in Fig. 3.8, the sample was rotated such that the surface normal forms an angle of 70.5° with the incident ion beam. This prolongs the geometric path of the ions through the oxide film and thus enhances the depth resolution of the RBS measurement by a factor of three. The depth resolution in the oxide film in this configuration was calculated with RESOLNRA [58] and is 43×10^{19} atoms/m^2 at the surface and 53×10^{19} atoms/m^2 at the deepest part (55 nm) of the thick oxide film. For the evaluation of the RBS spectra an average depth resolution of $\leq 50 \times 10^{19}$ atoms/m^2 (corresponding to 7 nm of WO_3) was applied for the oxide film.

The modeling of the depth-resolved oxygen concentration in the sample is realized by the fitting program "MultiSIMNRA" [68]. It uses multiple instances of SIMNRA (version 7.02) [63, 64] to simulate RBS spectra at different energies and varies the target elemental composition to give

the best fit to the experimental data. In MultiSIMNRA the oxide film is divided into several sub-layers with constant composition. The layer thickness is set equal to the depth resolution of the RBS measurement (50×10^{19} atoms/m^2 corresponding to 7 nm of WO_3). The concentration of O and W atoms in these sub-layers is then varied to optimize the fit to the experimental spectrum. As an example, the simulation results for a pure W sample as well as for WO_3 (55 nm) are shown in Fig. 3.8 and it is evident that they agree very well with the experimental data.

It is important to note that the size of the analyzing beam spot of 1 mm^2 is larger than the typical W grain size of 10–50 µm. For the thermally grown oxide films, the beam hence averages over many W grains with different oxide thicknesses. In SIMNRA such variation in film thickness can be described by defining a sub-layer of constant composition with a so-called "layer roughness". The influence of this thickness variation is also shown in Fig. 3.8 in which two cases are compared: A smooth oxide film (no roughness) with one where the known oxide thickness distribution [53] is taken into account. It is clear that the model with roughness provides a far better fit to the experimental data. It is obvious that the thickness variation affects only the left part of the low intensity step in the RBS spectra, i.e., the deepest part of the oxide films. As can be seen in Fig. 3.8, the high energy (and hence surface near) part of the spectrum is unaffected. This holds true as long as the backscattered ^{4}He does not stem from collisions with the underlying metallic substrate. Once this happens a gradual transition from the oxide film to the underlying W substrate leads to a smearing out of the step in the RBS spectrum in this energy region. In general, the same effect would be observed if an oxygen concentration gradient in the film would be present. However, the assumption of a gradient is not necessary as the know roughness distribution describes the measured spectrum very well. Consequently, the W-grain-dependent thickness variation of the oxide film can be fully accounted for in the RBS spectra and does not affect the quality of the obtained oxygen depth profiles.

For the study on D uptake (chapter 4) RBS measurements were performed for all samples before and after plasma exposure and the corresponding oxygen areal densities and depth profiles were determined. For the D release experiments (chapter 5) RBS measurements were only conducted prior to the D release, as the partial reduction and strong lateral inhomogeneity of the oxide after the release prohibited accurate oxygen depth profiles afterwards.

3.7 Scanning electron microscopy

Scanning electron microscopy (SEM) uses a focused electron beam with electron energies of several keV to probe the sample surface. The much higher energy and consequently smaller wavelength of the electrons allows a significantly higher resolution (in the range of a few nm) compared with the photons used for optical microscopy. To acquire a two-dimensional picture of the sample surface, the beamspot is scanned across the surface. Information on the sample is gained from (primary or secondary) particles that are emitted from the surface and detected by the SEM. The detected signal intensity from a certain beamspot (area on the sample) is then encoded by the brightness of the corresponding pixel in the SEM image. Those particles can be a) backscattered primary electrons (BSE) that recoil from collisions with atomic nuclei in the sample; b) secondary electrons (SE) that are knocked on by the primary (beam) electrons and c) X-ray photons that are created by an outer-shell electron falling to a position in an inner shell after an inner-shell electron is knocked out by a primary electron from the beam. The spatial (and especially depth-) resolution of these particles depends on the interaction volume in the sample from which they can escape to the surface and reach the detector, as is illustrated in Fig. 3.9 from [69].

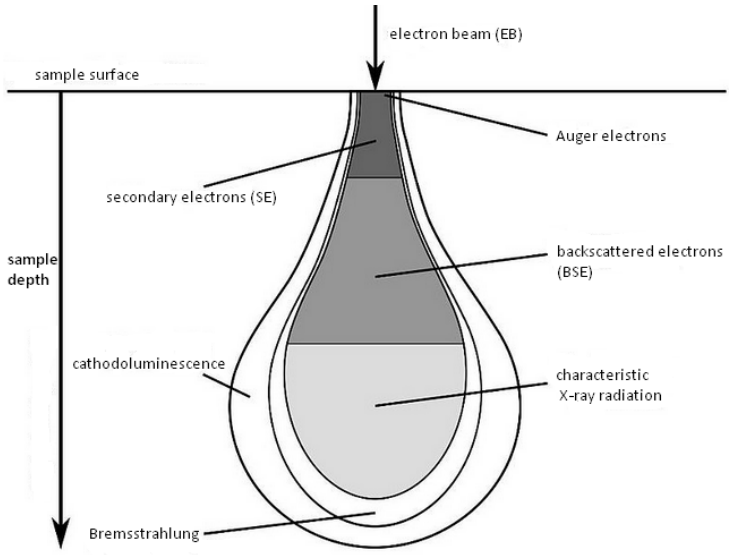

Figure 3.9 – Schematic representation of the electron interaction volume and the volume fractions from which particles (SE, BSE or X-rays) can escape the sample to be detected. [69]

The intensity of backscattered electrons depends on the atomic number (Z) of the elements in the sample. BSE images thus show a strong material-dependent contrast (also called Z contrast). Furthermore, the crystal orientation of the material plays a role, as primary electrons can be "channeled" deeper into the sample when they enter parallel to a crystal plane. As a consequence, the electrons are backscattered in larger depth and are less likely to escape the sample towards the detector. Thus, BSE images give also a crystal orientation contrast that shows, e.g., differently oriented grains in a metal in different gray scale values. The depth from which BSEs can leave the sample and be detected is about half of the maximum penetration depth of the primary electrons, as the BSE need sufficient energy to escape the sample after the backscattering event.

The secondary electrons in general have a rather low energy and thus have to be created very close to the surface in order to be detected. Consequently, small protrusion or sharp edges light up in SE mode, because the average path length to the next surface is smaller in these cases and more SEs can escape the sample. Thus, images in SE mode have an excellent surface sensibility and highlight small structures on the surface.

Lastly the X-ray photons contain direct information on the elemental composition of the sample. The energy differences between the outer and inner shells depend on the atom and the photon energies are thus characteristic for certain elements. The X-ray detectors are energy sensitive and the corresponding measurement technique is called energy dispersive X-ray spectroscopy (EDX). The drawback of this method is that X-rays can escape the sample from larger depths due the lower stopping they experience in material compared with electrons. Thus, the interaction volume from which an X-ray can stem is relatively large and the areal and depth resolution of the EDX image is lower than for BSE and much lower than for SE images.

In addition to the (non-destructive) imaging of the sample surface with an electron beam, the used SEM (FEI HELIOS NanoLab 600) is also equipped with an Focused Ion Beam (FIB). The ion beam can be used to prepare cross sections through the sample surface. The FIB source is tilted by 52° with respect to the electron beam. In order to prepare a cross section, first a coating is applied on the desired area of the sample by electron- or ion beam deposition (via cracking of a coating gas). The coating protects the surface edge of the cross section from rounding and is thus necessary for clean cuts through the surface near region. It is visible on top of the sample

surface in all FIB cross section images shown in this work. It should be mentioned already here that depending on the exact parameters of the ion beam and the coating, the FIB cuts sometimes create vertically aligned linear artifacts in the image that look like pearl strings (compare e.g. Fig. 4.1 a)). These artifacts also extend below the coating into the oxide film and metallic W underneath but are not a specific feature of the material.

After the coating, the sample is tilted to be perpendicular to the ion beam, which is then used to cut the sample. As ion beam cuts have typical dimension of µm in width and depth, the sample is not fully cut through but a slope is dug with the ion beam in front of the cut to allow imaging of the cross section. As the surface normal of the sample is tilted by 52° to align with the FIB, the cross section is tilted by 38° relative to the electron beam. Therefore, the vertical scale in the shown SEM image is compressed by a factor $\cos(38°) = 0.79$. This is the case for all FIB cross section images shown in this work.

Together with the SEM imaging, FIB cutting provides an excellent tool to study the thickness and also the structure of thin oxide films on W, as the high resolution of this method allows to resolve even the very thin (5 to 100 nm) oxide films that are studied in this work.

3.8 Ellipsometry

Ellipsometry is a non-invasive analysis technique from surface science for the characterization of systems of thin, transparent films on a reflective substrate. It measures the polarization change of light that is reflected from the sample to determine the complex refractive index and the optical film thicknesses. A detailed description of this analysis technique is given, e.g., in [70] and here only the fundamental principle is outlined.

The incident, (typically linearly) polarized light is reflected from the film surface or the interfaces of the transparent film(s) and the sample substrate. Due to back-reflection at the film surface, the beam can cross a transparent film multiple times, which leads to phase shifts and self-interference of the reflected light. With respect to the plane of incidence (spanned by the incident and reflected beam) the light can be polarized either parallel (p) or perpendicular (s). These two components are subject to different levels of attenuation and phase shifts in the material, which typically leads to an elliptical polarization of the reflected light. The polarization change is measured via an analyzer that is comprised of a rotating polarization filter and an light intensity sensitive diode. This yields the complex reflectance ratio of the material, which is expressed as an amplitude Ψ and a phase shift Δ between p and s polarized light. From the change of the p and s components of the polarization, one can infer the optical properties (refraction index n and extinction coefficient k) and the thickness d of the thin film(s). Since only two quantities are measured (Ψ and Δ), at least on of the film properties (n, k or d) has to be known to fully determine the system. Alternatively, several measurements of a system, between which only one property changes (e.g. film thickness), can be used to determine all three properties. It is also possible to analyze systems with multiple layers of transparent films by ellipsometry, but this of course increases the number of free parameters and additional information has to be inserted or gained by additional measurements to correctly model the results.

As only the relative intensity shifts are measured, ellipsometry does not need calibration via a reference beam and is quite stable against intensity fluctuations of the light source. In contrast to other optical measurement techniques, which are limited to a resolution comparable to the wavelength of the used light, ellipsometry also uses phase information of the light waves and can thus be used to measure film thicknesses that are much smaller than the wavelength of the

light. The measurement range of ellipsometry goes from a few angstrom to several µm and is thus ideally suited for the thin transparent oxide films on W studied in this work. Here, a Jobin Yvon PZ 2000 laser ellipsometer operating at a wavelength of 632.8 nm is used. The laser has a spot size of 10 µm×50 µm which is in the range of the typical grain size of recrystallized W. Thus, most data points are averages over several W grains which can have different oxide film thicknesses for the thermally grown oxide.

The measured data points are typically depicted in a Ψ-Δ graph. To interpret the data, an optical model of the layer system on the sample is needed. Besides the film thickness this model requires knowledge of the optical constants (n, k) of the layers. These optical constants are known for W and WO_3 but not for non-stoichiometric W oxides [71].

3.9 Thermal desorption spectroscopy

Thermal desorption spectroscopy (TDS) is an analysis method for the release behavior of atoms/molecules from solids at elevated temperatures. It can provide information about binding energies of atoms/molecules in the material, the number of desorbed particles and their desorption mechanisms. Here, it is applied solely to samples of the D *release* study (chapter 5). In the present case, D is trapped predominantly in material defects in the self-damaged W layer underneath the oxide film. The D is released from the defects once the sample temperature is sufficiently high for thermal de-trapping. In previous experiments with only thin natural oxide films, a double peak structure of the D release was observed [6]. Example for such TDS spectra of not-oxidized, self-damaged W reference samples will be discussed later and can be seen e.g. in Figs. 5.3, 5.4 and 5.6 in chapter 5. Details on the determination of binding energies of D traps in W from TDS spectra can be found elsewhere [13–15]. In this work, the focus lies on how the oxide film affects the release behavior, i.e., if the temperature of the D release peaks and the composition of released D-containing species are altered.

The ultra-high vacuum (UHV) device TESS (Thermal Effusion Spectroscopy Setup) was used for TDS. A detailed description of the setup is given in [72, 73]. The samples are loaded into a quartz tube that is connected to the main UHV chamber. Samples inside the tube can be heated by an external tubular furnace (single wire wound Gero SR 40-250/11), which can be moved over the tube. Several samples can be stored in a side arm of the tube far away from the heating area and can be moved to the heating area via a piece of nickel that is manipulated by an external magnet. Thus, batches of several samples can be measured under identical vacuum conditions. Furthermore, this setup has two advantages: a) it allows outgassing of the quartz tube prior to the sample measurement and b) it does not need a sample holder, which could contaminate the measurement by outgassing. The oven temperature is programmed and feedback controlled so that it undergoes a linear temperature ramp. The actual sample temperature is lower than the oven temperature and lags behind it depending on the ramping speed and the emissivity of the sample surface. Therefore, the temperature at the sample is measured separately via a shielded thermocouple touching the sample surface. The TDS measurements were all performed with a slow temperature ramp of 3 K/min from room temperature up to 1000 K (except for a single experiment with only 500 K, described in section 5.4). This slow ramp together with the inside thermocouple assures an excellent reproducibility of the sample temperature. Near the onset of the temperature ramp (T < 500 K), the reproducibility of the sample temperature is better than 10 K. For temperatures above 600 K, which are most relevant for D release, the variation is even smaller and lies well below 5 K. In all TDS spectra in this work, the temperature reading of this shielded thermocouple and not the oven temperature is shown.

The desorbed gases were measured with a Pfeiffer/Inficon DMM 422 quadrupole mass spectrometer (QMS) whose detector was operated in single-ion-counting mode. This allows applying Poisson statistics and assures negligible background noise. The following 15 mass channels were recorded with the so-called multiple ion detection mode: m/z = 1, 2, 3, 4, 12, 14, 16, 17, 18, 19, 20, 28, 32, 40 and 44. Residual backgrounds were measured before as well as after the temperature ramp and, in addition, also for ramps without a sample in the hot zone (as reference). Background subtraction and absolute calibration was conducted for mass channels 3, 4, 19 and 20 to derive absolute fluxes of D_2, HD, HDO and D_2O. The calibration procedure for HD and D_2 follows the description in [6]. The calibration of heavy water species will be discussed in detail in a separate upcoming publication [74] as a full description is beyond of the scope of this work. Here only a short outline of the principle shall be given: The calibration utilizes the fact that the absolute amount of D in the oxidized samples was additionally measured with NRA before and after TDS (see section 5.2). The absolute amount of D released in form of HD and D_2 is determined from TDS. The difference yields the absolute amount of D released in form of HDO and D_2O, which can be related to the measured counts in mass channels 19 and 20.

The TDS measurements were performed in two different campaigns for the three batches of samples that are discussed in section 3.5.2. The reference sample and the samples with 25, 50 and 100 nm thick oxides were in batch one. The samples with 5, 10 and 15 nm thick oxides were in batch two. The final batch contained only samples without D; two electro-chemically grown oxides with thicknesses of 20 and 40 nm and a thermally grown oxide with a thickness of 33 nm. They were exposed to a TDS ramp to 1000 K to analyze the purely thermal changes of the oxide film without the presence of D (see section 5.1).

Chapter 4

D uptake through thin tungsten oxide films

This chapter describes the effects that thin (33 to 55 nm), thermally grown surface oxide films have on the D uptake from a plasma into metallic W. It also discusses the partial reduction of the oxide films during D plasma exposure and the consequences this has for D uptake. The chapter is structured on the basis of several experimental campaigns with different plasma exposure conditions. Sections 4.1 and 4.2 are based on the first campaign with low D energy (< 5 eV/D) and low D fluence. The following sections (4.3 and 4.4) discuss the effects of higher D fluence and higher D energy/temperature, respectively. Along the experimental results a model of the W oxide/metallic W-system is developed and successively refined. At the end of the chapter the results are summarized and the consequences for laboratory experiments with a natural oxide film are outlined.

The results shown in 4.1 and 4.2 (except for 4.1.2) are based on a previous publication by the author and others [75].

4.1 Oxide film reduction by gentle plasma exposure - formation of a W-enrichment zone

In this and the next section (4.2) three different W samples were used: A sample with a thick oxide (55 nm), one with a thin oxide (33 nm) and a reference sample with only natural oxide (1–2 nm). They were prepared as described in sections 3.2 and 3.3 and then thermally oxidized (section 3.5.1). After this, they were exposed to gentle (5 eV/D) plasma at 370 K with a total fluence of 1.4×10^{24} D/m^2 in the device PlaQ (see section 3.4). They were analyzed with ion beam analysis and SEM imaging before and after plasma exposure.

In this section the results of several independent analysis methods for the oxide film thickness, the oxygen areal density and stoichiometric composition of the oxide are presented. Furthermore, the changes in surface morphology and depth-resolved oxygen concentration in the oxide film after D plasma exposure are discussed.

4.1.1 SEM images of cross sections through the oxide film before and after plasma exposure

The most direct way to visualize the changes of the oxide film after D plasma exposure is SEM imaging of FIB cross sections through the oxide film. Fig. 4.1 a) depicts such a cross

section of the 55 nm thick thermally grown oxide film before D plasma exposure. The oxide film is visible as a band atop the lighter gray of two different W grains and below the darker protective coating that is applied before the FIB cut. The vertical stripes across the picture are an artifact of the ion beam cutting. The oxide film coherently covers the surface of the W grains; it appears to be relatively smooth and shows no porosity. The thickness of the film was directly measured on three different W grains and is on average 53.9±1.5 nm. This agrees well with the oxygen amount measured with NRA and RBS (see section 4.1.3) assuming a nominal bulk density of WO_3 of 19.25 g/cm^3. However, due to the small size of the observation area, this is not necessarily representative for the full, grain-orientation-dependent thickness distribution of the oxide (see section 3.5.1 for details of the oxide thickness distribution). The average thickness of the oxide film on the three W grains measured here varies between 42.3±1.2 nm and 59.2±0.9 nm, which shows the large difference between individual grains.

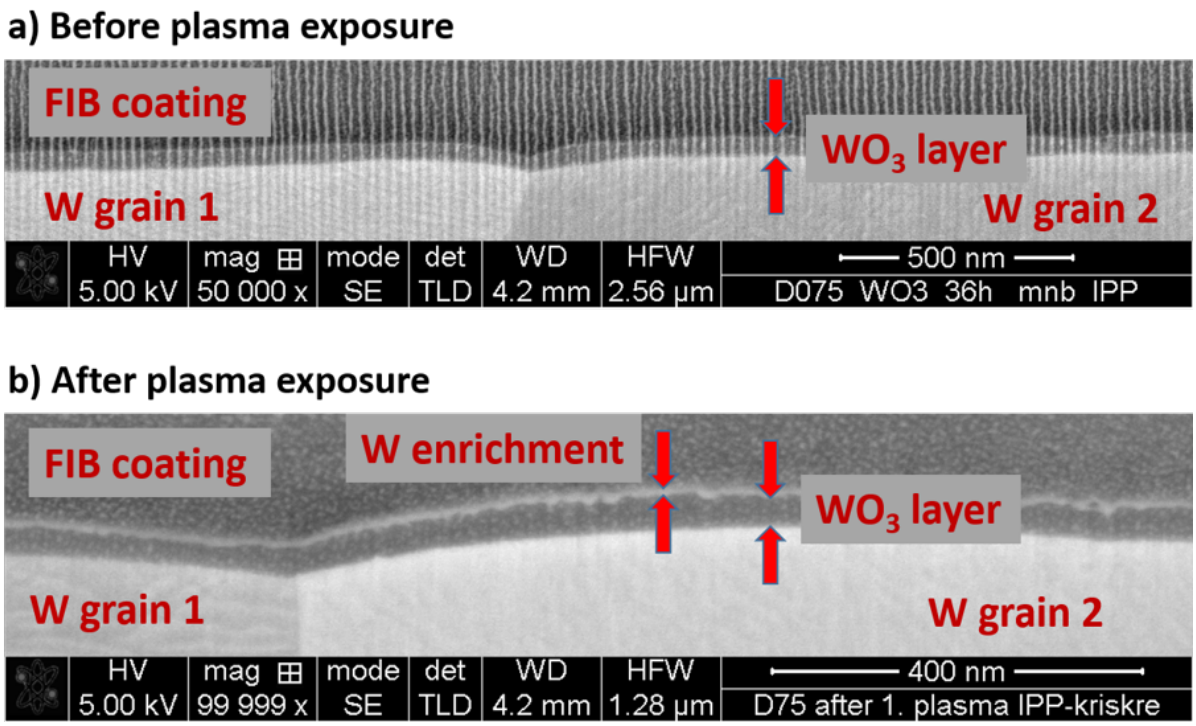

Figure 4.1 – SEM images of FIB cross sections through the originally 55 nm thick oxide film. a) before and b) after exposure to D plasma with <5 eV/D at a sample temperature of 370 K to a total fluence of 1.4×10^{24} D/m^2. Please note that the magnification differs by a factor of two between a) and b). The vertically aligned striped structure in a) is an artifact of the FIB cut through the coating and not a feature of the oxide film or metallic W.

Fig. 4.1 b) shows the oxide film on a different spot on the sample after plasma exposure. Please note the two times higher magnification. A thin, bright layer has formed on the surface of the oxide film, which indicates a material of higher Z number. This indicates that a at least partial reduction of the oxide film took place on the surface of the oxide film during plasma exposure and a thin layer of W-enriched oxide has formed on the topmost part of the film. The W enriched layer has a uniform thickness of 11.9±1.5 nm on the three measured W grains (again only two are shown) and seems to be independent of the original thickness of the oxide film.

4.1.2 Surface modification and crack formation

SEM images: The surface modification of the oxide film is investigated via SEM imaging. Figure 4.2 a) depicts a top-view image of the oxide film before plasma exposure. The film consists of many nano-sized grains (section 3.5.1) and homogeneously covers the surface without any obvious cracks. Fig. 4.2 b) shows a sample with identical oxide after exposure to the gentle (5 eV/D) plasma at 370 K sample temperature and a total D fluence of 1.4×10^{24} D/m^2. It is obvious that the oxide film has undergone strong surface modification and several cracks with lengths of a few hundred nanometer are visible in the image. Please note that due to the much higher contrast introduced by the cracks, the nano-crystalline structure of the oxide is no longer visible on the image after plasma exposure. However, there is no indication that the crystallinity of the oxide changes during plasma exposure. The crack formation cannot be explained by temperature differences between storage (room temperature) and plasma exposure (370 K) conditions, since the sample was oxidized at 600 K and has shown no cracks after cooling down to room temperature. Thus, the crack formation hints at a plasma-induced change in the oxide properties. The most likely explanation is a (partial) reduction of the oxide film surface, which would change the volumetric expansion of the oxide and lead to tensile stress at the surface. As discussed in section 3.5.1, the volumetric difference of W and WO_3 is about a factor of 3.4.

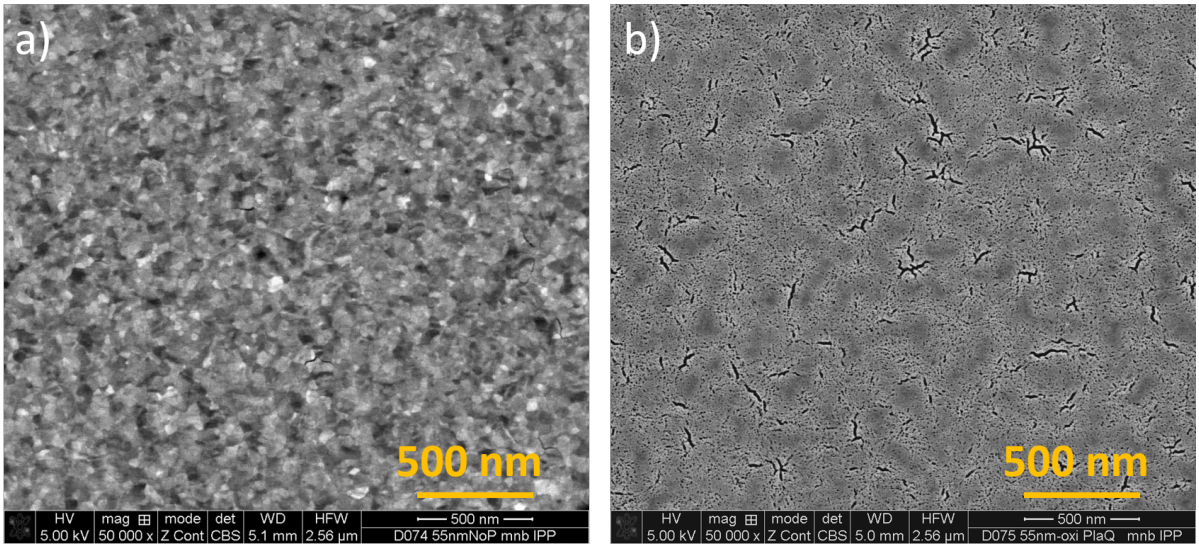

Figure 4.2 – Comparison of SEM top-view images of 55 nm thick thermal oxide. a) before plasma exposure and b) after exposure to gentle (5 eV/D) D plasma at 370 K sample temperature and a total D fluence of 1.4×10^{24} D/m^2

The width of these cracks and their extent into depth was investigated via a FIB cross section through the oxide film. This cross section is shown in Fig. 4.3 and several cracks in the oxide film are visible. Their depth is similar to the depth of the W-enrichment layer indicating that the cracks indeed form due to a change in oxide composition. Furthermore, the W-enrichment layer extends deeper into the oxide film at the position of the cracks which indicates that D ions from the plasma can enter the cracks and penetrate deeper into the oxide in their vicinity. However, under these gentle plasma exposure conditions neither the cracks themselves nor the W-enrichment layer beneath them extends through the full W oxide film so that the metallic W is still fully covered by not-reduced oxide.

Ellipsometry: Figure 4.4 shows ellipsometry measurements of a 55 nm thick thermally grown oxide after plasma exposure. The data is taken from a region of the sample that was partially

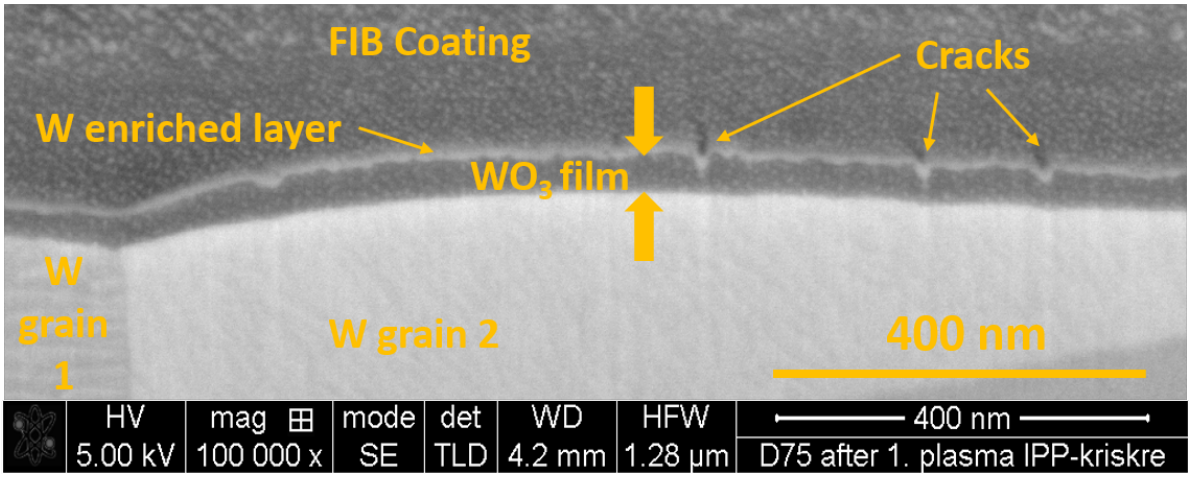

Figure 4.3 – FIB cross section through an originally 55 nm thick thermally grown W oxide film after exposure to a gentle (5 eV/D) D plasma at 370 K sample temperature and a total D fluence of 1.4×10^{24} D/m^2. The cracks that form during plasma exposure are clearly visible but they do not fully penetrate the oxide film.

sheltered from D plasma by a fastening screw. Fig. 4.4 b) shows a x-y map of the sample region and visualizes the sheltered area that is characterized by higher Psi values (green area) compared with the exposed (blue) area. These two areas correlate to the two black data clouds in image a), which shows the Psi-Delta graph (see section 3.8). The right data cloud in image a) (at Ψ values >35) corresponds to the area that was sheltered by the screw head. It coincides well with the predictions of an optical model for WO_3 on W that is shown in red in image a). This model shows the predicted Psi-Delta values for WO_3 from 1 to 55 nm thickness on W and each data point marks a 1 nm step in thickness. Note that the measurement spot size is 10×30 µm and hence comparable to the grain size of the W substrate. Therefore, the data points are spread along the red model curve due to the grain-dependent thickness of the oxide film.

The left data cloud (psi values 22 to 29) corresponds to the exposed sample area. Here the Psi-Delta values of the oxide film cannot be matched by the optical model for pure WO_3 any more. This data cloud can, however, be approximately described by a 42 nm thick WO_3 film with a 3 nm thick layer of metallic W on top, which is depicted as the orange branch of the optical model. This result indicates a change or (partial) reduction of the oxide film on the surface. Unfortunately, it is not possible to simulate a layer of partially reduced W oxide (e.g. WO_2), as no optical model for this case is available. Thus, it cannot be concluded from ellipsometry whether a full reduction of WO_3 to W or a partial reduction of WO_3 to sub-oxides (e.g., WO_2) takes place. Nevertheless, the ellipsometry measurements suggest that oxygen is removed by the plasma, leaving behind a W-enriched zone at the surface and thus confirming the results from the FIB cross sections above.

Chemical surface changes: According to literature, WO_3 can be removed from W by aqueous alkali hydrate solutions [34] and indeed it was found here that the oxide films can be easily removed by dipping into aqueous sodium hydrate solution (1.5 % NaOH). However, after plasma exposure a removal of the films was no longer possible. This shows that the surface of the oxide film undergoes changes during plasma exposure that protect it from chemical removal by NaOH, which agrees with the formation of a W-enrichment zone.

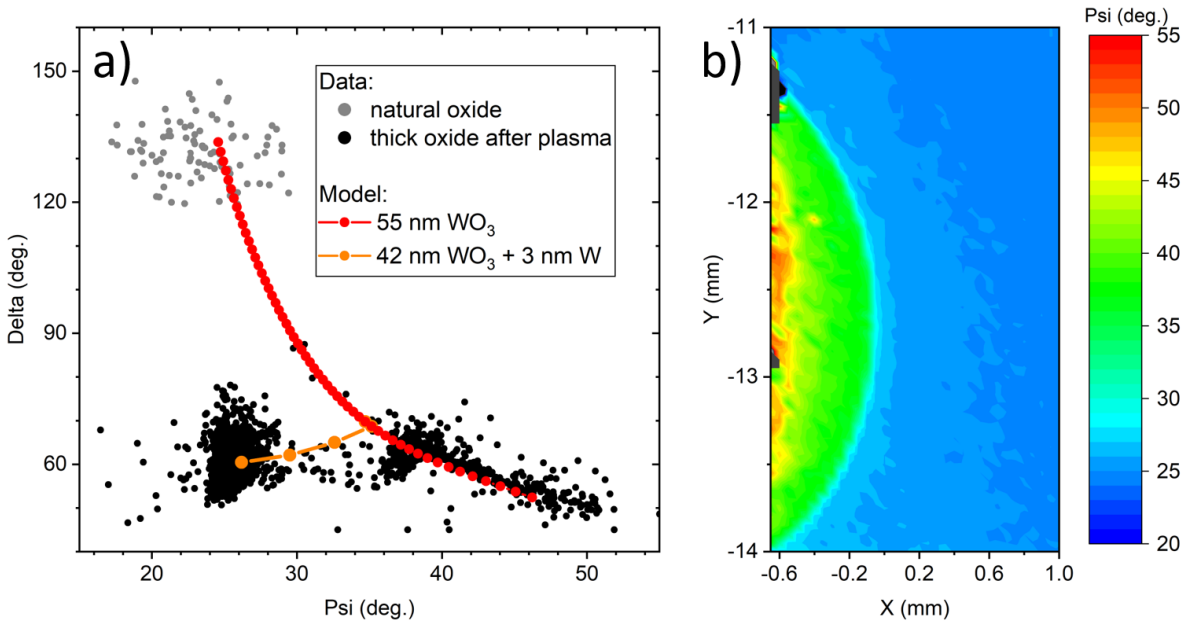

Figure 4.4 – Ellipsometry results: Image a) shows a Psi-Delta plot of an originally 55 nm thick oxide film (black) that was partially covered by a screw during plasma exposure. In addition, also W with only a natural oxide film is shown for reference (gray). An optical model for the expected Psi-Delta graph values of WO_3 for 1–55 nm thickness is shown in red and a modified model that shows 42 nm thick WO_3 with 1–3 nm metallic W on top is shown in orange. Image b) shows Psi values over x-y coordinates of the sample. The area of the oxide film that was covered by the screw is visible on the left and shows higher psi values (green color) compared with the area that was not covered (blue color). Correspondingly, the black data points in image a) show two different aggregation clouds. The one on the right coincides very well with the optical model for WO_3 and corresponds to the sheltered (green) area in image b). The black data cloud on the left in image a) is best described by the optical model of WO_3+metallic W (orange) and corresponds to the exposed (blue) area in image b).

4.1.3 Oxide areal density

The oxygen areal density before and after plasma exposure was determined by ion beam analysis via the nuclear reaction $^{16}O(^3He,p_o)^{18}F$ and backscattered ^4He atoms as described in sections 3.6.1 and 3.6.2. Figure 4.5 shows the result for the thin (initially 33 nm) and thick (initially 55 nm) oxide films derived from measurements with NRA (blue) and RBS (red). For both samples the oxygen areal density before and after plasma exposure is shown, as well as the difference between this two values. The NRA and RBS measurements of the thick oxide were performed on the same sample before and after plasma. The RBS measurements of the thin oxide were performed on two samples with nominal identical oxide thickness (identical samples oxidized for the same time under the same conditions) of which only one was plasma exposed. The numeric values to the data points in Fig. 4.5 are given in the appendix A.2.

From both NRA and RBS measurements, it is evident that a substantial amount of oxygen is lost from the sample during plasma exposure. Both methods agree very well and the amount of lost oxygen is reproduced within the uncertainty of the methods.

The loss of oxygen during plasma exposure is roughly equal (difference $< 10\,\%$) for the two oxidized samples and seems to be independent of the initial oxide thickness. This indicates that the oxygen removal process takes place mostly from the surface of the oxide film and is not a

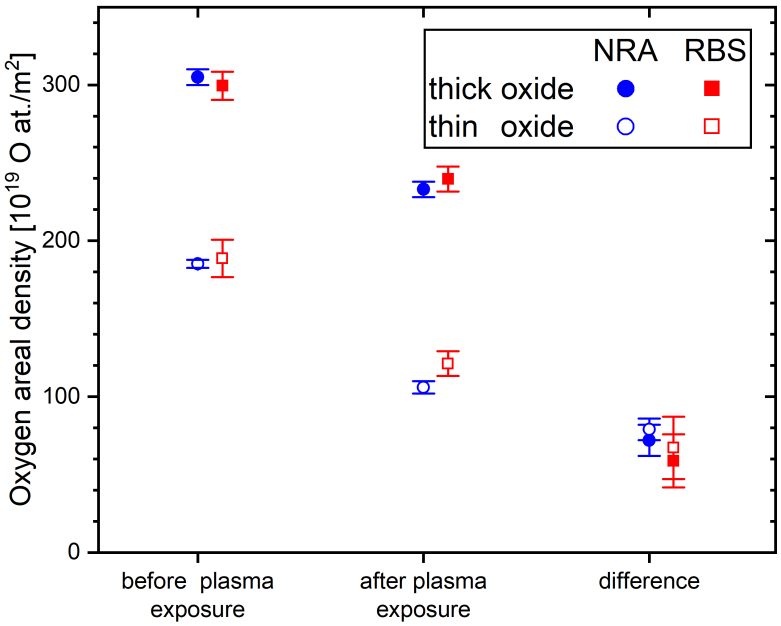

Figure 4.5 – Comparison of oxygen areal density for originally 33 and 55 nm thick oxide films before and after D plasma exposure (5eV/D) at 370 K sample temperature and a fluence of 1.4×10^{24} D/m^2. A remark to the units on the y-axis: 1×10^{19} O atoms/m^2 corresponds roughly to one monolayer of oxygen on the surface.

volume effect. This is noteworthy, since D is highly mobile in WO_3 and can diffuse inside the poly-crystalline oxide film within minutes at room temperature [40, 76].

In addition, D uptake is reported to cause a color change of the oxide [25, 40, 77] (see also section 2.3). Indeed, a rapid color change of the oxide film was observed during the "burn in" phase were only atomic D can reach the sample and within the first minutes of D plasma exposure where charged D reaches the sample. After that, a second slower color change occurred over the course of several hours of plasma exposure. A video analysis of the color change of the thick (55 nm) oxide during the "burn in phase" and plasma exposure can be found in the appendix A.3. The first (fast) color change can be attributed to the intercalation of D atoms into the WO_3 and the formation of tungsten bronze (D_xWO_3), which changes the optical properties of the oxide film. The fast color change has previously been reported, e.g., by Addab et al. [25] for similar conditions and it is also utilized commercially for gas sensors based on tungsten oxides [22, 23]. Note, however, that for these gas sensors a thin catalyzer (Pd or Pt) is used on the surface to dissociate the D_2 molecules into atoms, before they can enter the oxide. Accordingly, no color change was observed during D_2 molecular gas exposure prior to the "burn in" phase. The formation of tungsten bronze, and thus the color change, is expected to be slowly reversible during storage at room temperature [25] and indeed a partial reversal of the color change was observed over several weeks after plasma exposure.

The second, slower color change observed during plasma exposure is, in contrast, attributed to the gradual removal of oxygen from the oxide film in the surface-near region by the plasma. Such a removal of oxygen from tungsten oxide has been previously observed by Hopf et al. [20], although in a hydrogen plasma with much higher H energies of 200 to 400 eV compared with the <5 eV/D gentle D plasma used here. The oxygen loss leads to a change of the optical properties and also a thinning of the oxide film, which permanently changes the interference color of the film. The slow color change, thus, comes in addition to the fast color change induced by the intercalation of D atoms.

The average oxygen loss during the gentle plasma exposure is $76\pm9\times10^{19}$ O atoms/m^2, which corresponds to 13.5 nm of stoichiometric WO_3. With a total applied D fluence of 1.4×10^{24} D/m^2 this yields an oxygen loss rate of $5.4\pm0.7\times10^{-4}$ O atoms per incident D.

The thin natural oxide film has an areal density of $8.4\pm1.2\times10^{19}$ O atoms/m^2 (corresponding to 1.5 nm WO_3) before plasma exposure, according to NRA measurements. Under the assumption that it is removed in the same fashion and with the same speed as the thermally grown oxide films, it would take $1.6\pm0.4\times10^{23}$ D/m^2 to remove the natural oxide film during plasma exposure under the given conditions, i.e., $\approx 10\,\%$ of the fluence applied in this experiment. Therefore, it can be assumed that the natural oxide is fully removed during the early phase of the D plasma exposure.

4.1.4 Depth-resolved oxygen concentrations after plasma exposure

The RBS spectrum of the thick (initially 55 nm) oxide after plasma exposure is shown in Fig. 4.6. The measurement was performed with ^{4}He ions with 800 keV under an incidence angle of 70.5°. The experimental spectrum is shown in red and the simulated spectrum from SIMNRA in blue. A detailed explanation of the interpretation of such RBS spectra is given in section 3.6.2. For comparison with an RBS spectrum of the oxide film *before* plasma exposure, refer to Fig. 3.8. The distinct difference before and after plasma exposure is a peak at about 730 keV. This peak can be described by a higher local W concentration at the surface-near region of the oxide film after plasma exposure. For comparison, the simulated spectrum of a WO_3 sample without W-enrichment at the surface is shown as a gray dashed line in Fig. 4.6. This W-enrichment proofs that the removal of oxygen by the D plasma starts at the surface of the oxide film.

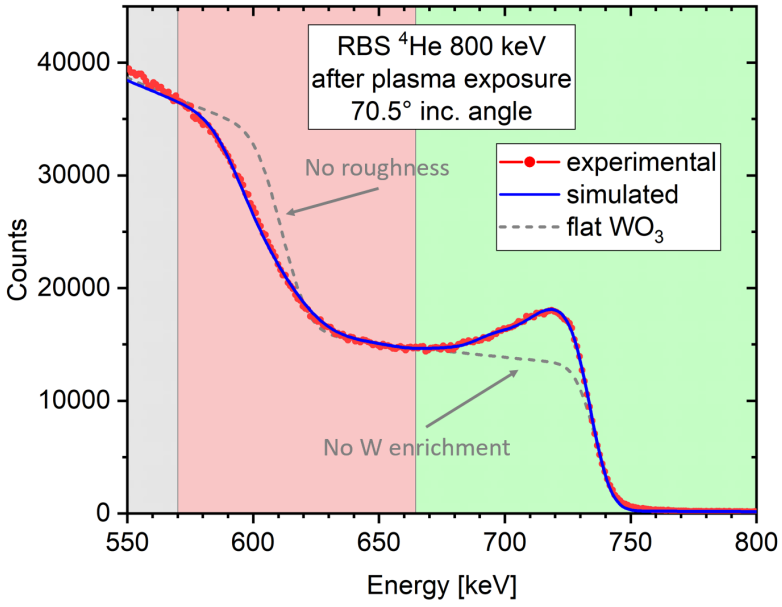

Figure 4.6 – Experimental (red) and simulated (blue) RBS spectrum for the thick oxide film after plasma exposure. The peak at about 730 keV shows the W-enrichment in the surface-near region of the oxide film. The background colors indicate the following parts of the spectrum: green: surface-near region of the oxide where the oxide thickness distribution has no effect on the RBS signal; red: deeper region of the oxide, where the RBS signal is influenced by oxide thickness distribution; gray: underlying W substrate.

For the high energy part of the RBS spectrum (shaded in green in Fig. 4.6), the backscattered He ions all stem from within the oxide film on all grains. No He ions detected in this energy interval reached the metallic W underneath. This region, nearest to the surface of the oxide film, can, therefore, be directly modeled without the need for further assumptions of the oxide thickness distribution. For the area shaded in red in Fig. 4.6, the W grain-dependent thickness variation [53] of the thermally grown oxide needs to be taken into account. For comparison, the simulated spectrum of a WO_3 sample without grain-dependent roughness is shown as a gray dashed line in addition. As most grains are close to the maximum in the thickness distribution, the difference between the two simulations is most pronounced for the deep part of the oxide film. However, due to technical limitations in the program SIMNRA a layer that incorporates a thickness distribution cannot be further divided into sub-layers. Therefore, the area shaded in red can only be represented as a single layer of constant elemental composition in the oxygen depth profiles. Nevertheless, as the relevant changes in oxygen concentration during plasma exposure appear only in the green-shaded area of the RBS spectrum (near surface region of the oxide film), this will not affect data interpretation. Finally the gray-shaded area in Fig. 4.6 marks the metallic W substrate underneath the oxide film.

The oxygen depth profiles derived from the RBS spectra of all samples are presented in Fig. 4.7. The color code of the background is the same as in Fig. 4.6. The area shaded in red is always represented by a single layer of constant composition, whereas the area shaded in green allows depth-resolved steps. The steps have equal thickness (50×10^{19} atoms/m^2) that is determined by the depth resolution of the RBS measurement in the oxide film. The upper axis of the plot shows the (approximate) thickness of the layers in nm under the assumption of stoichiometric WO_3 with a density of 7.16 g/cm^2. For the W enriched zones in Fig. 4.7 b) and c) this thickness scale is no longer accurate and serves only as an approximate frame of reference.

Fig. 4.7 a) shows the oxygen depth profile of the thick (55 nm) oxide before plasma exposure. It is derived from the RBS spectrum shown in Fig. 3.8. The W concentration is shown in red and the O concentration in blue. It is evident that the thick oxide film before plasma exposure can be described by WO_3 (i.e., 25 at.% W and 75 at.% O) over its full depth of 385×10^{19} atoms/m^2. After this, the metallic W begins. The slight increase of oxygen at the very surface (by about 1 at.%) can be attributed to a small mismatch of the simulation and the experimental spectrum. This is possibly due to electronic noise in the detector readout electronics, which causes the background of the RBS measurement (Fig. 3.8) to increases slightly stronger towards lower energies than predicted by the simulation. This in turn leads to a slightly higher O content near the surface (high-energy side in the spectrum). In any case, this O increase is barley significant. The uncertainty of the W and O concentration in the depth profile was derived by manually varying the concentration and the solid angle of the detector around the fitted values until obvious mismatch between the simulated and the experimental RBS spectra occurred. With this method, the error in the concentration is estimated to be <1 at.%.

Fig. 4.7 b) in turn shows the oxygen depth profile for the thick oxide sample after plasma exposure. The corresponding RBS spectrum is shown in Fig. 4.6. It is evident that the W concentration of about 40 at.% at the surface is significantly higher than the 25 at.% expected for stoichiometric WO_3. The W concentration decreases with distance to the surface and reaches the nominal 25 at.% at a depth of about 100×10^{19} atoms/m^2 corresponding to roughly 13.5 nm of stoichiometric WO_3. This shows that the oxide removal by the D plasma starts at the surface and most likely penetrates deeper into the bulk with increasing plasma fluence. It definitely does not occur homogeneously throughout the bulk of the oxide film. Due to the limited depth resolution of the RBS measurement, it is not possible to determine if the oxygen concentration decreases gradually towards the surface or if there is an abrupt jump in concentration. It can,

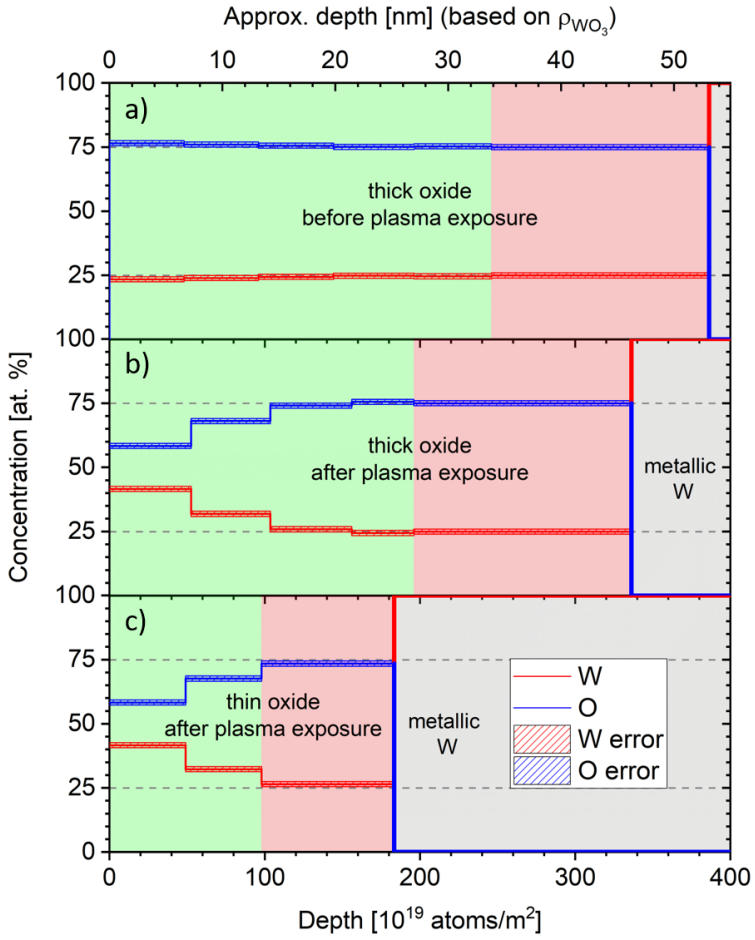

Figure 4.7 – Oxygen depth profiles derived from 800 keV ^{4}He RBS measurements: a) Thick oxide before plasma exposure (RBS spectrum shown in Fig. 3.8). b) Thick oxide after plasma exposure (from the RBS spectrum shown in Fig. 4.6). c) Thin oxide after plasma exposure (RBS spectrum not shown). The color code for the background is the same as in Fig. 4.6.

however, be excluded that WO_3 is fully reduced to metallic W at the surface before the oxygen loss can progress deeper into the oxide film. Such behavior would lead to a region of fully reduced metallic W at the surface with intact WO_3 underneath, but simulations of this case deviate strongly from the experimental spectrum in Fig. 4.6, even if one takes into account that this layer of pure W would form natural oxide on top again after the plasma exposure. The measured spectrum (and the same is true for the not shown RBS spectrum belonging to Fig. 4.7 c)) is much better represented by the simulation if one assumes that a partial reduction of the W oxide takes place across the first 100×10^{19} atoms/m^2 ($\approx$ 13.5 nm) of the oxide film. However, the D implantation depth in WO_3 for the used D energies is only 0.7 nm for 5 eV/D and 1.6 nm for 15 eV/D, according to simulations with SDTrimSP (v. 6) [78] when considering the average implantation depth plus a two σ interval (see appendix A.4). By comparing these values, it becomes clear that the kinetic energy of the incident D ions cannot be the immediate cause for the removal of oxygen from the film.

Fig. 4.7 c) shows the oxygen depth profile of the sample with thin oxide after plasma exposure. Here, the same trend as in Fig. 4.7 b) is visible. At the surface, the W concentration is also increased to about 40 at.%. In the next layer, it is closer to the nominal value of 25 at.% for WO_3. The deeper region of the oxide film can still be well described by stoichiometric WO_3, which matches the results for the thick oxide film. This shows that the removal of oxygen from

the surface near region of the oxide films is identical in both cases and is independent of the film thickness.

This partial oxygen loss in the near surface region agrees with previous experiments by Alimov et al. [21]. They have observed a thicker W-enrichment zone in the first 130 nm of 1–2 µm thick, thermally oxidized WO_3 layers after D plasma exposure at temperatures between 340 K and 515 K. They used a total D fluence of 10^{26} D/m^2, a D flux of 10^{22} D/m^{2}s and an energy of 38 eV/D. Despite all three critical parameters that could influence the thickness of the W-enrichment zone being one to two orders of magnitude larger than in the present case, they observed an increase of only one order of magnitude in the thickness of the reduction zone (130 nm compared with 13.5 nm in the present work). This is interesting as one could assume that the difference in D fluence (10^{26} D/m^2 vs. 10^{24} D/m^2) would already lead to a thicker reduction zone. Furthermore, the 1–2 µm thick oxide layer in their work exhibited strong cracking due to the different densities of W oxide and metallic W. These cracks might also cause a deeper oxide reduction zone compared with the thin, crack-free oxide films in the present work. All this implies that the depth-progression of the oxygen loss saturates or at least slows down drastically with increasing D fluence; possibly due to the growing W-enriched layer on top of the oxide film. To address this effect quantitatively, the oxygen loss rate was further studied at higher fluences of gentle D plasma as described in section 4.3.

Another interesting question is, which mechanism leads to the oxygen loss and the W-enrichment at the surface of the oxide film. It is possible to exclude preferential sputtering of the O atoms by the D plasma as the sole driver of this, because the overall depth of the oxygen loss region of 100×10^{19} atoms/m^2 (corresponding to 13.5 nm of stoichiometric WO_3 or 4 nm of metallic W) is much larger than the D ion implantation depth (1.6 nm for 15 eV/D). Furthermore, the D energy used here is far too small to allow direct sputtering of W atoms and the W-enrichment zone would quickly prevent further removal of atoms from the surface. A investigation of the sputter yield of W from W oxides by D at different D energies was also conducted in the present work and is described in section 4.5.

Another possibility for the oxygen loss could be that after the first step of chemical reduction of WO_3 by D atoms under formation of deuterium tungsten bronze (D_xWO_3), a second chemical reaction takes place that forms oxygen-containing molecules that become mobile within the oxide film. However, as the diffusion of D in the WO_3 layer is expected to be high [21, 40, 76], it is likely that chemical reduction of the tungsten oxide by diffusing D takes place across the full depth of the oxide film, as is indicated by the fast color change of the oxide film that was observed during D plasma exposure (see section 4.1.3). Therefore, chemical reduction by D atoms (formation of D_xWO_3) can be excluded as the rate-limiting step of oxygen loss, as it would lead to a uniform removal of oxygen across the full depth of the oxide film and not only close to the surface.

Thus, the following can be proposed as a possible mechanism for the oxygen loss in the near-surface region of the oxide film: While in a first step the reduction of WO_3 by D takes place across the full oxide film, the rate-limiting step is the diffusion of O-containing molecules from the place of creation to the surface. The oxygen loss from the sample is then driven either by thermal or ion-induced desorption from the surface.

However, since it became clear in the previous section that significant amounts of oxide remain on the sample surface after gentle plasma exposure, the most interesting question still remains: To what extent does the oxide film affect D uptake into metallic W?

4.2 D uptake during gentle plasma exposure

This section investigates how oxide film affects the D uptake into metallic W. To this end, several D depth profiles were measured on all three samples (thick, thin and natural oxide) with NRA at different time steps after the plasma exposure. The profiles were created from NRA spectra at several different primary ^{3}He ion energies. In order to achieve a very high depth resolution near the surface, the information from protons and α-particles created in the nuclear reaction were combined. See section 3.6.1 for details of the NRA measurements.

4.2.1 Deuterium depth profiles

Fig. 4.8 a) shows the D depth profiles for all three samples two days under vacuum after plasma exposure. The blue line represents the D concentration profile in the reference sample with only a 1–2 nm thick natural oxide film. The areal density of D retained in the reference sample is $31.9 \pm 1.6 \times 10^{19}$ D/m^2. Its D concentration profile extends about 1.3 µm deep into the self-damaged W, but does not completely fill it to its full extent of 2.3 µm. This is an expected outcome, as it reproduces the results of similar experiments under these conditions that previously have been conducted in the work group of the author [12, 44, 79].

The D depth profiles of the samples with thick and thin oxide film two days after plasma exposure are depicted in red and green in Fig. 4.8 a), respectively. They both consist of only a single D-containing layer close to the surface with no measurable amounts of D deeper in the samples. The depth resolution of the depth profiling with NRA in a WO_3 film is approx. 50 nm at the surface, which is about the same as the thickness of the thick oxide film (initially 55 nm). This directly confirms that the D in the sample with thick oxide (red in Fig. 4.8 a)) is located solely within the oxide film. For the thin oxide film (initially 33 nm; green in Fig. 4.8 a)), the depth resolution of NRA is larger than the film thickness and consequently this conclusion cannot be directly drawn from the measurement. Nevertheless, it is reasonable to assume, that also for the thin oxide film, D is retained only within the oxide. If D could penetrate through the oxide into the self-damaged W, the D concentration would extend deeper into the sample, which would be clearly visible in the D depth profile and also in the NRA spectrum itself (not shown).

Due to the limited depth resolution of NRA it is not possible to determine a depth profile of the D concentration within the oxide film itself. Therefore, it is not possible to conclude from NRA, if the D concentration within the oxide film has a gradient throughout the layer. Nevertheless, assuming a homogeneous distribution of D within the oxide film seems reasonable (at least for the not-reduced part of the oxide), considering that D is mobile within WO_3 at room temperature [40, 76]. This assumption is further supported by Alimov et al. [21] who found D diffusion in thick WO_3 oxide films over several µm already at temperatures of 340 K, i.e., lower than the 370 K used in this experiment. Therefore, in Fig. 4.8 a) the D concentrations in the oxide films (red and green) are shown as dotted lines under the assumption of homogeneous D distribution within the oxide films. The D concentration under this assumption is 1.3 at.% for the thick oxide and 0.9 at.% for the thin one. The difference may be an indication that the D is predominantly retained in the stoichiometrically unaffected part of the oxide film that consist still of WO_3 after plasma exposure. The fraction of this unaffected zone relative to the total thickness of the film is bigger for the thick oxide.

Independent of the D distribution within the oxide films, the absolute D areal density in these surface layers can be determined very precisely by the NRA measurement. The areal density in the oxide film is $4.02 \pm 0.28 \times 10^{19}$ D/m^2 for the thick oxide and $1.30 \pm 0.09 \times 10^{19}$ D/m^2 for

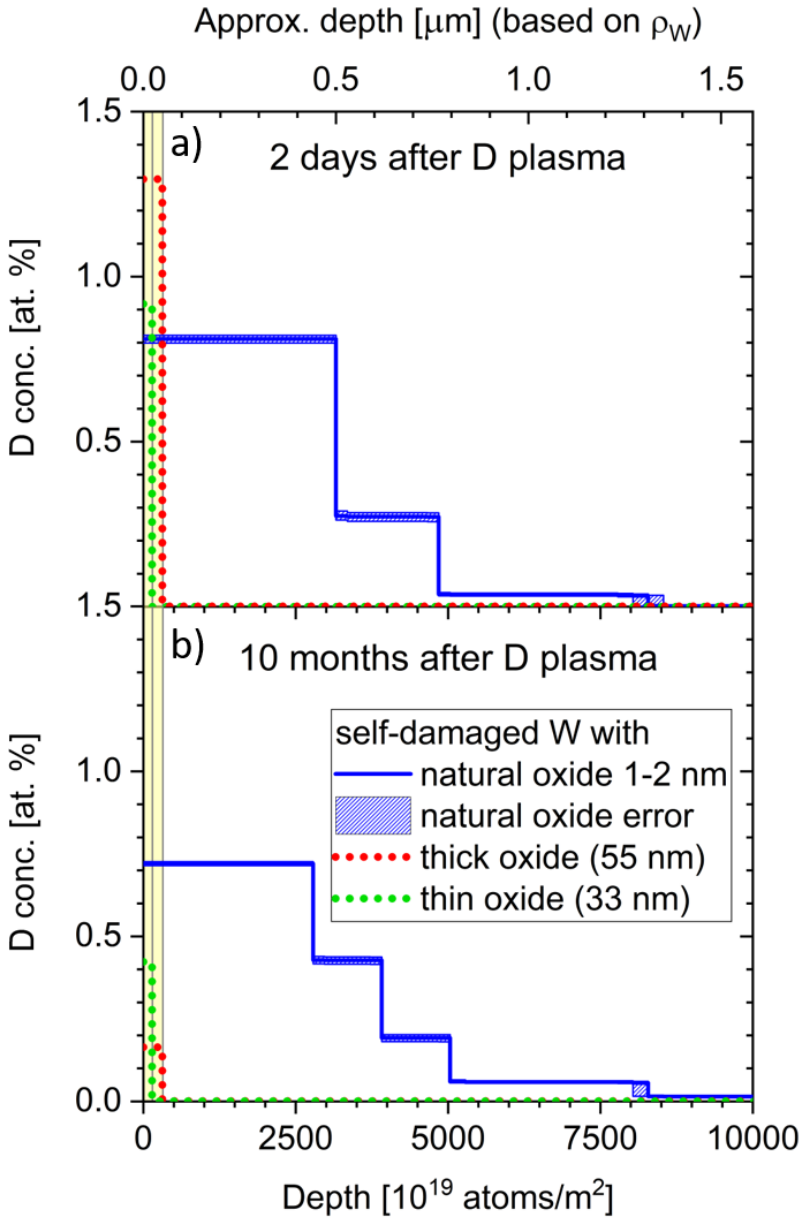

Figure 4.8 – Deuterium depth profiles measured with NRA after exposure to gentle D plasma with D energies of 5eV/D at a sample temperature of 370 K and a fluence of 1.4×10^{24} D/m^2. a) Depth profiles two days after plasma exposure. b) Depth profiles ten months after plasma exposure. The yellow background color indicates the approximate oxide film thickness after plasma exposure.

the thin one. The fact that the D retention in the thin oxide is disproportionately smaller than in the thick oxide, again suggests that the D is predominantly retained in the remaining, stoichiometrically unaffected WO_3 deep in the oxide film. When comparing the amount of this remaining WO_3 for the two oxide films (see Fig. 4.7 b) and 4.7 c)), it is obvious that the thick oxide film has about three times more WO_3 left than the thin oxide film. This corresponds very well to the difference in D retention in the two oxide films. In any case, the absolute D retention in the oxidized samples is significantly smaller (factor of 8 and 25 for the thick and thin oxide, respectively) than in the reference sample with only natural oxide that shows a retention of $31.9 \pm 1.6 \times 10^{19}$ D/m^2.

Thus, the D depth profiling with NRA clearly shows that oxide films of initially 33 and 55 nm thickness effectively block D diffusion into the (self-damaged) metallic W at 370 K. This is a new and unexpected result.

There is one study by Ogorodnikova et al. [24] who claims that D is retained deep in the bulk W beyond a WO_3 film of 100 to 400 nm thickness for thermally oxidized W samples after irradiation with D ions at an energy of 200 eV. However, this statement relies on a sole measurement of the D concentration in the sample with ^{3}He NRA at a single energy of 1 MeV, which corresponds to a probing depth of about 1 µm depending on the oxide thickness. With only one single energy and the detector setup used in [24], no depth profiling of the D concentration in the sample can be achieved. It is, therefore, not clear, how this measurement can yield information on whether D is located inside or beyond the oxide film.

In the present work, however, employing detailed RBS and NRA depth profiling with ^{3}He energies from 0.5 to 4.5 MeV and using the very surface sensitive alpha spectrum, made it possible to obtain a reliable picture of the depth distribution of both the oxygen and the D concentrations in the sample. Therefore, it can be concluded that for the thick oxide any D that is retained in the sample is retained within the oxide film. For the thin oxide, this is also strongly indicated. No D has penetrated through the oxide films into the self-damaged W after the here applied gentle D plasma exposure with D energies of 5 eV/D at a sample temperature of 370 K and a D fluence of 1.4×10^{24} D/m^2.

4.2.2 D release at room temperature

The D depth profile of the three plasma-exposed samples (natural, thin and thick oxide) was measured again after a waiting period of ten months. The samples were stored at room temperature in a desiccator under vacuum during this time. The D depth profiles after the waiting period are shown in Fig. 4.8 b).

The D content in the reference sample with the natural oxide (blue) was $29.8 \pm 1.5 \times 10^{19}$ D/m^2 after the waiting period, and has thus stayed about constant with a measured change of 6.6 % from the initial value of $31.9 \pm 1.6 \times 10^{19}$ D/m^2. This small relative difference is close to the experimental uncertainty. Therefore, only a very small amount of D is lost from the natural oxide sample. This was expected, since most of the D should be firmly trapped in defects in the self-damaged W underneath the natural oxide film and much higher temperatures are needed for a thermal release [12, 33]. A similar small reduction (in the order of 5 %) of the trapped D amount due to storage in vacuum was also observed in a dedicated study by Wielunska et al. [12].

But more importantly, the deuterium amount in the oxidized samples (red and green) has diminished drastically. From 4.02 ± 0.28 to $0.40 \pm 0.03 \times 10^{19}$ D/m^2 (90 % reduction) in the case of the thick oxide (red) and from 1.30 ± 0.08 to $0.59 \pm 0.04 \times 10^{19}$ D/m^2 (55 % reduction) in the

case of the thin oxide (green). From the strong reduction of D over time, one can conclude two things: First, the D must be mobile in the oxide at room temperature to be able to leave the oxide. Second, it does leave the oxide towards the surface and not towards the self-damaged W. Otherwise, it would still be detectable by NRA as the defects in the self-damaged W do not release trapped D at room temperature (see above). The first conclusion is already well known in literature, see e.g. [25]. The second conclusion, however, is new and leads to the interpretation discussed in the next section.

The observed reduction of the D content in the oxide over time leads to the question whether significant amounts of D could leave the oxide film already within the first days after D loading (i.e., the time usually needed to transfer the sample to the NRA setup and measure the content). To this end a dedicated study of the D loss over time at room temperature and elevated temperature has been conducted and is described in 4.2.3.

4.2.3 D loss from oxide over time

To investigate whether significant amounts of D are released from W oxide directly after D exposure, a dedicated study with a much thicker oxide film was conducted. The thicker oxide film allows a higher total D retention in the oxide and thus improves the accuracy of the measurement. Since the W grain-dependent thickness variations may pose a problem for thicker oxide films, a W single crystal with (100) orientation was used. The single grain orientation leads to a homogeneous growth of W oxide with constant thickness. The sample consists of a thin disc with a diameter of 10 mm and was thermally oxidized at 723 K for 5.5 h in the same setup and fashion as described in section 3.5.1. The resulting oxide areal density (measured by ^{3}He NRA at 4 MeV) was $3231\pm190\times10^{19}$ O/m^2. This corresponds to a thickness of 529 ± 31 nm for stoichiometric WO_3.

After oxidation, the sample was exposed to gentle D plasma in PlaQ (<5 eV/D) at 370 K for 65 minutes (D fluence: 2.2×10^{23} D/m^2). After that, it was cooled down in D gas with a pressure of 1 Pa and reached room temperature after 15 minutes. Immediately afterwards, the sample was transferred through air to the NRA setup and set under vacuum again. Then, the D and O signals were measured with ^{3}He NRA at 4 MeV in various time steps in the interval from 41 minutes to 27 h after the end of the plasma exposure on different locations on the sample. Since the goal of this experiment was to detect possible relative changes, only the integral counts from the D and O peak in the NRA spectrum are shown and no calibration to areal density was performed. After 22.5 h the sample was removed from the NRA chamber and broken in two halves. One half was inserted into PlaQ and heated to 500 K in vacuum (18 minutes heat up, 32 minutes constant T, 39 minutes cool-down to room temperature). Afterwards both halves were again inserted into the NRA chamber and two more measurements points were taken for both samples.

The results are shown in Fig. 4.9. The oxygen content (black symbols — right axis) stays constant over time and is not affected by exposure to air or heating to 500 K. The blue symbols show the D content for the full sample (first seven points) and in the unheated half after sample breaking (last two points). The D content stays constant within the uncertainty of the measurement of 3 % (relative changes for high counting statistics; see section 3.6.1 for details) over the first 22.5 h and it is also not affected by the (second) exposure to air (last two points). These results show that the D content does not significantly decrease during storage at room temperature within the first day (27 h) after D exposure at 370 K. Neither storage in vacuum (NRA chamber) nor exposure to air (for transfer and sample breaking) seem to affect the D content in

this time period. It should be noted, however, that from these ex-situ measurements it cannot be concluded whether significant amounts of D are lost immediately after plasma exposure, either upon first contact with ambient air or by a fast outgassing during the 41 minutes between the end of plasma exposure and the first NRA measurement. Nevertheless, one can conclude that the D contents measured within a few days after D exposure are comparable with each other and — apart from the potential initial loss — additional D loss from the oxide in significant quantity occurs only on a timescale of weeks or months for thermally grown oxide films.

Finally, the D content in the heated half is shown in red in Fig. 4.9 and a strong decrease in the D content (by 63 %) is visible. This indicates that the majority of D trapping (or binding) sites within the oxide are depleted at this temperature, but some still contain D and thus may have a higher binding energy. However, from this single exposure at one temperature it is not possible to determine the D binding energies of these sites within the oxide.

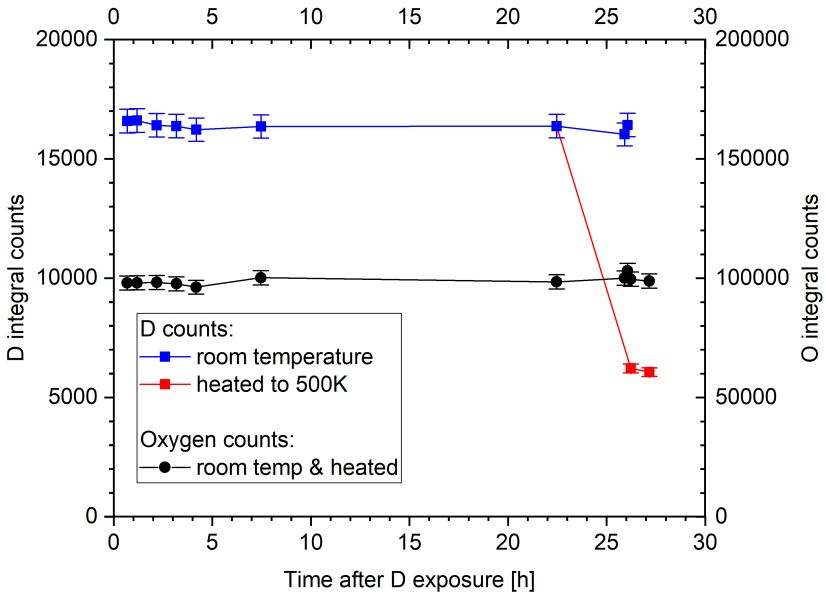

Figure 4.9 – Integral counts of the D and O peaks in the ^{3}He NRA spectrum during the first 27 h after gentle D plasma exposure at 370 K for heated and unheated samples.

4.2.4 Interpretation of results: Difference in heat of solution between W oxide and metallic W

The results from above indicate that tungsten oxide films act as a permeation barrier for D into W. This holds true even after a waiting period of ten months at room temperature in vacuum. D permeation into metallic W is not prevented by a limited transport of D within the oxide, but by the interface of W oxide to metallic W. Based on the current knowledge of the system, the following conclusions are made: During plasma loading, D is implanted beneath the surface into the oxide film (implantation range 0.7 nm for 5 eV/D). Within minutes [40], it diffuses throughout the full depth of the oxide film up to the interface and forms deuterium tungsten bronze (D_xWO_3). In contrast to a direct, plasma-driven implantation into the metallic W, the thermalized D in the oxide film does not possess enough energy to overcome the difference in the enthalpy of solution (Q_{Sol}) between WO_3 and metallic W, which is schematically illustrated in Fig. 4.10.

The enthalpy of solution of D in metallic W is 1.14±0.04 eV [29]. However, for D in WO_3 literature data is scarce. A study by Dickens et al. [37] (which appears to be the most substantiated), has found a slightly negative enthalpy of formation of −0.28±0.04 eV and this value is used for the schematic in Fig. 4.10. This value fits well with the observation by Ippolito et. al [80] that HIs can be absorbed in WO_3 from a HI-rich atmosphere at temperatures above 394 K when catalysts are present to assist with molecular dissociation (see activation barrier for H_2 desorption indicated in Fig. 4.10). Additionally, in the present study it was observed that D can desorb again into vacuum at room temperature over a timescale of months, which also indicated that the enthalpy of solution of D in WO_3 must be close to that of D_2 in vacuum. Consequently, the difference in the enthalpy of solution for D atoms in WO_3 and in W should be close to 1.4 eV. This energy difference is too high to be overcome by D atoms in WO_3 in the present experiment at 370 K. Note that the energy necessary for a diffusion step ΔE_{diff} for hydrogen in WO_3 is stated as 0.35 eV from DFT calculations [38] and as 0.4 eV from experiments [39]. For metallic tungsten, ΔE_{diff} for HIs was recently remeasured with high precision and is stated as 0.28±0.06 [30].

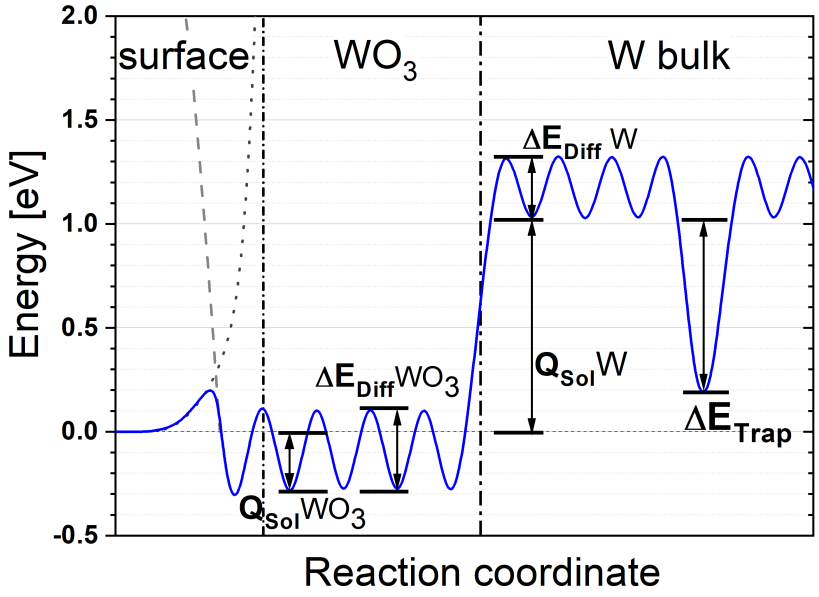

Figure 4.10 – Schematic representation of the energy landscape of D in WO_3 and W (blue). The dashed gray line at the surface marks the energy of a D atom. The dotted gray line marks the repulsive potential for the D_2 molecule close to the surface. At the intersection of these lines the dissociation of molecular D_2 to atomic D takes place. The heat of solution (Q_{sol}) and the energy necessary for a diffusive step (ΔE_{Diff}) for D in WO_3 and W are shown. In the self-damaged W bulk also a D trap with the binding energy ΔE_{Trap} is shown. A detailed discussion of the absolute values is provided in the text.

One can assume that the thin (1–2 nm thick) natural oxide film, present in many laboratory experiments, exhibits the same behavior and reduces or even prevents the D transport into metallic W at a temperature of 370 K. However, since the sample with only natural oxide showed significant D concentration in the self-damaged zone, it can be concluded that this effect only lasts until the natural oxide film is sufficiently reduced by the D plasma. The presented data cannot confirm this assumption, since the thermally grown oxide films have obviously not yet reached this state. They show only a partial oxide reduction in the surface near region

(100×10^{19} atoms/m^2). In larger depths, especially at the interface between oxide and metallic tungsten, the stoichiometric composition of WO_3 is still intact. A direct measurement of the reduction of the natural oxide is also not possible since it reforms before ion beam analysis can be applied. Therefore, the D fluence was extended to investigate if the thermally grown oxides can reach a sufficiently reduced state for D to enter metallic W. The results are discussed in the next section.

Lastly, it is worth mentioning that the proposed barrier mechanism acts only in one way. While the uptake of D from the WO_3 into the metallic W is reduced or blocked, the transport in the opposite direction should not be affected by the interface. It may, however, be affected by the oxide itself. The present experiments allow only to draw conclusion on D uptake. The effects that surface oxide films have on the release of D from self-damaged W have also been investigated in this work and are discussed in chapter 5.

4.3 Effects of higher D fluence at low D energy

This section describes a second experimental campaign that was conducted with the same samples as in section 4.1 and 4.2 but with a significantly higher D fluence, in order to investigate how the reduction of the oxide progresses and whether a higher D fluence leads to a breakdown of the D permeation barrier. The fluence was increased in several steps from the original 1.4×10^{24} to 3.0×10^{24}, 4.6×10^{24} and finally 1.6×10^{25} D/m^2. After each fluence step, D and O depth profiles were measured with IBA and the surface modification was investigated by SEM imaging and FIB cuts. Section 4.3.1 describes the changes and reduction of the oxide film, section 4.3.2 discusses the D uptake through the (partially reduced) oxide and section 4.3.3 provides a short summary and discussion of the results. The results presented in section 4.3 and 4.4 will also be published in a forthcoming peer-reviewed journal publication.

4.3.1 Oxide reduction and surface modification

Oxygen loss: Fig. 4.11 shows the changes of the oxygen areal density for the thick, thin and natural oxide (red, blue and black, respectively) as a function of applied D fluence as measured with NRA. Image a) shows the remaining oxygen and b) the loss of oxygen. The first three fluence steps are almost identical and correspond to plasma exposure times of 7, 8 and another 8 hours (1.4 and 1.6×10^{24} D/m^2, respectively). It is apparent that the additional oxygen loss decreases with each successive fluence step for both the thick and thin thermally grown oxide. A possible explanation for the saturation of the oxygen loss may be the growth of the W-enrichment zone that has formed after the first fluence step (see 4.1). A thicker enrichment zone would increase the distance the oxygen has to diffuse to reach the surface. The final fluence step is much longer (58 h or 1.2×10^{25} D/m^2), but causes only a very small additional O loss, indicating that the W enrichment zone blocks further O transport to the surface. Furthermore, the loss of oxygen follows the same trend for both oxide thicknesses and after the final step an almost identical amount of oxygen has been removed from both samples. This indicates that the oxygen removal by the plasma stays independent of the oxide thickness even for a higher D fluence. Apparently, both oxides are thick enough so that the oxygen loss saturates before they are fully reduced.

The natural oxide (black) reforms after each plasma exposure in ambient atmosphere during transit to the diagnostics. Therefore, the measured oxygen areal density is about the same in all measurements.

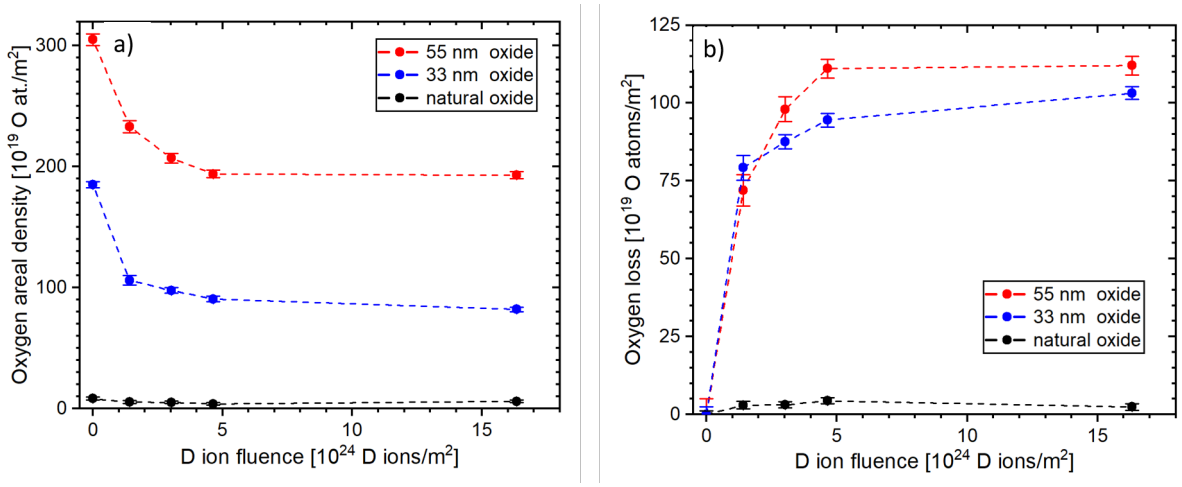

Figure 4.11 – Oxygen areal density evolution of the thick, thin and natural oxide films over D fluence as measured by NRA. The films have been exposed to D plasma at 370 K and D energy of 5 eV/D in several fluence steps to 1.4×10^{24}, 3.0×10^{24}, 4.6×10^{24} and finally 1.6×10^{25} D/m^2. The dashed lines serve only as an guide for the eye. a) shows the remaining oxide areal density on the sample surface and b) the loss of oxygen (in relation to the initial value) in the same units.

Growth of the W-enrichment zone: The W-enrichment zone was (re-)investigated with SEM imaging of FIB cross sections through the thin and thick oxide film after the 3th and 4th D fluence step. The thickness of the W-enrichment zone grew from the 11.9±1.5 nm after the first plasma exposure (see section 4.1.1) to 15.5±2.6 nm after 4.6×10^{24} D/m^2 (image not shown), which agrees well with the additional oxygen loss shown in Fig. 4.11. After the final fluence step to 1.6×10^{25} D/m^2, the W-enrichment zone did not grow further and shows a thickness of 14.7±2.7 nm (measured from the image in Fig. 4.13). Thus, the SEM images indicate that the thickness of the enrichment zones does not change during the last fluence step. However, due to the grain-dependent thickness distribution and the limited number of observed grains these values are not as representative as the NRA measurements in Fig. 4.11. Nevertheless, the SEM results are compatible with the observation that the oxygen loss saturates after a certain D fluence. This supports the hypothesis that the oxygen loss is slowed down by the growing W-enrichment zone, which hinders the diffusion of O-containing species to the sample surface. Eventually, the W-enrichment zone fully prevents further diffusion and stops its own growth. It acts as a barrier protecting a layer of not-reduced, stoichiometrical WO_3 beneath it. This should in principle create a stable state that prevents D uptake into the underlying W indefinitely for the given plasma exposure conditions, as the interface to the metallic W is still covered by a layer of stoichiometrical WO_3. However, as discussed in the next paragraph, surface modifications, such as crack growth, turn out to play an important role and the simple one-dimensional picture of the layer system has to be modified.

Surface morphology changes and crack evolution: Fig. 4.12 shows an SEM image of the initially 33 nm thick oxide film after exposure to the highest fluence of 1.6×10^{25} D/m^2 under gentle plasma conditions. The straight dark lines are grain boundaries of the underlying W substrate. It is obvious that strong crack formation has occurred in the oxide film. By comparison with Fig. 4.2 b) it seems that the cracks may have grown in number and in thickness since the first plasma exposure to a fluence of 1.4×10^{24} D/m^2, but the changes are moderate and are hard to quantify in the top-view images.

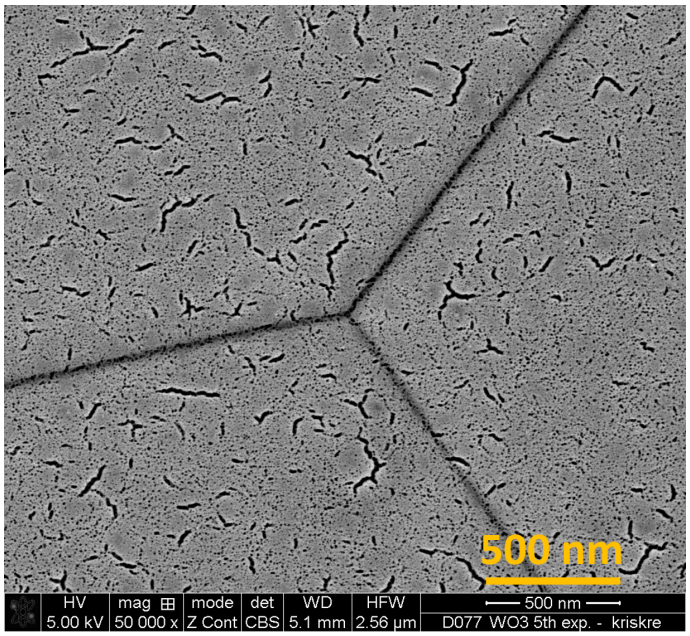

Figure 4.12 – SEM image of the originally 33 nm thick thermally grown oxide film after gentle (<5 eV/D) plasma exposure at 370 K to the highest D fluence of 1.6×10^{25} D/m^2. The straight, dark lines are grain boundaries of the W substrate. Apart from that, strong crack formation in the oxide film is visible.

The evolution of the W-enrichment zone and the cracks with D fluence is much better visualized by comparing a FIB cross section through the oxide film after the highest fluence (Fig. 4.13) with a cross section after the first exposure (Fig. 4.3). It is obvious that the cracks in the oxide film have strongly increased in width and depth after the higher D fluence (please note the higher magnification in Fig. 4.13). Furthermore, the cracks now (almost) completely penetrate the oxide film and form channels to the surface of the metallic W, which in these spots appears to be covered only by a very thin layer of remaining reduced W oxide. This shows that in the fraction of the surface area that consists of such deep cracks, the interface is no longer covered by intact WO_3. Thus, one could expect at least some D to enter the metallic W via these cracks, which will be discussed in the next section (4.3.2).

Most of the surface area is, however, still covered by an oxide film that consists of a W-enriched top layer (bright) with mostly intact oxide (dark) beneath. According to the model developed in 4.2.4, this indicates that for most of the surface area the oxide film should still prevent D uptake into the metallic W. It is, however, not possible to determine the exact composition and stoichiometry of the oxide film from the SEM images alone. Oxygen depth profiles with RBS are necessary to determine whether the remaining oxide is indeed still WO_3 or if it has been reduced (to some extent) by the higher D plasma fluence.

Oxygen depth profiles: The stoichiometrical composition of the remaining oxide film is investigated by oxygen depth profiles from RBS measurements. Fig. 4.14 shows such profiles after the highest D fluence of 1.6×10^{25} D/m^2 for the thin and thick oxide in a) and b), respectively. For the thick oxide, intact WO_3 is still present near the interface to the metallic W even after this high fluence. The W-enrichment zone at the surface, however, has a higher W concentration (48 %) than after the first exposure (40 %; compare with Fig. 4.7) and extends far deeper into the oxide film (150–250×10^{19} atoms/m^2 compared with 100×10^{19} atoms/m^2 after the first exposure). This shows that the oxide reduction is progressing both in intensity (W

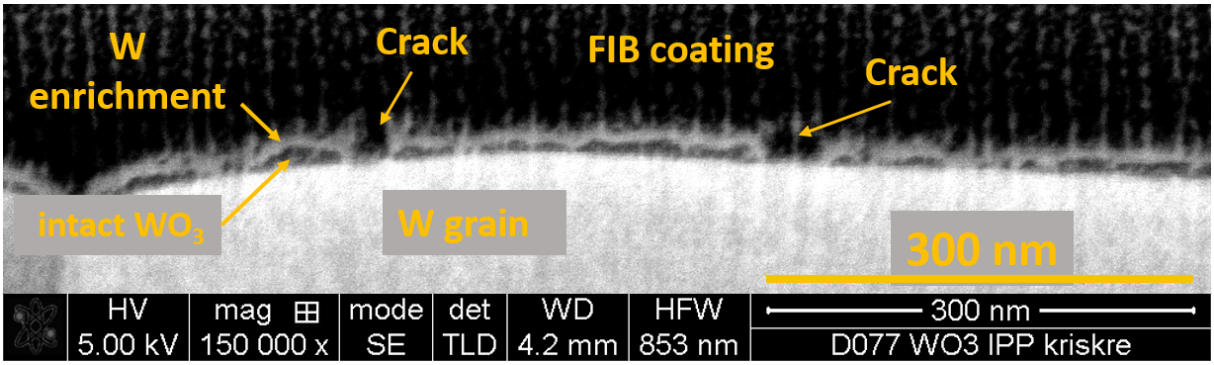

Figure 4.13 – FIB cross section through the oxide film shown in Fig. 4.12 after exposure to gentle D plasma to the highest fluence of 1.6×10^{25} D/m^2. The vertical stripes are an artifact of the FIB cross section.

concentration) and in depth.

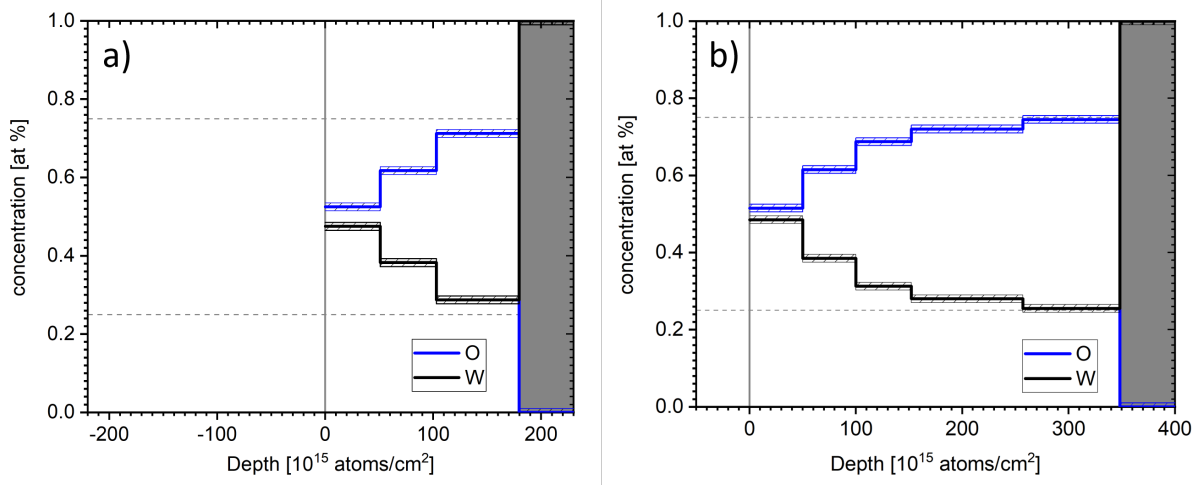

Figure 4.14 – Depth profiles of O and W concentration in the oxide film after exposure to the highest fluence of 1.6×10^{25} D/m^2 of gentle (5 eV/D) plasma at 370 K. a) shows the thin and b) the thick oxide film. Please note that in this graph the presentation of the oxygen depth profile is slightly different than in other graphs in this work and the interface to the metallic W is fixed to illustrate the thickness difference of the oxide films. The 0 on the y-axis marks the surface of the oxide film and the dark gray area on the right marks the metallic W.

However, the RBS depth profiles are affected by the strong cracking that penetrates through the full oxide film. In contrast to the first exposure, where the cracks occurred only in the topmost layer of the oxide and did not affect the surface near part of the oxygen depth profiles[1], the deeper cracks here affect the full film and lead to a pronounced lateral inhomogeneity of the oxide film. Due to the lateral inhomogeneity, the oxide film can no longer be described as a one-dimensional system consisting of layers with different oxygen concentration. As the separation into such a stack of layers is the basis for oxygen depth profiling with RBS, the method becomes unreliable and different oxide film thicknesses (areas with cracks vs. areas without cracks) cannot be distinguished from homogeneous layers with different oxygen concentrations by RBS alone. Consequently, the RBS-based depth profiles can no longer be assumed to accurately

[1] This peculiar feature of the RBS depth profiling may seem counter intuitive, but a detailed explanation is given in section 3.6.2

describe the stoichiometry of the oxide film and the W concentration will appear higher (due to the metallic W that lies at the surface in the areas with deep cracks). For the thick oxide this has only a minor effect as the oxide at the interface can still be described as WO_3 by the RBS measurement. For the thin oxide film (Fig. 4.14 a)), however, this effect is more pronounced, as the remaining oxide film is too thin and the fraction of surface area with deep cracks is too large, for the oxygen depth profile to be interpreted as an accurate description of the absolute stoichiometry of the oxide film.

Nevertheless, even for the thin oxide, the RBS profile still yields valuable information on the laterally averaged oxygen concentration. It clearly shows that the oxygen concentration is lower at the surface (W-enrichment zone) and close to WO_3 at the interface. The difference to stoichiometrical WO_3 can in this case be attributed to cracks that fully penetrate the oxide film. For the thin oxide film, it is thus not possible to determine from the RBS depth profiles alone whether the remaining oxide at the interface is still a layer of stoichiometrical WO_3 with cracks in between or if it is, in addition, also partially reduced. However, considering the results for the thick oxide film, which clearly shows intact WO_3, and the FIB cross section through the thin oxide film in Fig. 4.13, it seems reasonable to assume that the remaining oxide on the interface consists mostly of intact WO_3 also for the sample with thin oxide film.

This is an important result as it strongly indicates that the interface between W oxide and metallic W is in the same state as after the first plasma exposure for most of the surface area and should thus exhibit the same properties towards D uptake, i.e., prevent it completely with the possible exception of the fraction of the surface area that contains deep cracks.

4.3.2 D permeation into metallic W through slowly growing cracks

The D depth distribution was measured with NRA after each fluence step. For all but the last step the D depth profiles show that D does not penetrate into the metallic W and only accumulates within the oxide film. This indicates that the model assumption that intact WO_3 on the interface blocks D uptake also holds true for a higher D fluence.

After the last fluence step to at total fluence of of 1.6×10^{25} D/m^2, however, the depth profiles suggest that a small amount of D has passed into the metallic W. Fig. 4.15 shows the depth-resolved D concentration profiles for the thick, thin and natural oxide film after this last fluence step. The light green and red background marks the approximate thickness of the thin and thick oxide film, respectively. For the thin oxide it is obvious that D has penetrated beyond the oxide film into the metallic W. For the thick oxide, only a very small amount of D is located beneath the oxide film, which in principle could be an artifact of the deconvolution with NRADC. Furthermore, since the concentration of D in the oxide film is relatively high compared with the fraction beneath the film, it dominates the depth profile and complicates determining the exact amount of D that has entered the metallic W.

To gain direct evidence on how much D has penetrated into the metallic W, an attempt was made to remove the oxide film from parts of both samples by Argon sputtering with 200 V bias in PlaQ. The thin and thick oxide sample were partially covered by an W sheet and exposed to an Ar plasma for 85 and 200 seconds, respectively. Unfortunately, the Ar flux in PlaQ is not well quantified under these conditions and the sputter yield of the partially reduced oxide by Ar is not well known. Therefore, the necessary exposure time could only be roughly estimated and the oxide was not fully removed by the sputter process. Prolonged sputtering with Ar was also not an option as eventually even the metallic W would be sputtered at these energies. According to subsequent NRA measurements, for the thick oxide about 90 % or $221\pm6\times10^{19}$ O/m^2

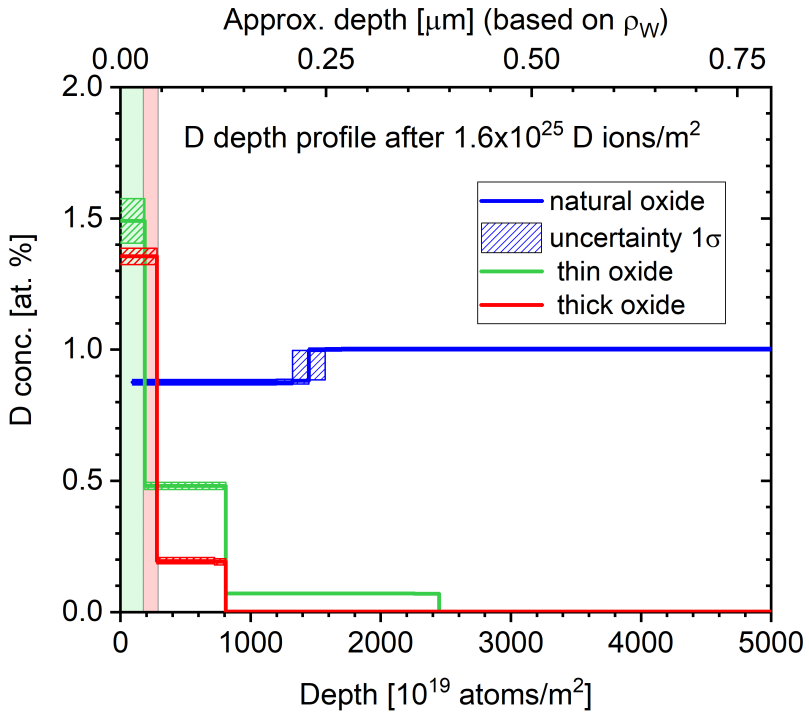

Figure 4.15 – D depth profiles for the thick (red), thin (green) and natural oxide (blue) after exposure to gentle D plasma to the highest fluence of 1.6×10^{25} D/m^2. The areas shaded in light green and red mark the approximate thickness of the thin and thick oxide film, respectively.

of the oxygen on the surface has been removed by the 200 s of Ar plasma (from 246±5 to 25.2±2.2×10^{19} O/m^2). Thus, much clearer information could be gained from the subsequent NRA measurement. Fig. 4.16 shows an SEM image of the thick oxide film after sputtering. The oxide film is mostly removed and the surface area is partially oxide free. Only small islands of oxide remain. The image has been taken in BSE mode, which is sensitive to the atomic number (Z) of the material (see section 3.7 for details) and thus the oxide islands appear darker than the metallic W.

For the thin oxide, on the other hand, the shorter sputter time (85 s) reduced the surface oxygen amount only by about 40 % or 38±4×10^{19} O/m^{2}to 60±3×10^{19} O/m^2). The most likely reason for the smaller relative sputter yield of the thin oxide is that the W-enrichment zone on top of the oxide film exhibits a higher resistance to Ar sputtering than the stoichiometric oxide below it. Once this protective top layer is removed, however, the underlying, not-enriched tungsten oxide is sputtered more quickly. This assumption is based on literature values from Guseva et al. [81] and Roth et al. [82], which indicate that W oxide has a lower sputter threshold and higher sputter yield compared with W[2]. Nevertheless, in both cases the Ar sputtering substantially reduced the oxygen amount and thus the amount of D that is stored in the oxide film. Thus, the D content in the underlying metallic W could be determined with higher precision.

The D depth profiles after Ar sputtering are shown in Fig. 4.17. The approximate oxide thicknesses of the thick and thin oxide are again marked by the shaded red and green area in the background. The formerly thick oxide (red) is now actually thinner than the originally thin oxide, but the naming convention is kept unchanged regardless. It is now discernible that also for the thick oxide sample some D has entered the metallic W. Since the oxide film is almost com-

[2]More details to this can be found in section 4.5, which investigates the sputter yield of W from W oxide.

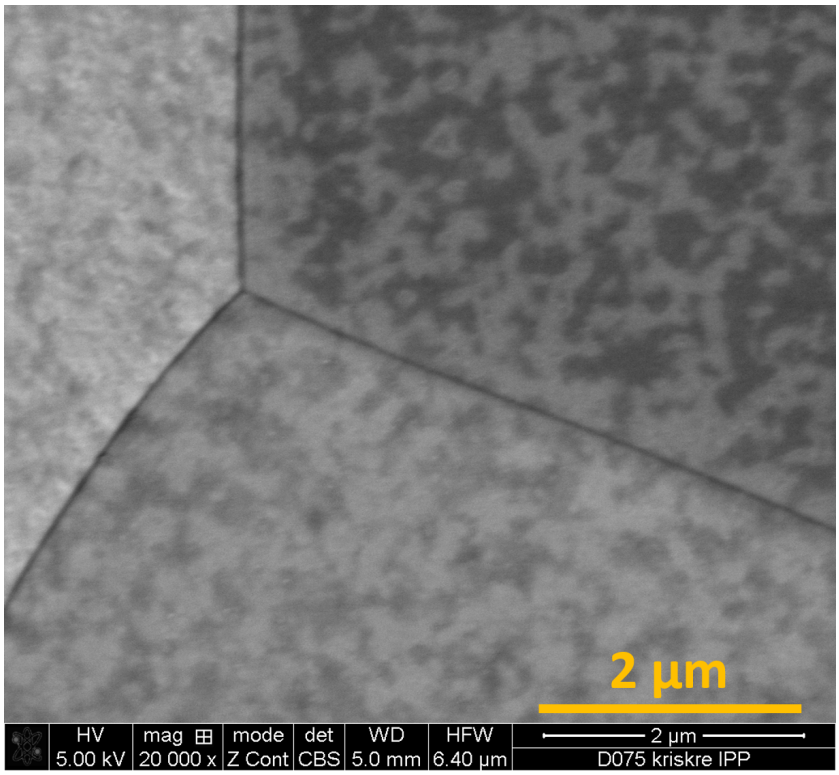

Figure 4.16 – SEM image of the "thick" oxide sample after sputtering with 200 eV Ar ions for 200 s in PlaQ. The oxide film is mostly removed and only small oxide islands remain on the surface. The oxide appears darker than the metallic W in this Z contrast image.

pletely removed, the amount can be estimated very well. For the originally thin oxide sample still some oxide remains and a clear separation between D in the metallic W and D in the remaining oxide is not possible. To get an approximate number of the D amount in the metallic W in this case, the D amount in the oxide film is estimated and subtracted from the total D amount. To estimate the D in the oxide film the concentration of 1.5 % is assumed and multiplied by the approximate oxide thickness. The same is done for the thick oxide. This yields an approximate D amount in the metallic W of 1×10^{19} D/m^2 for the thick oxide sample and 4×10^{19} D/m^2 for the thin oxide sample. These numbers have to be compared with the D uptake into the reference sample that was treated in exactly the same way but has only a very thin natural oxide film on top. For the reference sample the D uptake into metallic W was 145×10^{19} D/m^2.

4.3.3 Summary and conclusions of D uptake and oxide film reduction after high fluence at low D energies

In sections 4.1 to 4.3 it was investigated whether D can enter metallic W through 33 and 55 nm thick W oxide films after (prolonged) exposure to gentle D plasma (5 eV/D). A fluence series up to 1.6×10^{25} D/m^2 was conducted at a sample temperature of 370 K. After each fluence step, the D uptake and the changes of the oxide film were investigated with IBA and SEM. During the first three fluence steps (up to 4.6×10^{24} D/m^2), D was only retained in the oxide film itself and could not cross the interface into the self-damaged, metallic W. The oxide film showed reduction and a W-enrichment zone formed at the film surface (first 13.5 nm). In addition, cracks formed in the oxide but did not fully penetrate the oxide film.

At the highest fluence (1.6×10^{25} D/m^2), however, small amounts of D entered the metallic W.

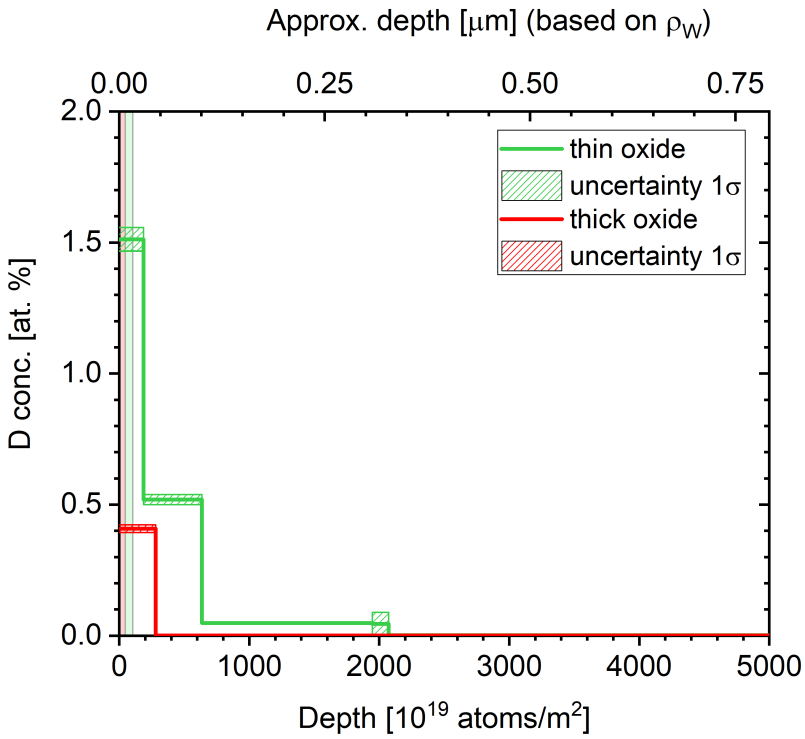

Figure 4.17 – D depth profile of the thick (red), thin (green) and natural oxide (blue) after Ar sputtering of the surface oxide film. The areas shaded in light green and red mark the approximate thickness of the remaining fraction of the thin and thick oxide film, respectively.

They are in the order of a few % compared with the much larger D uptake of the reference sample with only natural oxide. The thick and thin oxide block 99 % and 97 % of the D, that would otherwise enter the metallic W, respectively. Even after this highest fluence, the oxide film still covered most of the surface area and showed a W-enrichment layer on the surface with intact WO_3 underneath at the interface to the metallic W. However, detailed analysis of the surface modification of the W oxide films showed that after the highest D fluence cracks have fully penetrated the oxide film. In the small fraction of the surface area that is covered by such deep cracks, the metallic W is covered only by a very thin layer of reduced oxide. This suggests that the observed D uptake into the metallic W occurs only via these cracks.

Furthermore, the data on the oxygen loss and oxide reduction shows that the loss of oxygen from the oxide film has saturated above a D fluence of 4.6×10^{24} D/m^2. After that, the oxygen loss is almost zero (thick oxide) or very small (thin oxide). This suggests that the oxide will be long-time stable under these plasma exposure conditions and little to no further oxide reduction (oxygen loss) is expected. As the formation and growth of cracks is caused by shrinking of the oxide film with oxygen loss due to the volumetric difference between W and W oxide (see section 4.1.2), no further crack growth is expected.

The results suggests that thin (33 and 55 nm), thermally grown WO_3 films on W effectively reduce D uptake into metallic W up to a high D fluence of $> 1.6\times10^{25}$ D/m^2 under gentle plasma conditions (5 eV/D; 370 K sample temperature). D can only enter the metallic W through surface cracks, which constitute a small fraction of the total surface area and appear to be stable after a certain D fluence. This leads to the conclusion that the remaining stoichiometric WO_3 on the interface to the metallic W still prevents D from overcoming the energy barrier between WO_3 and metallic W, which confirms the results that were obtained in section 4.2.

However, partial oxide reduction and crack formation, eventually leading to D uptake into metallic W, show that the oxide film is fragile under D exposure and may lose its properties as a barrier when the oxide is sufficiently reduced. It is not clear at this point, whether W oxide films will also reduce D uptake under different conditions such as higher D energy or higher sample temperature, as both might lead to a stronger reduction of the oxide. In order to investigate whether thin natural oxide films might influence laboratory studies of D uptake, it is important to determine under which conditions and in which (reduction) state the oxide film stops to prevent or reduce D uptake. Only with this information will it become possible to make useful predictions under which conditions and after which D fluence the natural oxide film loses the property to prevent D uptake into metallic W. To this end, further experimental campaigns with higher D energies or higher sample temperature have been conducted and are described in the next section.

4.4 Influence of D energy and exposure temperature on D uptake and oxide reduction

To study the influence of D energy and sample temperature on the oxide reduction and D uptake through the oxide film, a series of D plasma exposure experiments has been conducted at different D energies and at higher sample temperature. For all experiments in this section, identically prepared samples were used. Each sample was polished, annealed, self-damaged and then thermally oxidized to a thickness of 55 nm, following the procedure described in sections 3.2, 3.3 and 3.5.1. The results presented in section 4.3 and 4.4 will also be published in a forthcoming peer-reviewed journal article.

4.4.1 Higher D energy

Higher D energies were realized by applying negative, direct current bias voltages of -30 V and -100 V to the sample holder during D plasma exposure. Together with the plasma potential of -15 V this respectively yields an effective energy of 15 and 38 eV per D for the majority species of D_3^+ molecular ions in the plasma source (see section 3.4 for details).

In order to probe the dynamics of the oxide reduction and D uptake process, two almost identical D fluence series of 2 h, 21 h (or 22 h) and 72 h were conducted for the two higher D energies at 370 K. The exact D fluence depends on the applied bias voltage and is stated individually for the different energies later in the text. After each fluence step, the D uptake was measured with NRA and the reduction of the oxide film was investigated with NRA, RBS and SEM imaging of FIB cross sections through the oxide film.

Furthermore, the maximum implantation depth of D (molecular) ions with these higher energies into W oxide was determined with SDTrimSP [78] in the same way as for low energy D (<5 eV/D) (see section 4.1). For the majority species (D_3^+, 94 % of the non-neutral D flux), the maximum implantation depth is 1.6 nm for -30 V bias and at 3.1 nm for -100 V bias. For the single charged D^+ minority species (3 % of the non-neutral D flux), the particle energies are 45 and 115 eV/D with a maximum implantation depth of 3.5 nm and 7.1 nm, respectively. Thus, in all cases the penetration depth of D from the plasma is much lower than the oxide film thickness of 55 nm and no direct implantation of D into the self-damaged W is possible.

Oxygen loss: Fig. 4.18 shows the oxygen loss as a function of D fluence for higher D energies in red (−100 V bias) and green (−30 V bias). The oxygen loss from the previously described D uptake experiments at floating potential (< 5eV/D; gentle plasma) are also shown for comparison in gray. It is apparent that the oxygen loss increases significantly with D energy. The oxygen loss after only 2 h exposure (about 6×10^{23} D/m^2) already surpasses the maximum oxygen loss observed after exposure to gentle plasma. After this first exposure at higher energies, 55 % and 40 % of the original oxygen content is removed from the samples for −100 V and −30 V bias, respectively.

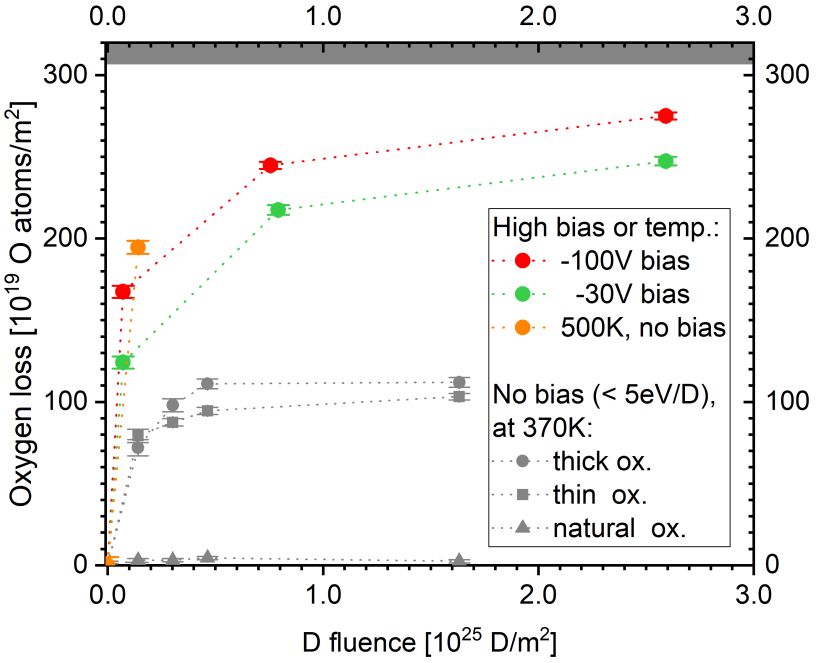

Figure 4.18 – Oxygen loss as a function of D fluence for sample bias voltages of −100 V (red) and −30 V (green) at 370 K and for a sample temperature of 500 K for floating potential (orange). For comparison, the oxygen loss as a function of D fluence for floating potential at 370 K (gentle plasma) is shown in gray. The original oxygen areal density on the sample prior to plasma exposure is 307×10^{19} atoms/m^2 and the dark gray band on top marks the area were all oxygen would be removed from the sample. Please note that the dashed lines connecting the data points serve only as an guide for the eye.

Similarly to the gentle plasma case, the oxygen loss per incident D decreases with D fluence. This indicates that also for higher D energies a W-enrichment zone forms at the surface of the oxide film and slows down oxygen loss. However, in contrast to the gentle plasma exposure, the oxide reduction does not appear to saturate completely for the higher D energies. The curves for both energies clearly show additional oxygen loss during the final D fluence step, although this step starts at D fluence where the oxygen loss from samples exposed to gentle plasma has already saturated. This shows that the process of dynamic oxide reduction carries on throughout all applied fluence steps. After the final fluence steps to 2.1 and 2.3×10^{25} D/m^2, 79 % of the oxygen is removed from the oxide film at −30 V bias and 89 % is removed for −100 V bias. Compared with the 37 % oxygen loss after the final fluence step during gentle plasma exposure (gray circles in Fig. 4.18), this illustrates the much stronger oxide reduction at higher D energies.

For D exposure at higher sample temperature at floating potential (orange in Fig. 4.18), the oxygen loss is far larger than for 370 K. After 7 h of exposure (1.4×10^{24} D/m^2) at 500 K, the

oxide film has lost 63 % of its oxygen content, while the film exposed at 370 K with identical D energy and fluence has lost only 24 %.

−30V sample bias (15 eV/D): Figure 4.19 shows the oxygen (left) and D depth profiles (right) after plasma exposure at −30 V bias for the three fluence steps. Figure 4.20 is arranged in the same fashion and shows SEM images of FIB cross sections through the oxide film (left) and top-view images of the oxide film (right) after each fluence step. Together these two figures provide a compact overview over the oxide reduction and D permeability of the oxide after plasma exposure at −30 V bias.

Comparing the oxygen depth profile after the first fluence step of 5.9×10^{23} D/m^2 (Fig. 4.19 a)) with that of an identical oxide film exposed to a gentle plasma to a fluence of 1.4×10^{24} D/m^2 (Fig. 4.5 b)), it becomes apparent that higher D energy caused much stronger reduction although the fluence was more than a factor two lower. Not only is the W-enrichment at the surface stronger for higher energy (51 % W vs, 42 % W), but also the remaining thickness of the oxide film is smaller (291 vs. 336×10^{19} atoms/m^2). Furthermore, the depth of the W-enrichment zone is larger for higher energy (150 compared with 100×10^{19} atoms/m^2). These values confirm that the D energy strongly influences the speed and depth of the oxide reduction.

However, for this low fluence at −30 V bias, the oxide still seems to consist of stoichiometric WO_3 at the interface to the metallic W. This is also indicated by the SEM image of the FIB cross section through the oxide film in Fig. 4.20 a). It shows that beneath the bright W-enrichment layer a homogeneous and almost completely intact film of darker not-reduced oxide remains and covers the metallic W. On the top-view image (right side in Fig. 4.20 a)) several cracks in the oxide are visible. However, in the FIB cross section along the three grains that are cut (only two are shown) the cracks are sparse and do not go deep into the oxide film. Compared with the first exposure to gentle D plasma (see Fig. 4.1 and 4.3) the cross section image of the oxide film looks very similar and the oxide film seems to have reached a comparable state of reduction (although with more oxygen loss and after significantly lower fluence). According to the model developed in section 4.2.4, the full coverage of the interface by intact WO_3 suggests that no D should be able to enter the metallic W as it cannot overcome the difference in the enthalpy of solution between WO_3 and metallic W. And indeed the corresponding D depth profile in Fig. 4.19 b) shows that D is only present within the oxide film (indicated in yellow in the graph) and does not penetrate deeper. The total amount of D in the oxide film is $1.67\pm0.12\times10^{19}$ D/m^2.

The situation changes after the second fluence step to 6.4×10^{24} D/m^2. The oxygen depth profile in Fig. 4.19 c) shows strong reduction of the oxide throughout its full depth. The W-enrichment at the surface has further increased and the overall oxide thickness has further decreased. The corresponding SEM image of a cross section through the oxide (Fig. 4.20 b)) shows growth of the W-enrichment zone and, in addition, also a strong and laterally inhomogeneous modification of the oxide film. On some parts of the sample (left grain and parts of right grain) the interface is still mostly covered by the darker, intact oxide. However, in other parts (especially the middle grain) the oxide film shows much stronger reduction. Several deep cracks are visible and in many places the bright W-enrichment zone has direct contact with the metallic W. Between these contact points, islands of darker, not-reduced oxide are still visible. Overall the reduction of the oxide seems to be further progressed than after gentle plasma exposure at the highest fluence of 1.6×10^{25} D/m^2 (see section 4.3). Consequently, a higher D uptake into metallic W can be expected although the total D fluence is more than a factor two lower compared with the highest fluence during the gentle plasma exposure. This prediction is confirmed by the D depth profile in Fig. 4.19 d), which shows a total retention of $14.0\pm0.7\times10^{19}$ D/m^2 of which $11.2\pm0.6\times10^{19}$ D/m^2 are located in the self-damaged metallic W beneath the oxide film. This

is about 11 times higher than the D in an identical sample (55 nm oxide) after exposure to gentle D plasma to the highest fluence (see section 4.3.3).

Furthermore, the inhomogeneity and roughness of the oxide film after this second fluence step is much more pronounced than the roughness after long exposure to gentle D plasma. This strong lateral inhomogeneity shows that the oxide film can no longer be described as a one-dimensional system consisting of layers with different oxygen concentration. As described in section 4.3.1, the RBS method can no longer be assumed to accurately describe the stoichiometry of the oxide film under these circumstances, but can still yield laterally averaged values of the O and W concentration. For example, the relative fraction of 63 % O and 37 % W at the interface to metallic W in the RBS depth profile in Fig. 4.19 c) do not necessarily mean that there is WO_2 at the interface. It can also indicate that there is no longer a closed layer of intact WO_3 and that the W-enrichment has reached the interface in some spots (as is the case). In order to distinguish between the two cases and to get an accurate two-dimensional picture of the reduction state, the RBS profiles have to be viewed in tandem with SEM images of the cross sections through the oxide film.

For the final fluence step to 2.1×10^{25} D/m^2 the same trend as above continues. The oxide reduction progresses even further and the oxygen profile in Fig. 4.19 e) shows again a reduction of the overall thickness of the oxide film and an increase in the W to O ratio of the oxide. The SEM image in Fig. 4.20 c) shows that the bright W-enrichment zone touches the metallic W in many places and only small islands of darker, not-reduced oxide are visible on the interface. Nevertheless, a substantial part of the interface area is still covered by this not-reduced oxide and on these parts D uptake should still be blocked according to the model assumption. As expected, the corresponding D depth profile in Fig. 4.19 f) shows substantial D uptake of $38\pm3\times10^{19}$ D/m^2. This is significantly higher than the $4.8\pm0.4\times10^{19}$ D/m^2 that is retained in an identical sample (55 nm thick oxide) exposed to a similar fluence (1.6×10^{25} D/m^2) of gentle D plasma (see section 4.3.2). However, the amount is still small compared with the $145\pm8\times10^{19}$ D/m^2 found in the reference sample with only natural oxide that was exposed to the same fluence of gentle D plasma (the corresponding depth profile is indicated in gray in Fig. 4.19 f) for reference). This shows that even for a D energy of 15 eV/D, a 55 nm thick thermally grown oxide film reduces D uptake into metallic W significantly (74 %) compared with a reference sample with only natural oxide, although the D fluence and D energy were higher than for the reference sample.

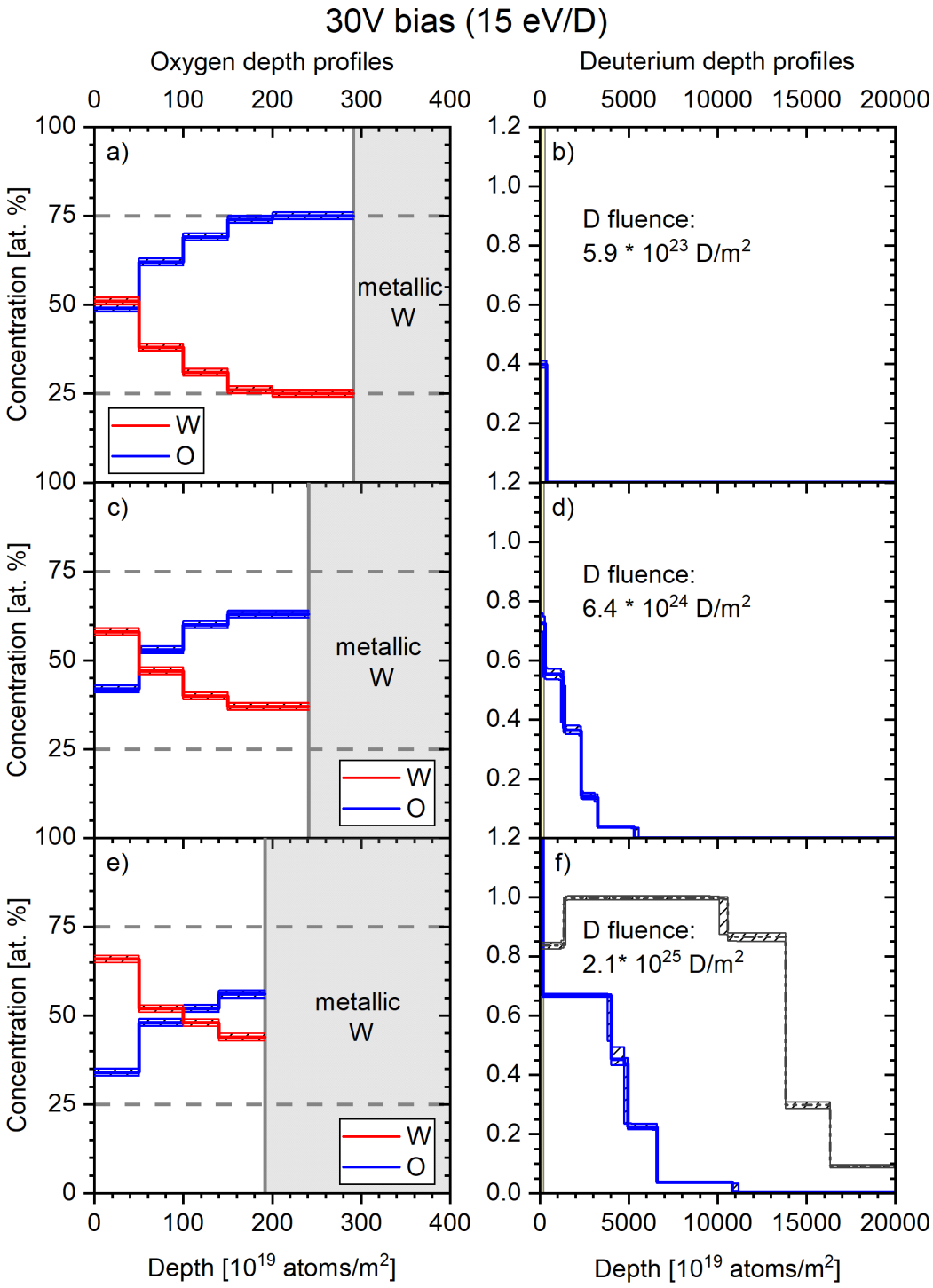

Figure 4.19 – Oxygen (left) and deuterium (right) depth profiles of samples with 55 nm thermal oxide after exposure to D plasma at 370 K and −30 V sample bias (15 eV/D) after different D fluence steps of: Top level (a, b): 5.9×10^{23} D/m^2 (2 h exposure time). Middle level (c, d): 6.4×10^{24} D/m^2 (22 h). Bottom level (e, f): 2.1×10^{25} D/m^2 (72 h). In f) also a reference D depth profile is shown in gray. It stems from a sample with only natural oxide that was exposed to 1.6×10^{25} D/m^{2}of gentle plasma. An areal density of 10^{19} atoms/m^2 approximately corresponds to one monolayer of atoms.

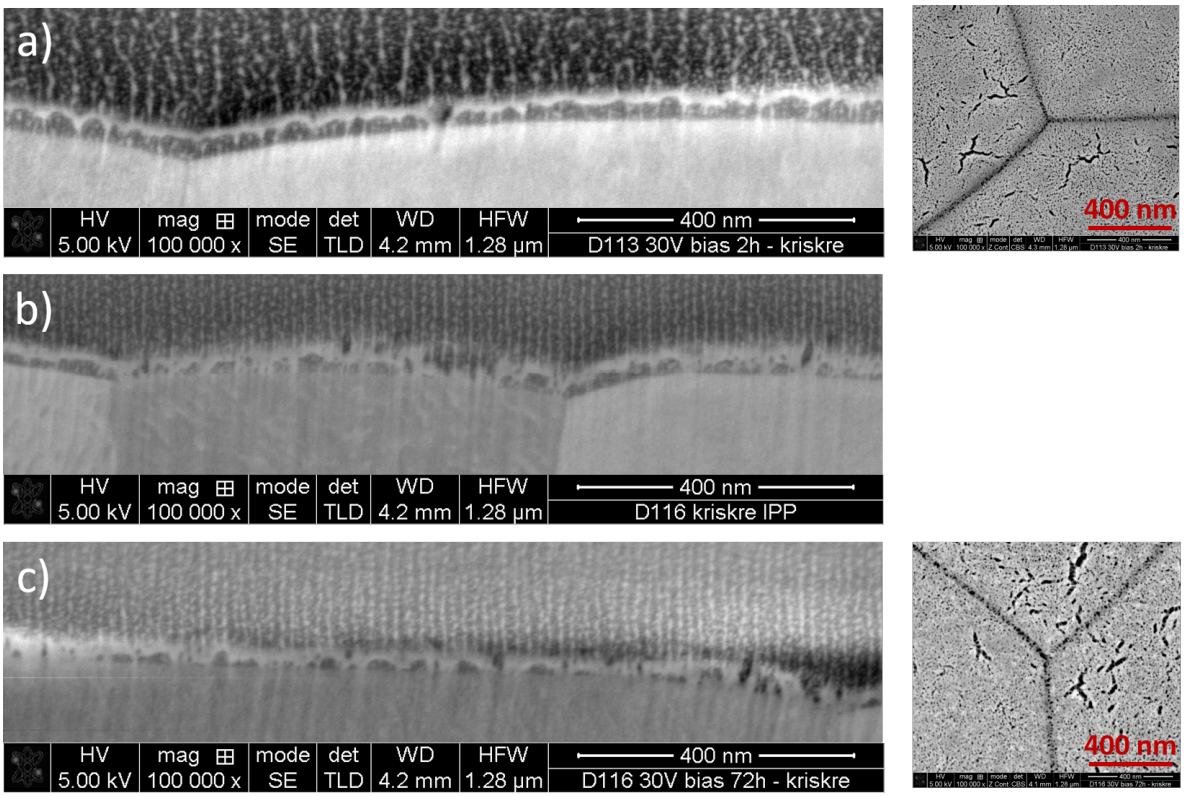

Figure 4.20 – SEM images of FIB cross section through the oxide film (left) and the corresponding top-view image of the oxide film (right) for different D fluence steps with -30 V bias (15 eV/D) at 370 K sample temperature. Fluence steps: a) 5.9×10^{23} D/m^2, b): 6.4×10^{24} D/m^2, c): 2.1×10^{25} D/m^2. The vertical stripes on the cross section images are an artifact of the FIB cut (see section 3.7 for details).

−100V sample bias (38 eV/D): For a sample bias of −100V (38 eV/D) the oxide reduction is even faster and stronger. The oxygen depth profile in Fig. 4.21 a) shows significantly stronger reduction after the first two hours of plasma exposure (6.5×10^{23} D/m^2) than for a similar fluence at −30 V bias. Furthermore, the interface to the metallic W shows signs of reduction. The oxygen concentration at the interface (measured with RBS) is less than the 75 at.% of stoichiometric WO_3. This indicates that the interface is bridged at least in some spots already after the first fluence steps at this high D energy. The corresponding SEM image of the cross section in Fig. 4.22 a) shows two well separable layers of bright W-enrichment zone on top and dark intact oxide below in most places. The bright W-enrichment zone appears to be of similar thickness than after a similar fluence at −30 V bias, but the oxide film shows more roughness, cracks and lateral inhomogeneity. In addition, the top-view images on the right side of Fig. 4.22 a) show stronger and thicker cracks compared with the lower energy. Together these findings indicate that the stronger reduction by higher D energies is mostly caused by the stronger roughening and cracking of the oxide film and not by a thicker homogeneous W-enrichment zone.

The corresponding D depth profile in Fig. 4.22 b) shows that a small amount of deuterium ($4.9\pm0.4\times10^{19}$ D/m^2) is retained in the sample of which about 4×10^{19} D/m^2 is located in the metallic W beneath the oxide (which is indicated in yellow). Due to the short exposure time and low fluence, the D is bound in traps near the surface and could not progress deep into the sample. It can, however, be excluded that it is retained only within the oxide film.

After the second fluence step (to 6.8×10^{24} D/m^2) the reduction has progressed substantially. The corresponding RBS oxygen depth profile in Fig. 4.21 c) shows a state of reduction that is comparable to the state after the highest fluence at −30 V bias (Fig. 4.19 e)) both in the actual oxygen depth concentration and in the overall areal density of the remaining oxide film. The SEM image of the cross section in Fig. 4.22 b), however, shows that the reduction is even further progressed. The remaining oxide film is extremely rough and inhomogeneous. It consists mostly of the bright W enriched layer and has only small and sometimes vertically aligned pockets of darker, not-reduced W oxide. Additionally, the top-view image on the right shows that the cracks have grown strongly and that the surface between the cracks shows strong porosity.

The corresponding D depth profile in Fig. 4.21 d), shows strong D uptake of $67\pm4\times10^{19}$ D/m^2 into the metallic W. This already surpasses the maximum D uptake after the final fluence step at −30 V by more than 75 % although the fluence is a factor of three lower. This shows that the interface between the oxide film and the metallic W is permeable for D at this point.

After the final fluence step (to 2.3×10^{25} D/m^2), the oxygen reduction has reached a completely new stage. The oxygen depth profile in Fig. 4.21 e) shows no gradient in oxygen concentration any more but a homogeneous and strongly W enriched state of 35 % O and 65 % W with an areal density of 126×10^{19} atoms/m^2. The corresponding SEM image of the cross section (Fig. 4.22 c)) shows that the oxide film is almost completely gone. Especially in the middle and middle right part of the image a rough structure is visible on the surface of the metallic W. This seems to be the remaining and fully W-enriched part of the oxide film. Some dark "holes" are visible which are most likely wide (former) cracks. No spots of darker, not-reduced W oxide are visible on the surface anymore and it seems likely that no intact islands of not reduced WO_3 exist in the oxide film any longer. However, the fact that there is still a considerable contribution of oxygen measured by RBS (35 %) in the former oxide film indicates that the W oxide is not fully reduced to metallic W by the D bombardment.

According to NRA, the remaining oxygen areal density is $32\pm2\times10^{19}$ O atoms/m^2, which is about four times higher than the oxygen areal density measured for natural oxide on W before plasma exposure. This suggests that re-oxidation in ambient atmosphere after plasma exposure can only account for about 25 % of the oxygen that is found on this sample. It should, however,

be mentioned that the strong roughening of the remains of the oxide film (see Fig. 4.22 c) may increase the surface area of the W sample, which would increase re-oxidation and could in principle also explain the higher amount of remaining oxygen in the ex-situ measurements. With the present ex-situ diagnostic, it is not possible to clarify whether the measured oxygen is due to stronger re-oxidation, small spots of still intact WO_3 or due to a more homogeneous distribution of a sub-stoichiometric W oxide that is very resistant to both preferential sputtering of oxygen and chemical reduction by D. Unfortunately, the stoichiometry of this remaining oxide cannot be precisely determined due to the lateral inhomogeneity of the remaining film. In areas with deep cracks and thin remaining oxide film, backscattered ions from the underlying metallic W interfere with the signal from the oxide film and thus the W concentration within the oxide film will be overestimated by RBS.

Nevertheless, the D depth profile in Fig. 4.21 f) shows a strong D uptake of $130\pm7\times10^{19}$ D/m^2 into the metallic W after this highest fluence at -100 V bias. This D uptake is close to the fully filled reference sample with only natural oxide ($145\pm8\times10^{19}$ D/m^2), which shows that the oxide film in this highly reduced state is very permeable for D.

Two conclusions can be drawn from these results: 1) It is likely that the oxide film cannot be fully reduced by D plasma under the given exposure conditions (-100 V bias, 370 K exposure temperature and a maximum fluence of 2.3×10^{25} D/m^2) and an oxide with an O concentration of about 35 % remains. 2) The remaining, strongly reduced oxide only slightly reduces D uptake into metallic W. This means that the enthalpy of solution for D in this reduced oxide is high enough (closer to metallic W) for D to cross over the barrier into metallic W at a temperatures of 370 K.

As the probability to overcome the potential energy barrier depends on the temperature of the thermalized D, it may be possible for D to enter the metallic W even across an intact interface at a higher temperature. Such an exposure at an elevated temperature (500 K) has been investigated and is presented in the next section.

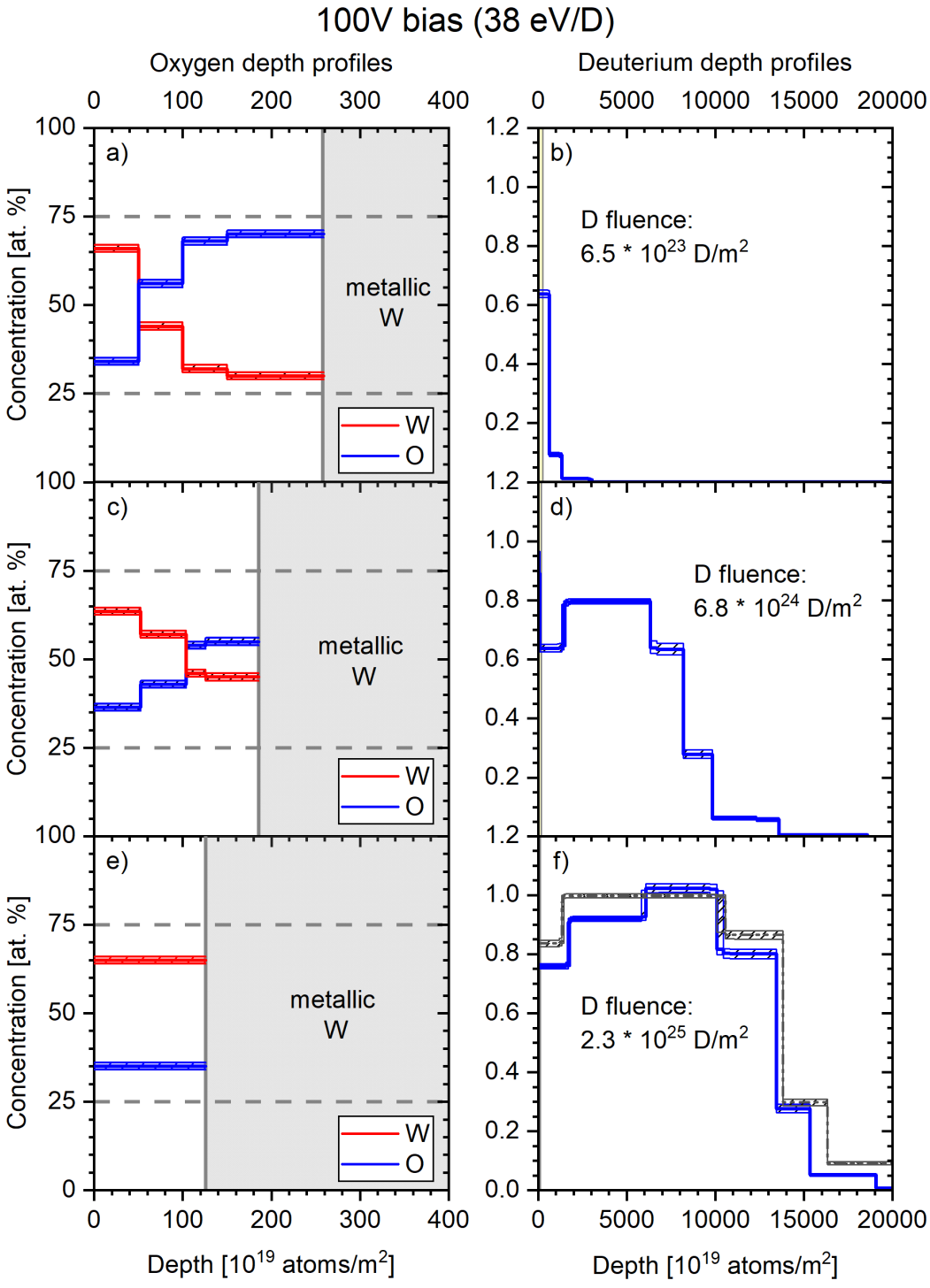

Figure 4.21 – Same as in Fig. 4.19 but for −100 V bias (38 eV/D). Please note the slightly different fluence steps due to the energy-dependent D flux.

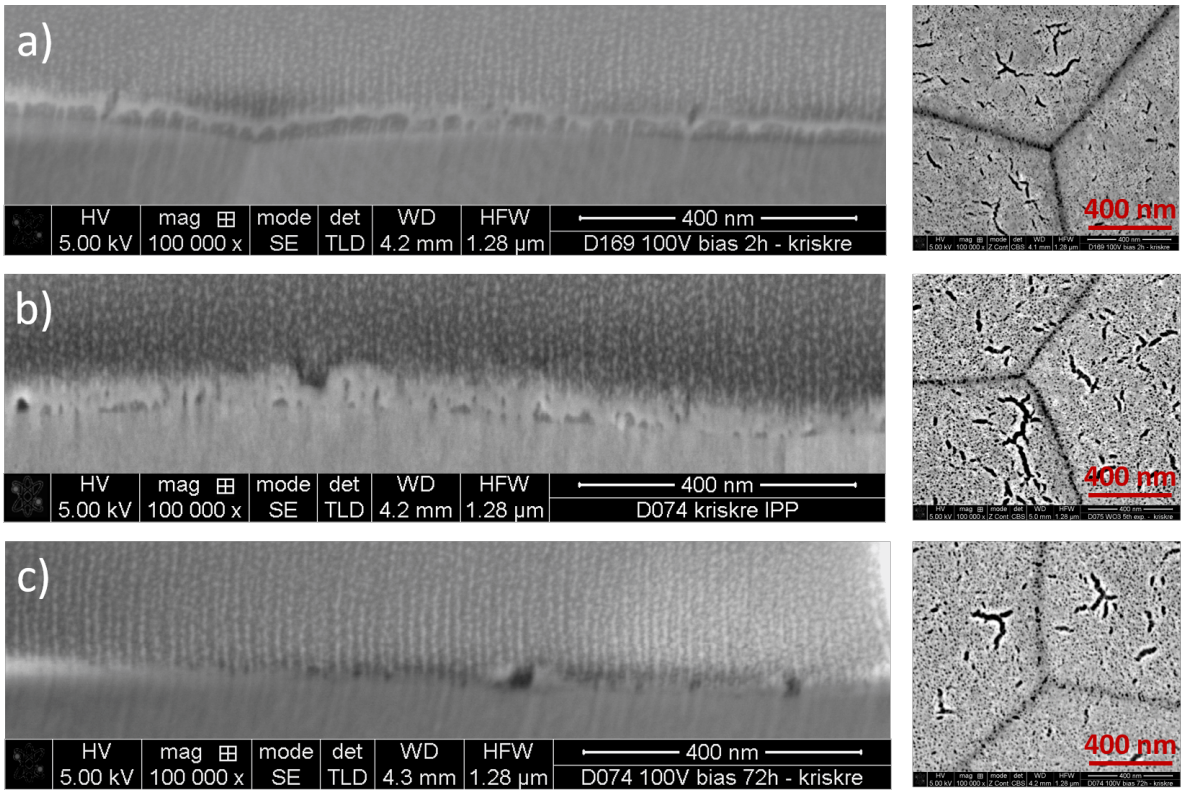

Figure 4.22 – Same as in Fig. 4.20 but for -100 V bias (38 eV/D). a) 6.5×10^{23} D/m^2 (2 h exposure time); b) 6.8×10^{24} D/m^2(21 h exposure time) and c) 2.3×10^{25} D/m^2 (72 h exposure time).

4.4.2 Higher sample temperature (500 K)

The influence of higher sample temperature on D uptake through W oxide is interesting under two aspects: 1) It accelerates the reduction process of the oxide under D plasma exposure (Fig. 4.18) and 2) it might enable D to overcome the potential energy barrier between W oxide and metallic W, even before the oxide is reduced.

Here one sample with 55 nm thick thermally grown oxide (identical to the samples used in section 4.4.1 and to the thick oxide sample used in sections 4.1 to 4.3) was exposed to gentle plasma (<5eV/D) at 500 K instead of the 370 K used before. The sample was exposed for 7 h amounting to a D fluence of 1.4×10^{24} D/m^2, which is identical to the fluence used for the first gentle plasma exposure that is described in section 4.1 and 4.2. Thus, the effects of the sample temperature on oxide reduction and D uptake can be compared directly for otherwise identical conditions.

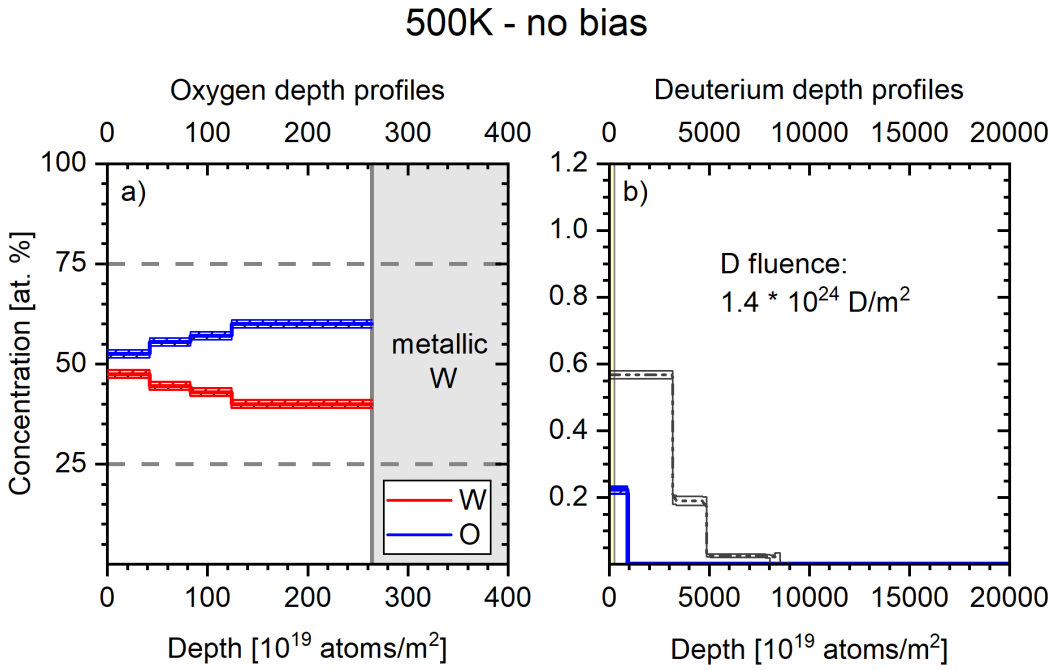

Figure 4.23 – Oxygen (left) and deuterium (right) depth profiles of samples with 55 nm thermally grown oxide film after exposure to gentle (<5 eV/D) plasma at 500 K to a fluence of 1.4×10^{24} D/m^2. The gray profile in b) depicts the D concentration in a reference sample with only natural oxide that was exposed at 370 K but otherwise identical conditions. The reference profile was scaled by a factor of 0.7 to account for the lower fill level of D trapping sites at 500 K and thus allows a direct comparison with of the D uptake of the measured sample.

Fig. 4.18 shows the oxygen loss as a function of D fluence for all D uptake experiments. For the sample exposed at 500 K (orange), the oxygen loss of 195×10^{19} O/m^2 is far larger than the loss for the sample exposed at 370 K under otherwise identical conditions (72×10^{19} O/m^2). This shows that oxide reduction strongly depends on sample temperature and an increase by 130 K increases the oxygen loss by a factor of 2.7. This strong difference poses the question if the oxide reduction at high temperatures resembles the reduction at lower temperature (W-enrichment layer formation, cracking) or if other processes take place.

The corresponding oxygen depth profile in Fig. 4.23 a) shows that the oxide reduction is much more homogeneous compared with previous findings. The reduction zone goes through the

full depth of the oxide film and shows a concentration of 60 % O and 40 % W in its deeper half. While a clear drop in the oxygen concentration is visible near the surface, the reduction there is only slightly stronger than for the exposure at 370 K at floating potential (see Fig. 4.7). However, compared with D exposure at higher D energies at a about a factor of two lower fluence (Fig. 4.19 and 4.21 a)), the surface near W-enrichment zone at 500 K is smaller and less strongly reduced. This shows that D exposure at a higher sample temperature does increase the W-enrichment at the surface, but the effect is less pronounced than for an increase in D energy.

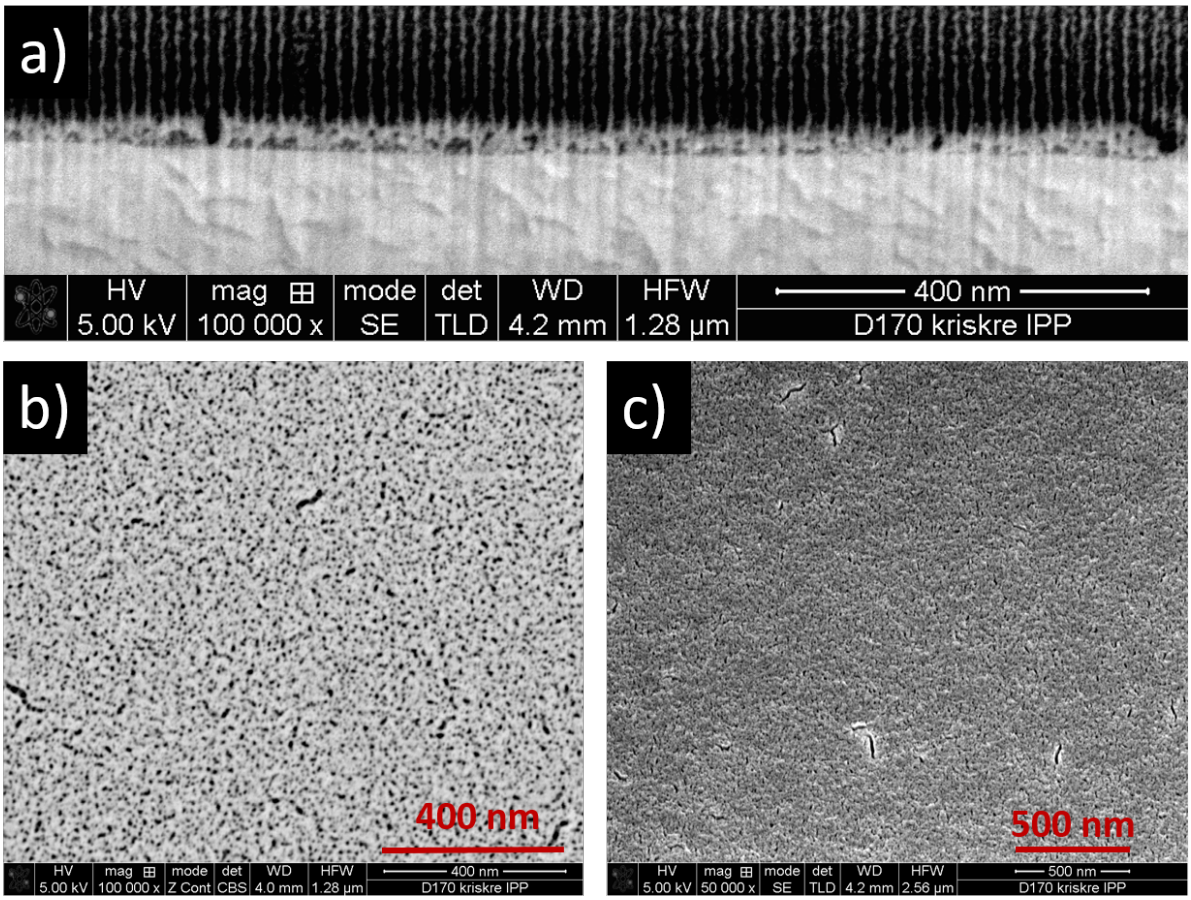

Figure 4.24 – SEM images of an originally 55 nm thick thermally grown W oxide film after exposure to D plasma at 500 K at floating potential (< 5 eV/D) to a fluence of 1.4×10^{24} D/m^2. a) FIB cross section through the film, b) top-view SEM image and c) SEM image of oxide film under 52° to surface normal.

The corresponding SEM image of the cross section through the oxide film in Fig. 4.24 a) shows that the oxide film is significantly roughened at the surface but appears to cover the metallic W almost completely. There are only a few cracks visible in the cross section in image a) or in the top-view images in b) and c), but they go all the way through the oxide to the surface of the metallic W. The image in c) is taken under an angle of 52° towards the surface normal and has a two times lower magnification than b). It shows a strong roughening of the sample surface and the oxide film appears to be spongy with many small pores. The most striking feature, however, is the absence of a clearly separated W-enrichment zone in the cross section in Fig. 4.24 a). In contrast to D exposure at lower temperature, the W-enrichment/oxide reduction is much more diffuse and appears to be spread out through most of the oxide film. However, small spots of darker not-reduced oxide are visible at numerous places throughout the oxide as well. The density of not-reduced oxide spots is lower near the surface and higher at the interface where small islands of not-reduced oxide still cover some of the interface to the metallic W. This more

irregular form of W-enrichment may be caused by the pores which form open pathways for oxygen containing molecules to reach the surface and diffuse into vacuum even from larger depth.

In any case, from the partial coverage of the interface with intact oxide one could expect that D uptake into the metallic W is reduced but not prohibited. The D depth profile in Fig. 4.23 b) indeed clearly shows that D (blue) is located both inside the oxide film and in the metallic W. The D concentration is, however, very low (0.22 at.%) with at total D retention of $2.5\pm0.2\times10^{19}$ D/m. This clearly shows that the oxide film strongly decreases D uptake even in this reduced state at 500 K. However, to make a quantitative estimate of the factor by which D uptake is reduced, the temperature-dependent filling of the traps in the self-damaged W (and also of the oxide) has to be taken into account. According to previous measurements of D uptake into self-damaged W with only natural oxide films at various temperatures under floating potential in PlaQ [83], the maximum D concentration in the self-damaged W is 30 % lower for 500 K than for 370 K. To allow a direct comparison of the reduction of D uptake by the oxide, the D depth profile from a reference sample with only natural oxide that was exposed at 370 K but otherwise identical conditions was scaled by a factor of 0.7 to account for the lower D uptake at 500 K and plotted in gray in Fig. 4.23. The scaled D uptake of the reference sample was calculated to be $22.3\pm1.6\times10^{19}$ D/m^2, which shows that the oxide film reduced D uptake by almost 90 % compared with a sample with only a natural oxide film for the given exposure conditions. This result indicates that even at 500 K, D cannot overcome the difference in enthalpy of solution between the remaining WO_3 and the metallic W.

However, due to the strong reduction of the oxide film at this elevated temperature, it can be expected that most of the intact WO_3 will be reduced at higher fluence, even at this low energy. Based on the oxygen loss at this D fluence (Fig. 4.18) it can be estimated that the oxide reduction per D fluence at 500 K and floating potential (<5 eV/D) is comparable to the oxide reduction at 370 K at a sample bias of −100 V (38 eV/D). Together with the much more diffuse oxide reduction zone (due to the formation of pores) this indicates that also the oxide at the interface will be fully reduced at higher fluence, which would allow mostly unhindered D uptake into the metallic W (similar to the case at −100 V sample bias in section 4.4.1).

4.5 Sputter yield of W from W oxide during D plasma exposure

From the results above it is clear that oxygen is removed from the oxide film during D plasma exposure. The process takes place already for gentle exposure conditions (<5 eV/D, 370 K) and accelerates for higher D energies. However, it is not clear if also W atoms can be removed from the oxide by sputtering with D from the plasma.

As a reminder: The charged D flux in PlaQ consist of 3 % D^+, 3 % D_2^+ and 94 % D_3^+ (see section 3.4). The energy of these (molecular) ions is determined by the plasma potential of approx. −15 V plus the sample bias and is shared equally between the individual D particles in the molecular ions (D_2^+ and D_3^+) when their bond shatters upon impact on the target. Consequently, the D with the highest energy in this work stems from D^+ during experiments with −100 V sample bias. Together with the plasma potential they have a maximum energy of 115 eV. For metallic W the literature value for the sputter threshold by D^+ ions varies between 160 eV [81] and 229 eV [84]. In any case, it is above the highest D energies in this work and it can be assumed that metallic W is not sputtered.

For W oxide on the other hand far lower threshold energies for sputtering of W by D are reported in literature: 65 eV by Guseva et al. [81] and even 15 eV by Roth et al. [82]. The investigation by Roth et al. used a 2 keV, magnetically separated D_3^+ beam, which was decelerated in front of the target, so that a single, well-defined D energy was ensured. The fraction of highly energetic neutralized D atoms in the beam was measured and its effect on the target was corrected. To create W oxide, they introduced a oxygen rich atmosphere (oxygen partial pressure: 1×10^{-2} Pa) in their sputter chamber before and during sputtering with D at room temperature. This created a natural oxide film on the W target but may also have caused sputtering by knock-on oxygen atoms from the gas. They found a sputter yield of 1×10^{-4} W/D for 38 eV/D and a sputter yield of about 2×10^{-4} W/D for 115 eV/D. Guseva et al., on the other hand, created W oxide by thermal oxidation of W at 700 °C which lead to an oxide film of about 50 nm thickness. They measured the sputter yield and threshold energy with field ion microscopy for short D irradiation pulses with a very small D fluence of $<10^{19}$ D/m^2. They used D^+ ions by D gas ionization and accelerated the ions to the target by a short negative voltage pulse. Thus, also in their case, the nominal energy of the D ions is well-defined and other D ion species can be neglected. Due to the short pulses and low fluence, the W oxide should be largely intact WO_3 even after irradiation in their case. They have found a sputter yield of about 1×10^{-4} W/D at a D energy of 115 eV but claim that no W is sputtered for energies of 38 eV. Both these results indicate that direct sputtering of W atoms from the oxide by D ions may take place in the D uptake experiments in this work and both publications agree on the sputter yield at 115 eV/D within a factor of two. However, the results disagree at the energy threshold for sputtering. Since the majority of D (97 %[3]) in the experiments at −100 V bias in the present work has an energy of 38 eV/D, the exact position of the energy threshold for sputtering will have a huge impact on the W sputter rate in this case.

The question whether W is sputtered from the oxide is relevant for two reasons: 1) It may influence the erosion of the oxide film and, if W is indeed sputtered, this will eventually lead to a complete removal of the oxide film for a sufficiently high D fluence. 2) A lower sputter threshold for W in oxidized surface films may cause higher W erosion by the plasma in fusion reactors (if significant surface oxidation occurs in a reactor). In this work, dedicated experiments to determine the sputter yield of W from W oxide have been conducted for energies of 5 to 15 eV/D (floating potential) and 38 to 115 eV/D (−100 V bias). It is, however, not possible to directly determine the W loss from the massive W samples. Weight loss measurements are impaired by the weight loss from oxygen removal and the weight gain by D uptake during plasma exposure. Direct determination of W loss by RBS is also not possible due to the background of the massive W sample.

Therefore, special samples were prepared to determine the W sputter yield. They consist of 15×12 mm^2 silicon plates which are coated with a thin layer of W by magnetron sputter deposition. The surface of the W layer is then electro-chemically oxidized (see section 3.5.2). Thermal oxidation is not possible for these samples due to diffusion and intermixing of W atoms with the Si substrate at elevated temperatures. After the oxidation, the samples consist of a thick Si substrate, a metallic W layer in the middle and a WO_3 film on top.

These samples are then analyzed with RBS to determine the thickness of the oxide film and the underlying metallic W layer with high precision. The uncertainty for W quantification is estimated to be $<1\%$ in the present case. In a next step, the samples are exposed to D plasma in PlaQ at the same conditions as the other D uptake samples, i.e., 370 K sample temperature and floating potential or −100 V bias, respectively. Afterwards, the samples are again measured by RBS and the oxygen and W loss is determined via fitting with SIMNRA [64]. The RBS

[3] The 94 % D_3^+ molecular ions carry 97 % of the total charged D flux.

measurement method is identical to the one used for determining the oxygen depth profiles on the massive W samples and is described in detail in section 3.6.2. Here ^{4}He atoms at 800 keV under an incidence angle of 60° were used.

4.5.1 No sample bias

One of these Si samples with the W and W oxide films upon it was exposed to D plasma at floating potential (5 to 15 eV/D) to a fluence of 1.21×10^{25} D/m^2 (58 h). Prior to D plasma exposure, the sample consisted of a WO_3 film with an areal density (thickness) of $329\pm4\times10^{19}$ atoms/m^2 (44 ± 0.5 nm) on a metallic W layer with an areal density of $147\pm1.5\times10^{19}$ W/m^2 (23 ± 0.3 nm) on a Si substrate. The RBS profiles before and after plasma exposure are shown in Fig. 4.25. In both cases, the oxide is visible by the lower step at the high energy side of the spectra and after plasma exposure also the W-enrichment is visible by the small peak near the cut of energy (see section 3.6.2 for details on RBS). However, the potential W loss from the oxide film cannot directly be determined from the spectra and the data has to be fitted by simulations with SIMNRA to extract quantitative information. Those fits are also shown in Fig. 4.25 and it is clear that they match the data well. The total W areal density in the metallic W and the oxide film before plasma exposure is $229\pm2.3\times10^{19}$ W/m^2 and after D plasma exposure it stayed constant and is $228\pm2.3\times10^{19}$ W/m^2. Considering the uncertainty of the RBS measurement and the fitting with SIMNRA (see section 3.6.2), this shows that W is not sputtered from W oxide by D plasma exposure with D energies of 5 to 15 eV/D.

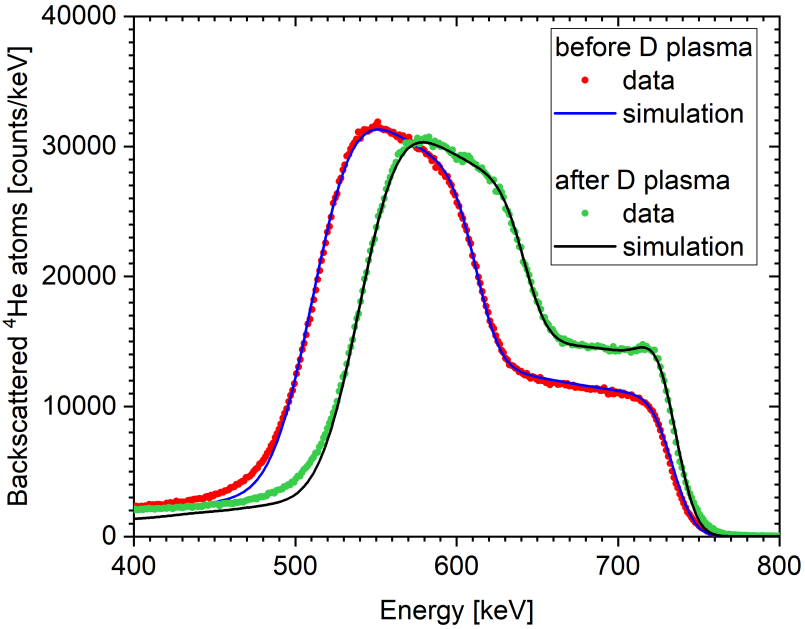

Figure 4.25 – RBS spectra and corresponding SIMNRA simulations for W oxide on W on Si substrate before and after exposure to plasma at floating potential (5 eV/D to 15 eV/D) at 370 K. Spectra taken with 800 keV ^{3}He ions at 70.5 ° angle of incidence. For details on the interpretation of the spectra see section 3.6.2.

Together with the result that the W-enrichment zone reaches a stable state after a certain D fluence at these energies, this indicates that the oxide film will be stable up to a very high D fluence of $\gg 1.6\times10^{25}$ D/m^2 (if it has a sufficiently high initial oxide thickness) and will continue to reduce D uptake under these conditions (gentle plasma, 370 K).

4.5.2 −100 V sample bias

The situation is different for plasma exposure at −100 V bias (D energies of 38 to 115 eV/D). There the initial areal density of the oxide film is $388\pm4\times10^{19}$ atoms/m^2 (52±0.6 nm) and the underlying W film has an areal density of $225\pm2.3\times10^{19}$ W/m^2 (36±0.4 nm). The difference in total W areal density to the first sample (section 4.5.1) comes from slightly different parameters during magnetron sputtering. The difference in oxide thickness is caused by a dark current flowing over the Si sample during electro-chemical oxidation (see section 3.5.2), which varies strongly with the exact placement and contact of the electric clamps to the Si and sputter-deposited W. The resulting oxide film is thicker than for the previous one but still very homogeneous. To assure that the full depth of the W oxide and W film is reliably measured by RBS, the angle of incidence of the ^{3}He ion was reduced to 60°, which reduces the path length of the ions through the film. Nevertheless, the total W amount is very reliably quantified with RBS regardless of the exact thickness of the metallic W layer and the oxide film.

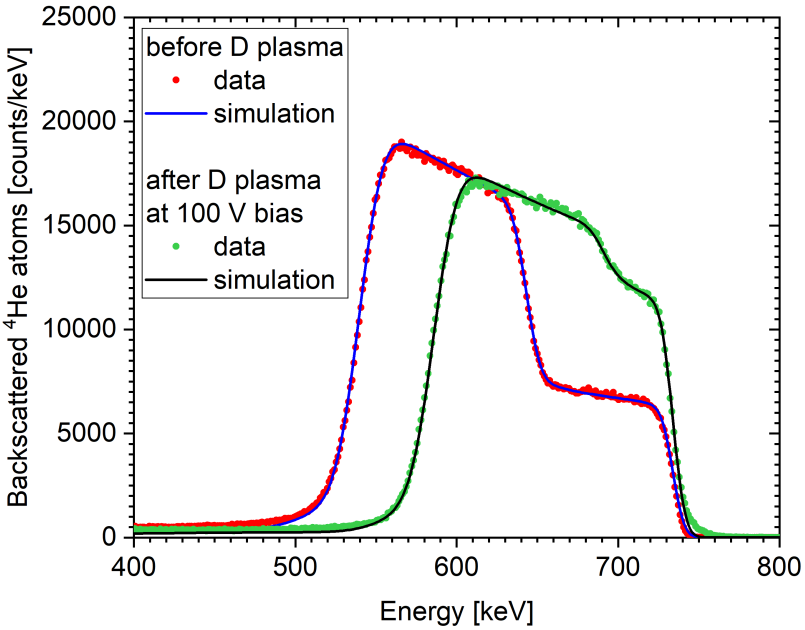

Figure 4.26 – RBS spectra and corresponding SIMNRA simulations for W oxide on W on Si substrate before and after exposure to plasma at −100 V sample bias (38 eV/D to 115 eV/D). Spectra taken with 800 keV ^{3}He ions at 60 ° angle of incidence. For interpretation of the spectra see section 3.6.2.

Figure 4.26 shows the RBS spectra and the corresponding simulations with SIMNRA before and after exposure to D plasma at −100 V bias to a D fluence of 1.6×10^{25} D/m^2 (49 h). As expected, the areal density of the metallic W layer did not change during plasma exposure and was $225\pm2.3\times10^{19}$ W/m^2 in both cases. However, the W areal density in the oxide film dropped from its initial $90\pm1.0\times10^{19}$ W/m^2 to to 78×10^{19} W/m^2 after D plasma exposure. This W loss of 13 % is well above the uncertainty of the RBS measurement method, which shows that W is indeed sputtered from the oxide film at these energies (38 eV/D to 115 eV/D). Under the assumption that W can be sputtered already by ions with 38 eV/D and that the sputter yield is not dominated by the higher energy minority species, the resulting sputter yield is 5.6×10^{-5} W/D. This value agrees within a factor of two with the one found by Roth et al. [82] for 38 eV/D. However, when assuming that only the minority species (3 %) with the highest energy (115 eV/D) contributes to W sputtering, the resulting sputter yield would be 1.9×10^{-3} W/D, which is a fac-

tor of 10 to 20 higher than the values from Roth et al. [82] or Guseva et al. [81], respectively. This discrepancy indicates that the minority of higher-energy D ions is not the sole driver for W sputtering, but that also D ions with lower energy (38 eV) contribute to W sputtering from the oxide.

A very recent work by Tu et al. [85] has also investigated the sputtering of W from W oxide with RBS. They have deposited W oxide directly by magnetron sputtering and investigated the energy range from 50 to 100 eV/D for a lower D fluence of 1.2 to 1.8×10^{23} D/m^2. They found W loss in the range of 1 % and claim to observe a W sputter yield of $2.98\pm1.30\times10^{-3}$ and $5.35\pm2.00\times10^{-3}$ for 50 and 100 eV/D, respectively. This sputter yield is about two orders of magnitude higher than the yield determined in this work. However, the low percentage loss of W observed by Tu et al. seems to be close to the uncertainty limit of the measurement method and their values may have a larger uncertainty than they claim. Furthermore, the ion species distribution in their case was 9.4 % D^+, 86.2 % D_2^+ and 4.4 % D_3^+ and the given energy values correspond to their majority species D_2^+. This means that for both energies they had significant contribution of D^+ ions with double the nominal energy which may have affected the resulting sputter yield.

Another possible reason for the different sputter yields may be due to the larger D fluence in the present work. It is not clear if the sputter yield of W from the oxide changes when the oxide is reduced by the D bombardment. During the plasma exposure at -100 V bias the total areal density of oxygen on the sample was reduced from 291 to 44×10^{19} O/m^2 in the present work. This significant change of the oxide film and the corresponding W enrichment at the surface could affect the binding energy of W in the oxide and thus the threshold energy and sputter yield for W atoms. Indication for such a behavior of the W enriched oxide was also observed during oxide removal with Ar sputtering, which has been described in section 4.3.

As a last point, it should be mentioned that one cannot exclude a contribution from impurity sputtering by oxygen atoms, i.e., oxygen atoms that are sputtered from the sample, ionized by collisions with electrons in the plasma and then accelerated towards the sample by the plasma sheath potential. This possibility is most likely a factor in the study of Roth et al. and less likely for the study by Guseva et al. (due to the short D pulses of only a few microsecond duration) but it can never be ruled out as a contributing factor.

Together all these results indicate that with a sufficiently high D fluence at energies of 38 eV/D or above, oxide films on W can in principle be completely removed including the W bound in the oxide film. However, assuming a constant sputter yield of 5.6×10^{-5} W/D for D exposure at -100 V bias, it would require a D fluence in the order of 10^{26} D/m^2 to completely remove the initial 55 nm thick oxide films that are used for most experiments in chapter 4. As a consequence for the D uptake experiments with -100 V bias conducted in this work, a W loss of about 17 % can be assumed to take place during exposure to the highest measured fluence (2.3×10^{25} D/m^2). The possibility to sputter W atoms at this high energy may also contribute to the much stronger reduction and erosion of the oxide film that has been observed in section 4.4.1 compared with D exposure at lower energies.

4.6 Summary of D uptake through surface oxide film on W

In this chapter D uptake through 33 to 55 nm thick, thermally grown surface oxide films into metallic W was investigated for various plasma parameters. In addition, also the reduction of

the oxide film during D exposure was examined. Several D fluence series were conducted in the range of 10^{23} to 10^{25} D/m^2 for D energies of < 5 eV/D to 38 eV/D at a sample temperature of 370 K. For < 5 eV/D, also a high temperature exposure at 500 K was conducted.

After each fluence step, the D uptake into the oxide and the metallic W was investigated with depth-resolved deuterium concentration profiles based on NRA measurements. To determine the corresponding reduction state of the oxide, the oxygen areal density and the depth distribution of oxygen within the oxide film were measured with ion beam analysis (NRA and RBS). This was supplemented by SEM images of the surface and FIB cross sections through the oxide. Together these methods allow drawing a detailed picture of the dynamics of the oxide reduction during D exposure and the resulting changes of its ability to prevent D uptake into metallic W.

One main results is that as long as metallic W is fully covered by a film of stoichiometrical WO_3, D uptake into metallic W is prevented. This permeation barrier effect is, however, not caused by a limited transport of D within the oxide, but by the interface between W oxide and metallic W. D is thermalized within the W oxide film and cannot overcome the difference in the enthalpy of solution between W oxide and metallic W (see Fig. 4.10). According to a study by Dickens et al. [37] the enthalpy of solution of D in WO_3 is slightly negative and is given by -0.28 ± 0.04 eV. This is much lower than the enthalpy of solution of D in metallic W, which is stated in literature as $+1.14\pm0.04$ eV [29]. Consequently, the difference between the enthalpy of solution for D in W oxide and metallic W is expected to be about 1.4 eV, which is too high for D to overcome at moderate temperatures. This was experimentally validated for sample temperatures of 370 K and was indicated for temperatures of 500 K in this work.

However, D from the plasma (partially) reduces the oxide and, in addition, cracks form within the oxide film during plasma exposure. Both processes degrade the ability of the oxide to prevent D uptake when the reduction reaches the interface. The degradation of the barrier effect is proportional to the fraction of the interface where the oxide is reduced or cracked. It has been found that the speed and extent of the reduction depends strongly on D energy and on sample temperature. For all D energies examined here, a W-enrichment zone forms at the surface of the oxide film and grows to a width of 100 to 150×10^{19} atoms/m^2. Since D is highly mobile within the oxide film [40], this shows that the oxide reduction is not governed by the availability of D but by the diffusion of oxygen-containing molecules towards the surface. If the availability of D would be the rate-limiting step, a uniform reduction throughout the full extent of the oxide film would take place.

The observations in this work indicate that the oxide reduction is a two-step process: First D diffuses through the full film under formation of so-called deuterium-tungsten-bronze D_xWO_{3-x} and then, in a second step, O-containing molecules (most likely OD or D_2O) form and diffuse towards the surface. However, the reduction process is slowed down by the W-enrichment zone, as oxygen from deeper inside the film has to diffuse through it to reach the surface and be released. Consequently, the oxygen loss rate for all exposure conditions is largest at the beginning of the D plasma exposure and then slows down with increasing fluence as the W-enrichment zone grows.

For exposure to gentle D plasma (<5 eV/D, 370 K), initially 33 and 55 nm thick oxide films reach a stable state when the W-enrichment zone at the surface prevents further reduction. In this case, the interface to metallic W is still fully covered by intact WO_3 and would prevent D uptake into metallic W in principle indefinitely. However, at a very high fluence of 1.6×10^{25} D/m^2, cracks growing through the oxide film begin to reach the interface to the metallic W and D can enter the metal at these spots. Since the cracks cover only a small fraction of the surface area, the D uptake is still strongly reduced by 97 % and 99 % for the thin and thick oxide films, respectively, compared with a reference sample with only natural oxide.

At higher D energies (15 and 38 eV/D) or sample temperatures (500 K), the oxide reduction progresses significantly faster and laterally more inhomogeneous. Eventually the reduction reaches the interface to the metallic W and D can enter the metal. After plasma exposure at 15 eV/D to the highest fluence of 2.1×10^{25} D/m^2, a large fraction of the interface area is still covered by not-reduced oxide and D uptake is reduced by 74 % compared with the reference sample. For exposure at −100 V bias (38 eV/D), however, the D uptake after the highest fluence of 2.3×10^{25} D/m^2 is almost the same as for the reference sample and the permeation barrier effect of the oxide has almost vanished. At this point, the oxide film on the sample is no longer visible in FIB cross sections, but the RBS-based oxygen depth profile shows a thin layer consisting of approximately 35 % oxygen and 65 % tungsten on the surface. With the current ex-situ diagnostics, it is not possible to clarify whether the oxide film is fully removed during plasma exposure (the measured oxide could be caused by increased natural re-oxidation due to an increase of the surface area during plasma exposure) or if a thin layer of oxide remains on the sample surface even during plasma exposure. In any case, the oxide is either fully removed, or does at least not significantly hinder D uptake into metallic W. The areal density of this remaining layer is 126×10^{19} atoms/m^2 and thus much larger than the implantation depth of D into the material, even if one conservatively assumes the same implantation depth as in WO_3 (7.1 nm for 115 eV/D) but assumes the density of metallic W for the thickness of the layer (20 nm). This indicates that if some oxide survives during plasma exposure, the difference in the enthalpy of solution for D between the remaining, strongly reduced oxide and metallic W is sufficiently diminished for D to cross the interface after it is thermalized within the reduced oxide.

In addition also the sputter yield of W from W oxide by D has been examined. The results show that for floating potential (5 eV/D) no W is sputtered from the oxide and only oxygen is lost. However, for higher energies (38 eV for the majority D species and up to 115 eV for the minority) W is indeed sputtered from the oxide, although the energy is not sufficient to sputter W from a metallic W lattice. This shows that for D plasma exposure at this energy the oxide is not only reduced but also eroded by sputtering of W atoms. This implies that for these or higher energies, the oxide film can be completely removed from metallic W.

4.7 Implications for natural oxide films and outlook

The above discussed results show that the natural oxide will be reduced very fast even by gentle (5 eV/D) plasma exposure at 370 K. Since it was shown that the oxygen loss is fastest at low D fluence, it is likely that the natural oxide will be fully reduced for an even lower fluence than the $1.6\pm0.4\times10^{23}$ D/m^2 estimated from the first experiments (see section 4.1). For higher D energies or sample temperature, the reduction process is accelerated further.

However, the results also indicate that even after plasma exposure at higher D energy at a significantly higher fluence, a thin oxide layer with an approximate composition of 35 % O and 65 % W remains on samples with an initially 55 nm thick oxide film. This indicates that also for the reference samples with only natural oxide films, a small amount of not-reducible oxide may remain on the surface after D plasma exposure. While the experiments at high D energy have shown that after reduction of the oxide to this state the D uptake is no longer significantly reduced compared with a natural oxide, no direct comparison to a W sample without any oxide was possible during the ex-situ experiments conducted in this work. In order to fully exclude an influence of this possibly remaining oxide on D uptake in W, it would be necessary to use an in-situ experimental setup capable of combining sputter removal of the natural oxide, D plasma

exposure and ion beam analysis of the D and O content in a single device.

According to NRA measurements, the natural oxide film on W has an areal density of only $8.4 \pm 1.2 \times 10^{19}$ atoms/m^2 (corresponding to 1.2 nm of WO_3) and it can be assumed that this thickness decreases during reduction. Assuming a reduction to a ratio of 35 % O to 65 % W, the resulting areal density of the reduced natural oxide would be 3.2×10^{19} atoms/m^2, which corresponds to a thickness of 0.5 nm (conservatively) assuming the same density as for WO_3. This is below the implantation depth of D even for the gentle conditions (0.7 nm for 5 eV/D). Consequently, one can assume that in this case the remaining reduced natural oxide will not be a barrier for D uptake in the sense that it prohibits D from entering metallic W. The remaining oxygen on the surface could, however, influence the out-diffusion of D that is implanted directly below the surface during plasma exposure and thus alter the total D uptake. Such effects could, however, not be measured with the current experimental setup and a thorough treatment of this remaining open question would also require an in-situ experiment with the above mentioned capabilities.

Chapter 5

D release through thin tungsten oxide films

This chapter discusses the effects of thin (5 to 100 nm) surface oxide films on the thermal release of D from ion-damaged W. D release studies are commonly used to determine the total D retention in (damaged) W and to quantify the binding energies of D in material defects. Any effects of a (natural) oxide film on the D release behavior would affect these values and pose an unaccounted discrepancy between the ex-situ laboratory studies and a reactor scenario. Therefore, it is important to estimate at which thickness (or quantity of oxygen) surface oxide films significantly influence the release spectra

As for the experiments for D uptake, W samples with high purity (99.97 wt.%) were prepared by polishing, annealing and self-damaging with W ions, as described in sections 3.2 and 3.3. Differently than for the uptake experiments, the defects in the material were decorated by exposure to gentle D plasma in PlaQ prior to oxidation, so that the self-damaged zone could act as a D reservoir (see section 3.4). In a next step, the D-filled samples were oxidized electro-chemically at room temperature, to avoid thermal release of D during the oxidation process. The electro-chemical oxidation method also yields WO_3 but in amorphous form and with a homogeneous oxide thickness (see section 3.5.2). Lastly, the outgassing of D through the oxide films was investigated by thermal desorption spectroscopy (TDS; section 3.9). After each step, the D and O amounts in the samples were measured by nuclear reaction analysis. In addition, the reduction of the oxide films after TDS were investigated by SEM imaging of the surface and of FIB cut cross sections through the film.

The results shown in this chapter are based on a previous publication by the author and others [86].

5.1 Effects of high temperature (1000 K) annealing on electro-chemically grown W oxide films

During TDS measurements, the samples experience high temperatures up to 1000 K, which in itself may already facilitate significant changes within the oxide film. To quantify the effect that the outgassing of D has on surface oxide films on W, it is necessary to separate these thermally-induced changes from D-induced changes. Therefore, “empty” samples (batch three; see section 3.4) without D but with thermally and electro-chemically grown W oxide films were exposed to a standard TDS cycle with a heating ramp of 3 K/min to 1000 K and were held at this temperature for 3 h. The changes in the oxide film were investigated via SEM imaging and NRA measurement of the oxygen areal density. The samples from this third batch were only polished and oxidized but not self-damaged or D-filled.

SEM imaging: Fig. 5.1 shows SEM images of a 40 nm thick, electro-chemically grown W surface oxide before and after heat treatment (3 K/min ramp to 1000 K and holding for 3 h at this temperature). The images were both taken in SE mode and have the same magnification but show two different spots on the same sample. In image a), before heat treatment, four different W grains are shown and the grain boundaries are clearly visible. All grains are covered by a homogeneous, smooth oxide film as expected after oxidation (compare with section 3.5.2). After annealing to 1000 K (image b)), the sample shows a crystalline-like, striped surface structure. This can be interpreted as a temperature-induced transformation of the originally amorphous, electro-chemical oxide to a nano-crystalline oxide. Such a transformation has been previously reported in literature and is stated to take place at temperatures above 660 K [87]. Furthermore, small cracks have formed on isolated spots in the oxide film. As the SEM image in Fig. 5.1 b) is taken in the edge-sensitive SE mode, the edges of these cracks appear bright. In some cases, the cracks are wider and enclose small areas that appear to be depressions. It seems likely that in these cases small portions of the metallic W surface lie uncovered. Examples for such areas are marked by the arrows in Figure 5.1 b).

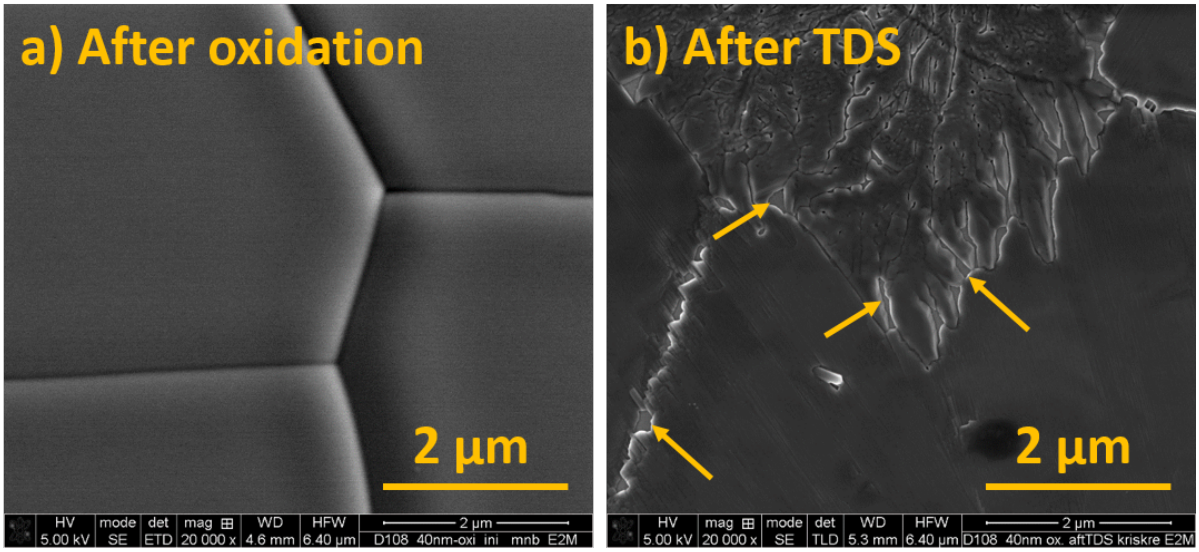

Figure 5.1 – SEM top-view images of a D-free W sample with a 40 nm thick electro-chemically grown W oxide film: a) directly after oxidation, b) after exposure to the same TDS procedure (3 K/min temperature ramp to 1000 K in vacuum) that was used for the D-containing samples. The arrows mark cracks in the oxide film, were the underlying metal appears to be exposed. Both images are taken in SE mode.

The same trend is visible for a thinner 20 nm thick electro-chemically grown oxide, which is shown in the appendix A.5. It should, however, be noted that the thin (20 nm) electro-chemical oxide shows more small areas where the oxide film has de-laminated and the metallic W is visible compared with the thicker (40 nm) film shown in Fig. 5.1. Nevertheless, also there the oxide film is mostly still intact. For comparison, also a 30 nm thick thermally grown oxide film has been studied (images in the appendix Fig. 5.1). In this case, the oxide film is mostly intact and only small regions with snowflake-like cracks in the oxide film are visible after heating.

NRA: The results of the NRA measurement of the oxide areal densities before and after the high temperature exposure are listed in Tab. 5.1. They show no or only a very minor loss of oxygen for the thick (40 nm) electro-chemically grown oxide and for the thermally grown oxide (33 nm). For the thin (20 nm), electro-chemically grown oxide, the oxygen loss in the order of

10 %, which is in accordance with the SEM images (A.5). This confirms that up to 1000 K, the oxygen amount on the samples is (mostly) stable and no or only small amounts of oxygen are lost due to, e.g., evaporation of WO_x molecules. Consequently, any significant loss of oxygen during TDS with D-filled samples must stem from interaction with the outgassing D.

Sample	Oxygen areal density (10^{19} O atoms/m^2)			
	As grown	After 1000 K	Difference	Difference (%)
20 nm electro-chem. ox.	117.9±2.8	104.4±2.7	13.5±3.9	12±4
40 nm electro-chem. ox	226.8±3.5	221.0±3.5	5.8±5.0	2.5±2.2
30 nm thermal ox.	163.8±3.1	166.8±3.2	-3.0±4.5	-1.8±2.8

Table 5.1 – NRA measurements of oxygen areal density of "empty" (D-free) samples with different surface oxides before and after exposure to 1000 K during TDS.

5.2 Deuterium depth profiles

This part focuses on the evaluation of the D depth profiles that were obtained by NRA in chronological order of the experimental steps; i.e, after D loading, after oxidation and after TDS. For each measurement, a different spot on the sample was chosen to exclude ion-beam-induced effects on subsequent measurements. The profiles are shown for one representative sample with an oxide thickness of 100 nm, but all other samples behave in the same fashion. Details of the D depth profiling technique with NRA and its uncertainty quantification are described in Section 3.6.1.

The first D depth profile was determined after the defects in the self-damaged W were decorated by exposure to gentle D plasma (5 eV/D) D at 370 K, but before oxidation[1]. It is represented by the black line in Fig. 5.2. The maximum D concentration is determined by the material defects that follow the damage profile, which is represented by the gray dashed line (with units on the right y-axis). Note that the defect concentration saturates above a certain damage level and the D concentration is thus flat-topped [5]. Therefore, this shape of the D retention is expected and coincides well with previous measurements on such samples under identical conditions [6]. The D concentration in the self-damaged zone is about 1.6 at.% and the areal density of D in this sample is $196\pm6\times10^{19}$ D/m^2. Furthermore, it is evident that the D concentration in the bulk W is negligible in comparison to the D concentration in the self-damaged zone.

The red line in Fig. 5.2 represents the D depth profile measured after the electro-chemical oxidation. In the self-damaged zone, it coincides very well with the previous profile (black), which indicates that the D remains trapped in the defects there. However, at the surface where W is converted to W oxide (light gray area), the D concentration is significantly lower (0.14 at.%) than for the first (black) D profile. This shows that most of the trapped D is released from W when it is converted to oxide. However, since this affects only a small portion of the D-containing self-damaged area, the total amount of D in the sample stays constant within the measurement uncertainty and lies at $197\pm6\times10^{19}$ D/m^2 after oxidation. Thus, the fraction of D

[1] A natural oxide film is of course present on the sample, but cannot fully prevent D uptake during plasma exposure (see chapter 4).

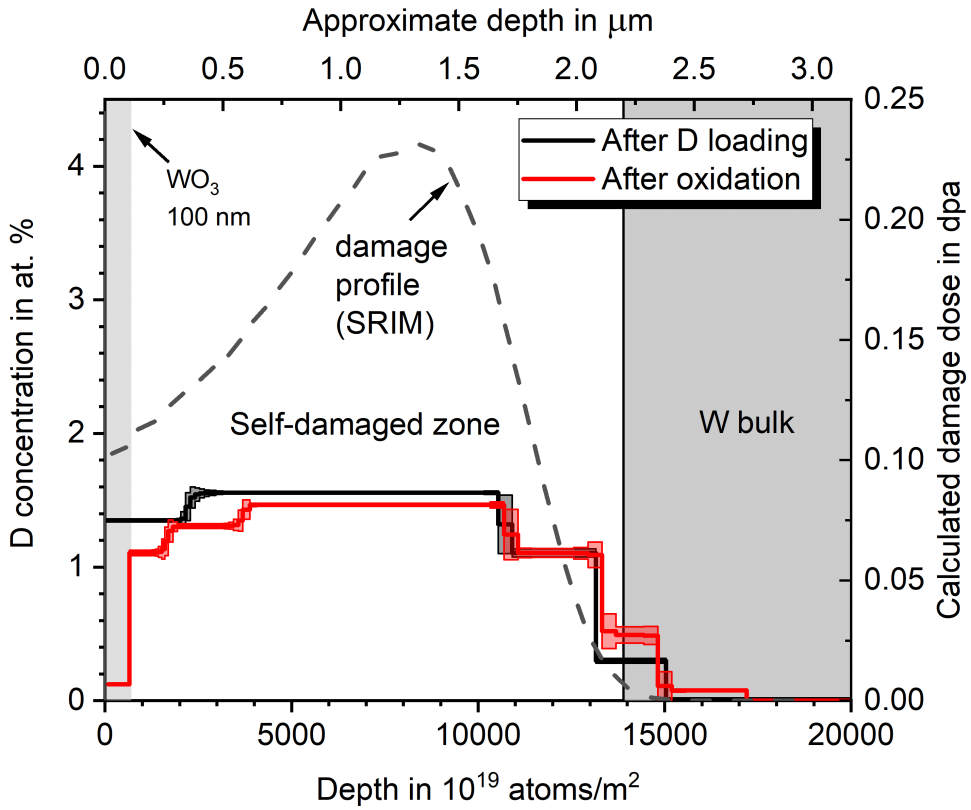

Figure 5.2 – D depth profiles of a 100 nm thick electro-chemically grown oxide after D plasma exposure (black) and after oxidation (red). The lower x-axis shows the areal density and the upper x-axis shows the approximate depth from the surface assuming a W oxide density of 7.26 g/cm^3 and W bulk density of 19.25 g/cm^3. The dashed gray line shows the calculated damage profile in dpa according to SRIM (units on the right y-axis). The light gray area on the left marks the oxide film after oxidation and the dark gray area on the right marks the un-damaged bulk W.

that is released during electro-chemical oxidation is negligible, as intended with this oxidation method at room temperature.

A third NRA measurement was performed after TDS exposure to 1000 K for all samples. In all cases, no remaining D was detectable with NRA which shows that all D was completely released from the samples during TDS.

5.3 TDS results

This section will discuss the TDS experiments with temperature ramps of 3 K/min up to 1000 K for various oxide thickness from 5 to 100 nm. Details on the TDS setup or measurement procedure can be found in section 3.9.

5.3.1 QMS signals of the natural and 100 nm oxide sample

To illustrate the effects that oxide films have on TDS spectra, it is instructive to compare a sample with only natural oxide (reference) with a sample with a 100 nm thick oxide film. Figure 5.3 a) shows such a comparison and depicts the background subtracted quadrupole mass

spectrometer (QMS) signals of mass channel 3 (HD) and 4 (D_2) (left y-axis) as function of time for the natural oxide (black) and the 100 nm thick oxide (red). The thin gray line (right y-axis) shows the temperature ramp.

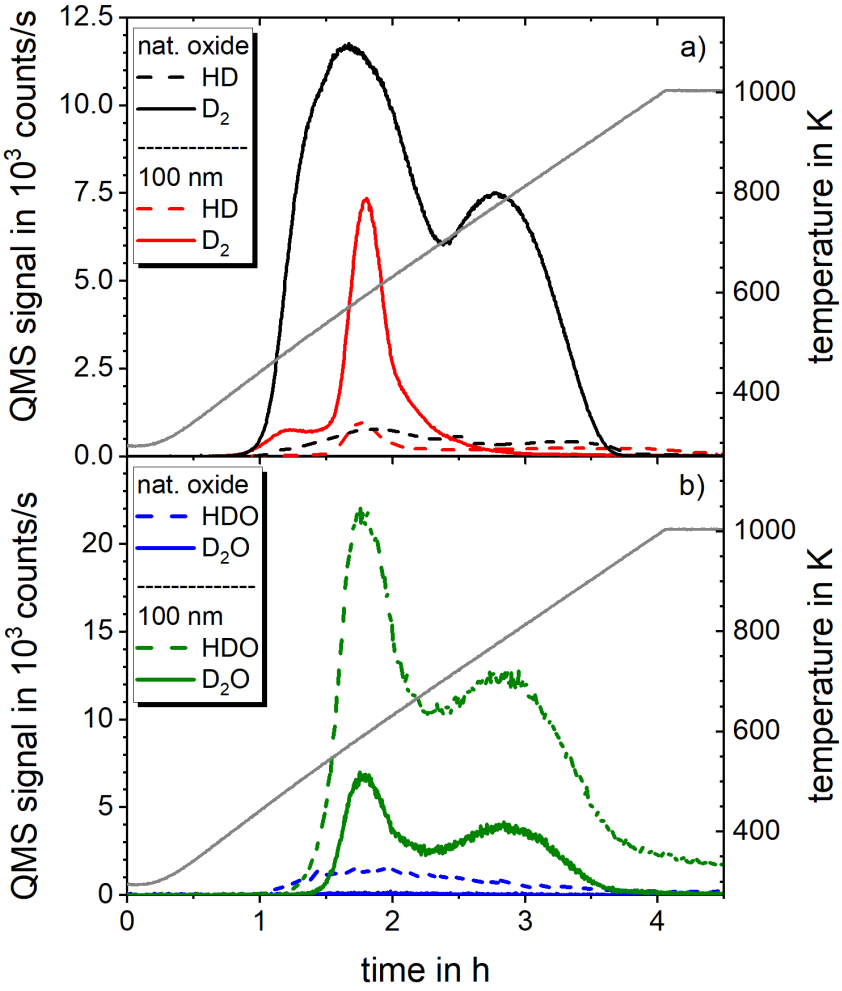

Figure 5.3 – Background-corrected QMS signals of natural oxide and 100 nm thick oxide during a 3 K/min ramp to 1000 K: a) D_2 and HD signal; b) HDO and D_2O signal (heavy water). The temperature ramp is indicated in gray with units on the right axis.

The D_2 signal for the natural oxide (solid black line) shows two distinct peaks, which coincide well with previous studies of such samples [6, 14, 15]. The double peak structure shows that D is trapped either in different defect types or in defects with multiple, fill-level-dependent trapping energies in the self-damaged zone. Depending on the trapping energy, D is released at higher or lower sample temperature. Furthermore, the onset of D release occurs at 410 K, which is as expected, since the samples were plasma-loaded at 370 K and traps that can release D at this temperature have already done so during the loading.

The QMS signal from the 100 nm thick oxide (red lines) shows a strongly different release behavior. The HD and D_2 signals seem to be much weaker for the oxidized sample, especially for high temperatures. While the onset of D release starts at the same temperature for both samples, the signal of the 100 nm oxide rises much slower and stays at a constant and low plateau from 475 K to 540 K before it starts to rise again. The maximum of the first release peak occurs significantly later (at 595 K) and is significantly lower than for the reference sample, which reaches tits maximum already at 565 K. After the first peak, the D_2 signal of the 100 nm oxide strongly decreases with temperature and stays far below the signal of the natural oxide

until it vanishes at about 825 K. Especially, the second D_2 peak (which is measured for the natural oxide sample at 770 K) has completely vanished for the oxidized sample. Integrating over time, there are about 80 % less D_2 counts for the 100 nm oxide than for the natural oxide sample. The HD signal behaves qualitatively similar as D_2 but on a much lower level.

This shows that the presence of a 100 nm thick oxide film on the surface has a strong influence on the D release from W. Furthermore, since the D depth profiles from NRA show that all D is released from the sample after TDS to 1000 K (see section 5.2), this result immediately raises the question what happened to the remaining D, as it obviously was released in a form other than D_2 or HD.

Figure 5.3 b) gives a possible answer to this question. It shows the QMS signals of mass channels 19 (HDO) and 20 (D_2O) for the same two samples. For the natural oxide, virtually no D_2O is detectable and only small amounts of HDO are released. For the oxidized sample, this is clearly different and there are strong signals for HDO and D_2O. Furthermore, these heavy water signals again show two clear peaks, similar to the D_2 release from the natural oxide sample. The first notable increase of the heavy water signal is measured at a temperature of 475 K, which coincides with the start of the plateau phase of the D_2 signal. and the first peak is reached at about the same temperature as the first D_2 peak. The second (high temperature) peak reaches its maximum at the same temperature as for the natural oxide sample (770 K), although it now consists only of heavy water instead of D_2 or HD.

This clearly indicates that D interacts with the oxide film during release and that it is converted to heavy water species during the release process. However, since Fig. 5.3 shows background subtracted QMS counts, the results are so far only qualitative. Nevertheless, these results also show that for low temperatures (first peak) D is not partly converted to heavy water and the release is delayed to higher temperatures or later times. At high temperatures (second peak) the release is not delayed (same peak position for natural oxide and 100 nm thick oxide) but the D is (almost) completely converted to heavy water species before it is released.

No significant contribution was detected in any of the other measured mass channels.

For further understanding of this conversion mechanism it is necessary to quantify the heavy water contribution. Typically, calibrating and hence quantifying water molecule fluxes is not possible or requires at least a special setup, as these molecules can stick onto the chamber walls on their way to the QMS [88]. However, due to the additional NRA measurements of the total D amount in the samples before and after TDS, such a calibration was possible in the present case. As discussed in section 3.9, the comparison of the total amount of released D (NRA) with the amount of D released as HD or D_2 (TDS), allows to obtain the absolute amount of D released in form of HDO and D_2O during TDS. This value can then be related to the measured counts in mass channels 19 and 20 to yield the calibration factors for heavy water. Based on these calibration factors, absolute fluxes of D/s in the form of D_2, HD, HDO, and D_2O will be discussed in the following sections.

5.3.2 Reactions of outgassing D with oxide and production of heavy water

Fig. 5.4 shows the quantified out-flux of D in the unit of D-atoms/s for electro-chemically grown oxide films with small thicknesses up to 15 nm. The graph depicts: 1) D-containing molecules without oxygen (the sum of HD + D_2, solid lines) and 2) heavy water molecules (the sum of HDO + D_2O, dashed lines). For comparison, a reference sample with only natural oxide is included (blue lines).

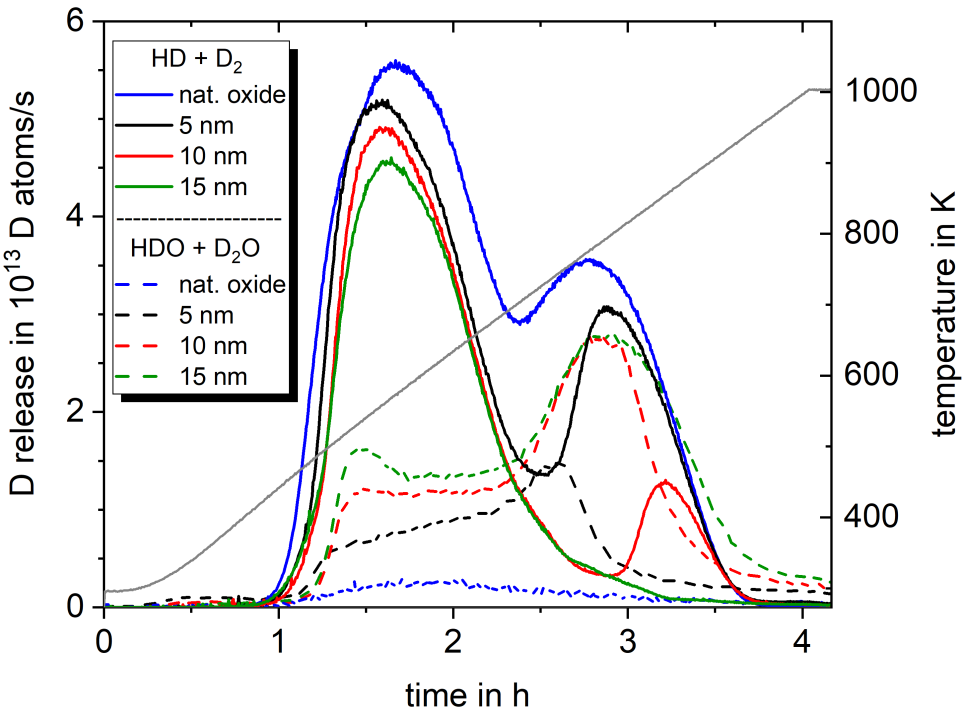

Figure 5.4 – Quantified D release in form of deuterated molecular hydrogen isotopes (HD + D_2; solid lines) and heavy water (HDO + D_2O; dashed lines) for thin oxide samples with varying thickness of the oxide film. The temperature ramp is indicated in gray with units on the right axis.

For the sum of the HD and D_2 desorption, a small shift to higher temperatures of the first release peak is visible with increasing oxide thickness, which indicates a delay of the D release. The reference sample was exposed in a different batch and its release signal is thus slightly shifted, with respect to the other samples. Furthermore, one can see that D release in form of heavy water molecules sets in already during the low-temperature peak at about 490 K. It forms a sharp step-like rise, followed by a relatively constant plateau up to about 700 K. The height of the plateau increases with increasing oxide thickness. For the natural oxide, no such feature is visible and the release of heavy water stays very low during the full TDS. This serves also as a check, that the heavy water signals of the oxidized samples is not just created from reactions of desorbing deuterium with possible oxygen contamination of the chamber walls, but stems directly from a reaction of outgassing D with the oxide film on the samples. This clearly shows that already at relatively low temperatures (490 K) the outgassing D chemically reacts with the oxide film and produces heavy water.

The behavior of the second peak, however, is even more curious. There, the sum of the HD and D_2 desorption shows a clear peak for the natural oxide (solid blue line), which becomes smaller and appears later with increasing oxide thickness until it completely vanishes for the 15 nm thick oxide (solid green line).

Since D is already thermally de-trapped from the defects in the self-damaged W at these temperatures, the D that is "missing" from the HD and D_2 desorption flux in the second peak has to be released in form of other volatile species, i.e., heavy water molecules. And indeed, the dashed lines which represent the heavy water molecules show a rise when the HD + D_2 signal in the second peak is lower than expected from the natural oxide. The green lines (15 nm oxide) clearly show that for temperatures above 700 K, D is released almost exclusively as heavy water. In this case, the oxide film is thick enough to supply enough oxygen to interact with all released

D. The situation changes for the 10 nm thick oxide (red lines). Here, the heavy water signal drops roughly at 3 h (about 800 K). This drop is accompanied by an increase in HD and D_2 desorption, which indicates that the oxide on the surface has been fully reduced to heavy water species and released into vacuum. Once the oxide is fully removed, the remaining D desorbes in form of HD and D_2 in the same way it would do for a sample with only natural oxide. For the 5 nm thick oxide (black lines) this effect is even more pronounced and the changeover sets in at a lower temperature, as less oxygen is available and the oxide is fully reduced earlier.

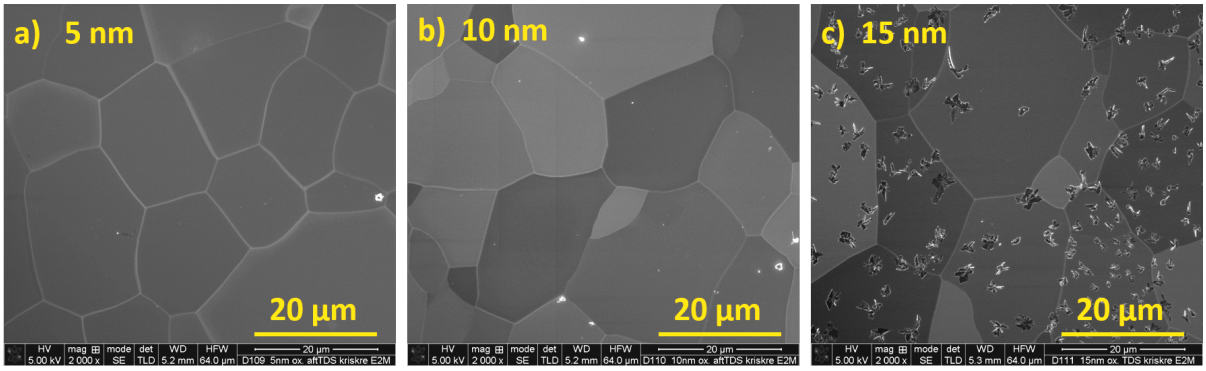

Figure 5.5 – SEM images in SE mode of the second batch of self-damaged, D loaded and electrochemically oxidized W samples after D release during TDS up to 1000 K. In all images different W grains are visible in different shades of gray and the grain boundaries appear as slightly brighter lines between them. In a) and b), the thin surface oxide films (originally 5 and 10 nm, respectively) are completely removed. In c), some remnants of the originally 15 nm thick oxide film remain. They are distributed in small islands on the otherwise clean W surface.

The assumption that the observed rise of the HD + D_2 signal occurs only after all oxygen in the oxide film is consumed is supported by the SEM images of the sample surface after TDS, which are shown in Fig. 5.5. For the originally 5 and 10 nm thick oxide films in Fig. 5.5 a) and b), the oxide is completely removed from the surface. For the originally 15 nm thick oxide film in Fig. 5.5 c), however, some oxide is remaining on the surface. This is in agreement with the interpretation of the TDS spectra for this sample, where heavy water production continues until all D is released from the sample. Obviously, all D stored in the self-damaged zone underneath the oxide was completely released before all oxygen available in the oxide film was converted to heavy water.

The remaining oxide in Fig. 5.5 c) is not distributed homogeneously across the W surface, but is clustered in small islands on an otherwise oxide free W surface[2]. Please also note that for SEM imaging, the samples were carried through air and thus a natural oxide film (invisible in the SEM images) has re-formed on the sample surface. The oxide islands visible in Fig. 5.5 c) cover a much smaller fraction of the surface area than the clean W. However, the dominant release channel of D towards the end of this TDS run was still heavy water. This observation indicates that although most of the D reaches the surface at a spot where the oxide was already removed, the D atoms diffuse across the surface until they reach an oxide island where they form heavy water before being released. The average distance between two neighboring oxide islands is in the range of several µm to several 10 µm. This indicates a high mobility of D

[2]Please note that for this apparently "oxide free" surfaces it might be possible that the last one to two monolayers of oxygen are more strongly bound than the rest of the oxide and thus might remain on the surface, even during D release at high temperatures. Therefore, the terms "oxide free" or "clean" are used here only to denotes that surfaces have no more than one or two monolayers of oxide.

atoms on the sample surface. It should be noted that D atoms that reach the surface cannot immediately desorb, but have to find another D atom and recombine to a D_2 molecule before they can be released as molecule (see section 2.1). As only minor contribution of D_2 and HD are visible in the D release as long as oxide is present, the mean free path of D on the W surface is larger than 1–10 µm before it meets another D atom. This also indicates that D that reaches an oxide island is bound there and remains until a second D atom reaches the spot and forms a water molecule that is then released.

Oxide thickness in nm	O amount in 10^{19} atoms/m^2	O/D ratio in %
natural oxide	8.4 ± 1.2	4.2 ± 0.5
5	30.0 ±1.4	13 ± 0.7
10	59.8 ± 1.9	26 ± 0.9
15	84.4 ±2.2	37 ± 1.0

Table 5.2 – Ratio of oxygen to D for different oxide thicknesses

Furthermore, the results in this section allow an estimate of when surface oxides become relevant for D release signals in TDS in general. As heavy water quantification in TDS is very difficult, the D_2 and HD signals are often the only ones that can be evaluated quantitatively. Therefore, it is important to estimate at which thickness (or quantity of oxygen) surface oxide films significantly influence the release spectra of these two mass channels. From Fig. 5.4 it is obvious that even the 5 nm thick oxide film significantly alters the $D_2 + HD$ spectra; especially the position and magnitude of the high temperature peak. For the natural oxide, on the other hand, the ratio of heavy water signal to $D_2 + HD$ signal is negligibly small and it can be assumed that the release behavior is not strongly affected. However, it is important to keep in mind that the present study used self-damaged W, which has a D retention that is orders of magnitude higher than for un-damaged W. Thus, for experiments that use un-damaged W, even the small amounts of oxygen in the natural oxide film could influence the D release.

Considering the SEM images in Fig. 5.5 a) and b), it is clear that the oxide can be completely removed by outgassing D, if enough D is available. Thus, it is reasonable to assume that the ratio of O atoms on the surface to D atoms in the sample is the decisive quantity that determines whether or not the oxide film influences the D release. In the present case, the total amount of D that was retained in the self-damaged W (as measured by NRA) is 2.3×10^{21} D/m^2 for the samples with thin oxide (5, 10, 15 nm) and 2.0×10^{21} D/m^2 for reference sample with natural oxide. The amount of oxygen (also measured by NRA) in these samples and the ratio of O/D is given in Tab. 5.2.

In case of the natural oxide, the oxygen amount is in the order of eight monolayers which gives a ratio of oxygen to deuterium of 4.2 %. This indicates that for O/D ratios of <5 % the effect of heavy water formation on D release during TDS seems to be negligible. However, it cannot be fully excluded that a very thin (one to two monolayers thick) oxide film remains on the W surface, which could affect the recombination of D atoms to D_2 and HD molecules that is necessary for release from the surface. To fully exclude such a possibility, an in-situ study with very clean surfaces would be needed.

For the 5, 10 and 15 nm thick oxides the situation is different. By comparing the O/D ratios in Tab. 5.2 with the D release spectra in Fig. 5.4, it becomes evident that for O/D ratios of > 10 % (5 nm thick oxide), the oxide film already strongly affects the D release spectra. If the O/D ratio is > 30 % (15 nm thick oxide), the D release spectra is completely dominated by the oxide film in the sense that the second (high) temperature peak vanishes completely in the $D_2 + HD$ signal and is only present in the heavy water signal.

5.3.3 Comparison of the total D release for all different oxide film thicknesses (5 to 100 nm)

It has been shown above that surface oxide films can alter the molecular species in which D is released from W. However, in order to asses if an oxide film affects also the release temperature and thus the determination of binding energies of D in W defects, a comparison of the total D flux is necessary. Fig. 5.6 shows the total D flux derived by summing up the quantified contributions from HD, D_2, HDO and D_2O for samples with different oxide thickness.

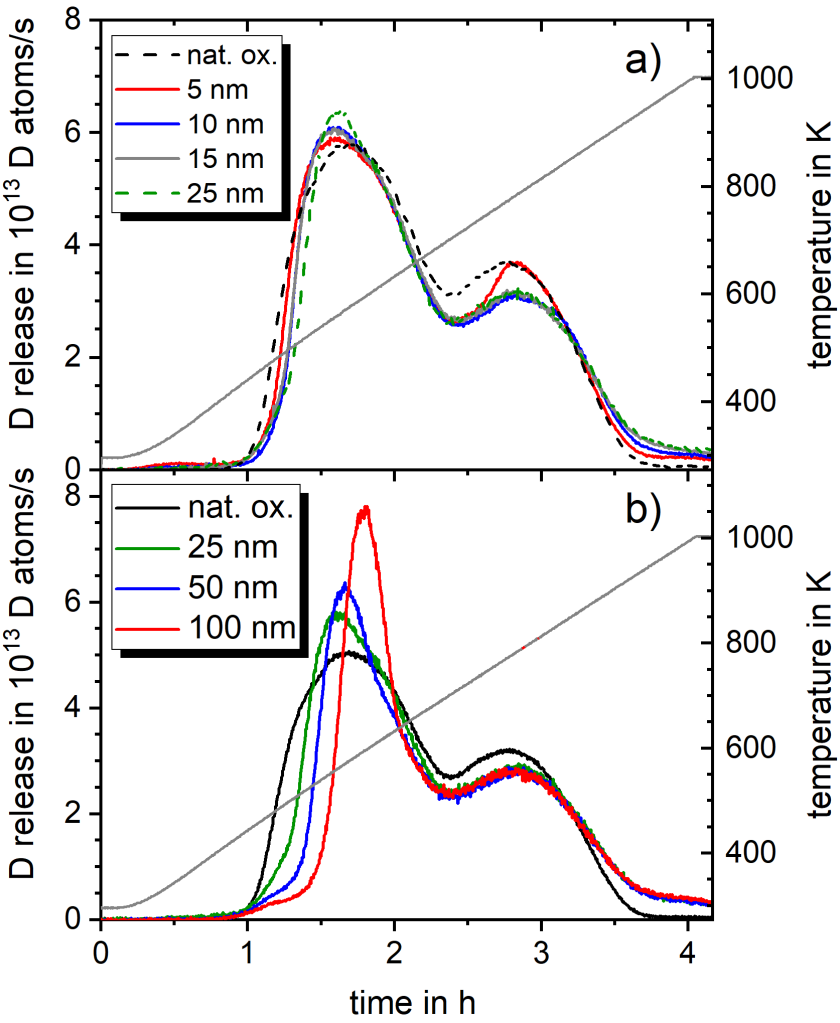

Figure 5.6 – Total D release: a) thin oxide films of 5 to 25 nm; b) thicker oxide films of 25 to 100 nm. The natural oxide signal is shown in both graphs for comparison. In a) the signals for the natural oxide and the 25 nm thick oxide are scaled by a factor of 1.15 to match the D content of the other samples shown in a); see text for details. The solid gray line shows the temperature ramp (units on the right y-axis).

Figure 5.6 a) shows the samples with thin oxide films (second batch) of 5 nm (red), 10 nm (blue) and 15 nm (line). Additionally, it shows the reference sample with only natural oxide and the 25 nm oxide film from the first batch (black and green dashed line, respectively) to allow a direct comparison of the different thickness regimes. Note that the signals from the natural oxide and the 25 nm thick oxide (batch 1) have been scaled by a factor of 1.15 to match the higher D content in the samples with thin oxides (batch 2). Details about the different D loading conditions between these two batches are described in section 3.4.

It is obvious that the total D release of all samples has remarkably similar peak shapes. The sum spectra in Fig. 5.6 a) show two distinct peaks for all oxide thicknesses, i.e., the total D release spectrum matches the expected general shape of the release in form of $D_2 + HD$ of the natural oxide sample. However, a slight difference between the samples is visible. With increasing oxide thickness, the left flank of the first peak slightly shifts to higher temperatures, indicating a delay in the D release already at these thin oxide thicknesses.

Figure 5.6 b) presents the total D flux from samples of the first batch, i.e., natural (black), 25 nm (green), 50 nm (blue) and 100 nm (red) thick oxide. For these thicker oxide films, the shift of the first peak is much more pronounced than for the thinner ones. The first peak maximum shifts from 560 K for the natural oxide to 590 K for the 100 nm thick oxide. It is worth mentioning that the release of D from trapping sites in the self-damaged zone is thermally activated and thus is not affected by the oxide film on top of the self-damaged zone. This means that the D release from the traps in the self-damaged zone occurred in the same manner for all oxide thicknesses. The peak shift in the release spectrum of the sample with thick oxide films thus shows that the oxide films delay the D on its way to the sample surface. As the oxide film itself shows a high D retention at temperatures around 500 K (see Fig. 5.11 in section 5.4), the delay can be explained at least in part by re-trapping (or chemical binding) of D in the oxide film. This indicates that only after all trapping or binding sites in the oxide are filled with D, the D that is released from the self-damaged zone can pass through the oxide and reach the surface. The oxide film thus acts as a sink or reservoir for outgassing D.

However, it is worthy to mention already at this point that the ramp-&-hold experiments, which are discussed in the next section (5.4), indicate that the oxide film acts not only as a sink for D but also as an transport barrier that reduces D release from the sample even after the oxide is filled with D.

Furthermore, with increasing oxide thickness, the first peak becomes narrower but higher and the amount of D that is released in the first peak decreases slightly. The first peak contains 63 % of the total D release for the sample with natural oxide, 59 % for the 25 nm, 56 %, for the 50 nm and 53 % for the 100 nm thick oxide. The shift of the peak position and the change of the quantity of released D in the two peaks shows that in this case also the calculation of binding energies of D in defects in W (that can be derived from such TDS spectra) would be affected by the oxide film.

When using self-damaged W and samples with only natural oxide, which is common for experiments that determine D trapping energies in displacement-damaged W, the amount of stored D is very large compared with the amount of oxygen in the oxide film. Consequently, the natural oxide film will be reduced early on by the first outgassing D, which means that heavy water formation will play only a minor role and the expected peak shift due to the oxide will be small. Thus, it can assumed that the natural oxide will not significantly influence the D release behavior from W in these cases. For experiments with un-damaged W with only few defects, however, even the natural oxide may significantly influence the positions and relative quantities of D release during TDS even when considering heavy water as an additional release channel

for D and monitor the total D release as is done in Fig. 5.6. Thus, even the natural oxide may influence the determination of binding energies of D in material defects in these cases.

The second (high-temperature) peak has a very similar shape and position for all samples; only the natural oxide shows a slightly higher maximum at slightly lower temperatures (770 K instead of 785 K). Furthermore, for the high-temperature side of the second peak, the curve of the natural oxide (black) falls off fast, whereas the curves of the oxidized samples decay slower. The D signals of the oxidized samples surpass the black curve at about 3.3 hours and thus the D release has a high temperature tail in these cases. This effect can be attributed to the "wall sticking" of heavy water molecules that are released by the oxidized samples. In contrast to the natural oxide where almost no heavy water is formed, this leads to a delayed signal as heavy water is repeatedly adsorbed and released from the chamber walls before it reaches the QMS.

5.3.4 Oxide film changes after D release

Fig. 5.7 shows SEM images of the thicker oxide films (25, 50 and 100 nm) after D release during TDS up to 1000 K. The surface morphology of the oxide films is changed drastically by the outgassing D. In the case of the 25 nm thick oxide film (Fig. 5.7 a)), snowflake-like structures are visible on top of a smooth surface. The elemental composition of the sample surface was checked with energy-dispersive X-ray (EDX) mapping, which is shown in Fig. 5.8 for a different spot on the same sample. There, it is clearly visible that the snowflake-like structure represents the remaining W oxide while the area in between consists of smooth, oxide-free W. This shows that the reduction of the oxide film is not a homogeneous process but leads to two-dimensional modifications of the film. Please note that the different gray scales of the metallic W surface are caused by two different W grains that are visible in Fig. 5.7 a).

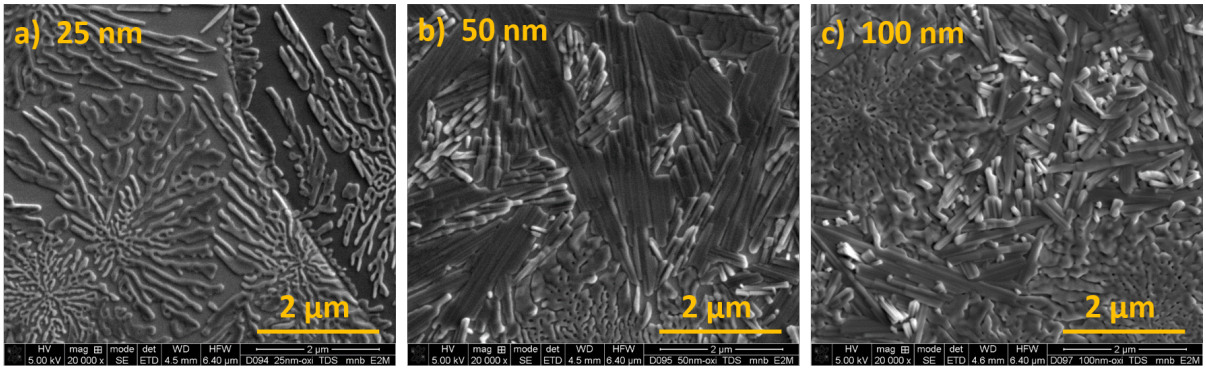

Figure 5.7 – SEM images of self-damaged, D loaded and electro-chemically oxidized samples with thicknesses of 25, 50 and 100 nm after D release during TDS up to 1000 K taken in SE mode with identical magnification.

For thicker oxide films (50 and 100 nm) in Fig. 5.7 b) and c) the surface is still mostly covered by the oxide film. Nevertheless, the film shows strong modification of either columnar crystal structures or coral-like structures. Comparing these images to the annealed D-free reference sample shown in Fig. 5.1 b), it is obvious that the changes during D release far surpasses those of the solely temperature-induced oxide modification.

For the thinner oxide films (5, 10, 15 nm), SEM images of the surface after D release have already been shown in Fig. 5.5. There the surface was completely free of oxide in the self-damaged area except for the 15 nm oxide, which contained some small oxide islands. For these samples, it is interesting to take a closer look to the region at the edge of the self-damaged

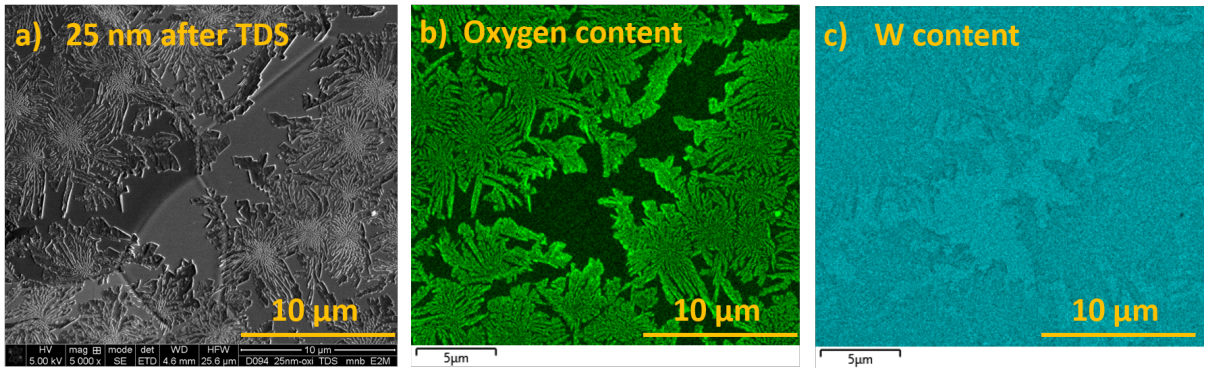

Figure 5.8 – Energy-dispersive-X-ray (EDX) mapping of the 25 nm thick oxide film (different spot on the same sample as in Fig. 5.7 a)) after TDS: a) SEM image in SE contrast, b) oxygen signal and c) W concentration.

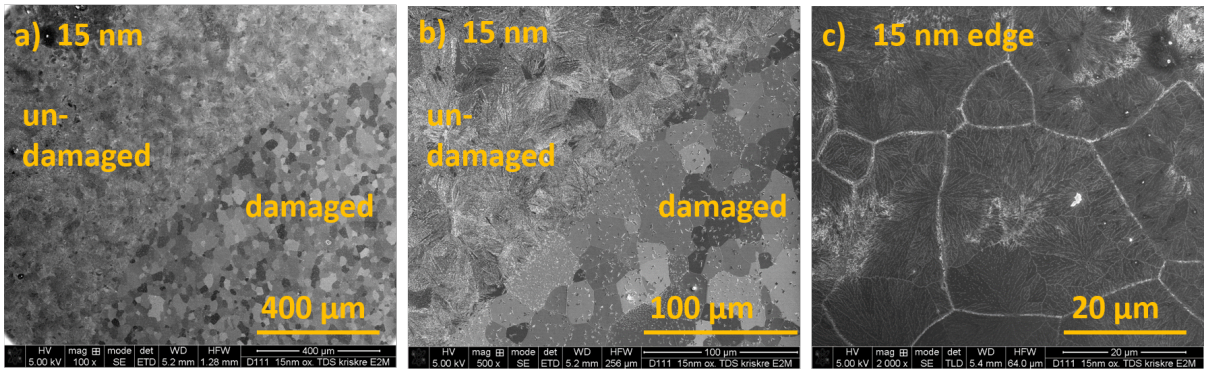

Figure 5.9 – SEM images in SE mode of the edge of the self-damaged zone for the originally 15 nm thick oxide film after TDS. The round edge is due to the shape of the mask holding the sample. a) Overview over the edge region, where the top left is not self-damaged and thus the W underneath the oxide contains only little D. b) Same with higher magnification. The edge between the two regions is clearly visible. In the undamaged part, a closed oxide film is retained after TDS. c) A magnified image of the un-damaged zone. The oxide shows only minor reduction by outgassing D, since the D amount underneath was much smaller in this region.

zone, where the sample has been shielded by the Molybdenum mask during the W ion bombardment (see section 3.3). SEM images of the edge separating the damaged and un-damaged zones are shown for the 15 nm thick oxide in Fig. 5.9. The borderline between the two zones is clearly visible in Fig. 5.9 a) and b). In the D-containing damaged zone most of the oxide film is removed, as discussed above. However, in the un-damaged zone the oxide film is still mostly intact and covers the surface area almost completely. This area is shown in higher magnification in Fig. 5.9 c). The film still shows some modification that goes slightly beyond the alteration that one would expect from the high temperature exposure alone (compare section 5.1). This is the case because even in the annealed and un-damaged W, some small amount of D is retained after the plasma exposure. The quantity of D is, however, too small to cause significant removal of the 15 nm thin oxide film.

The situation changes when looking at the edge region of the originally 5 nm thick oxide film that is shown in Fig. 5.10. Here even in the un-damaged zone a significant portions of the oxide film is removed from large parts of the surface area and only small, needle like oxide islands remain. This is similar to the case of the 15 nm thick oxide that was partially removed in the damaged zone. This result indicates that the amount of D stored in an un-damaged and

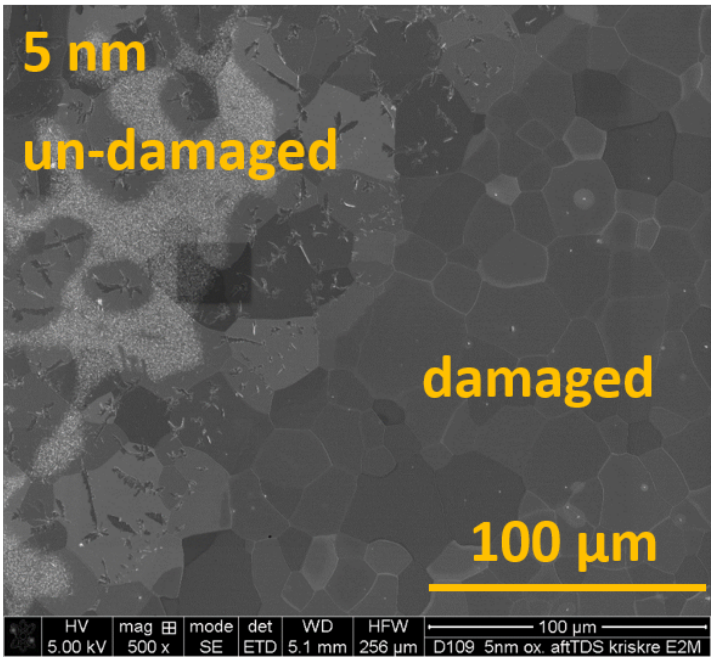

Figure 5.10 – SEM image of the edge of the originally 5 nm thick oxide film. The oxide is removed completely above the damaged area and only partially removed above the undamaged area, where needle like oxide islands remain. The dark square is an artifact of a previous SEM image with higher magnification.

annealed (2000 K) W sample is not enough to fully remove a 5 nm thick oxide film during TDS up to 1000 K. This again indicates that for laboratory experiments with un-damaged, annealed W even the natural oxide film (1–2 nm) may have a significant influence on TDS spectra.

5.4 Ramp-and-hold experiments to 500 K

In order to further study the before-mentioned D reservoir and transport barrier effect of the oxide film, the D release from one additional sample with 100 nm thick oxide from the first batch was analyzed by TDS with a lower maximum temperature. The sample was first ramped with 3 K/min to 500 K and then cooled down immediately by retracting the oven. Afterwards, it was exposed to a second ramp to 500 K and held at this temperature for 3.5 h. This temperature was chosen as D_2 desorption shows a peculiar plateau starting at this temperature (see Fig. 5.3 a)). As mentioned before (see discussion of Fig. 5.3 b)) this temperature is just slightly above the roughly 475 K where the production of heavy water sets in. Thus, the goal of the ramp-&-hold experiment is to study how D is transported through the oxide film at this reduced temperature and how the film is modified by the outgassing D and heavy water production in this case.

5.4.1 D depth profiles and O content

The D depth profile after the first heating ramp to 500 K is shown in Fig. 5.11 in blue. For comparison the D depth before TDS (black and red) are also shown. As is evident that there is an accumulation of deuterium in the oxide film after the ramp. Analysis of the depth profile yields that about 11 % ($22\pm0.7\times10^{19}$ D/m^2) of the D that was originally retained in the sample ($197\pm6\times10^{19}$ D/m^2) was transferred from the self-damaged zone to the oxide film. Assuming

a constant D concentration throughout the oxide film, the local concentration of D in the oxide is 3.3 at.%. The total D amount after the ramp is $193\pm6\times10^{19}$ D/m^2. Thus, only approximately 2 % of the D that was originally retained in the sample was released during the ramp, although this is barely significant considering the uncertainty of the measurement method.

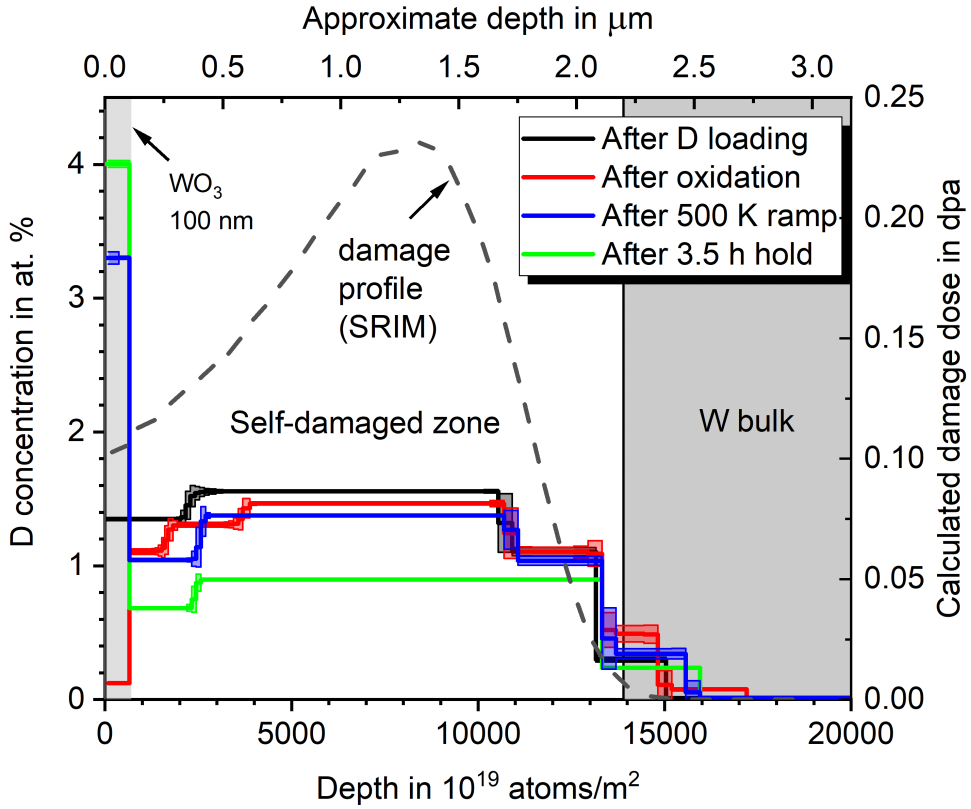

Figure 5.11 – Depth profiles of a 100 nm thick electro-chemically grown oxide after a 3 K/min ramp to 500 K (blue) and after a second identical ramp and a 3.5 h hold (green) at 500 K. The gray dashed line shows the calculated damage profile in dpa according to SRIM (units one the right y-axis). For comparison the depth profiles before TDS are also shown (black and red).

After this first ramp and subsequent NRA measurement, the same sample was reinstalled in the TDS setup and was again ramped to 500 K and held at that temperature for 3.5 h. The deuterium depth profile after the holding period is represented in green in Fig. 5.11. A small additional amount of D was transferred from the bulk to the oxide film such that 13 % ($26\pm0.8\times10^{19}$ D/m^2) of the originally retained D are trapped in the oxide film after the holding period. The corresponding average D concentration in the oxide film is now at 4.0 at.%. The total D areal density of the oxide and the self-damaged zone underneath was measured to be $143\pm5\times10^{19}$ D/m^2. Thus, another 25±4 % of the originally retained D was released during the holding period. This is about eight times more than during the previous step (ramp only).

In total 27±4 % of the retained D was released from the sample during these two experiments according to NRA. Consequently, the D concentration in the damaged-region decreased from originally 1.6 at.% to 0.9 at.%. As the oxygen areal density (also measured by NRA) changed only by a minor amount during these two experimental steps, it is reasonable to assume that the oxide thickness after the holding time is comparable to that after oxidation.

5.4.2 Desorption spectra

Figure 5.12 a) and b) show the D_2 (red) and HDO (blue) desorption fluxes for ramp and hold experiments to 500 K. The signals for HD and D_2O follow the same behavior as D_2 and HDO, respectively, but at a lower level and are thus omitted in the graph for sake of a concise presentation. The temperature ramps are shown as straight black lines with units on the right y-axis. Fig. 5.12 a) shows the D release from a reference sample with natural oxide that was ramped only once to 500 K and held there. Fig. 5.12 b) shows the D release from a sample with a 100 nm oxide that was ramped first to 500 K, cooled down and ramped again to be held at that temperature for 3.5 h. The color code is kept the same in a) and b). However, the absolute scales for the desorption fluxes differ by a factor of 20. In both images, the D_2 desorption fluxes of 'full' TDS spectra (ramped up to 1000 K) of identical samples are shown in gray for comparison. The two samples with the natural oxide stem from a previous study and underwent identical preparation as the samples from the present study [6]. Comparing the D_2 desorption fluxes from the "full" TDS samples (gray) with the ramp-&hold-samples (red) for both natural oxide and 100 nm oxide (Fig. 5.12 a) and b), respectively), one can see again the excellent reproducibility of the data. In both cases the initial D_2 desorption fluxes for the ramps to 500 K are identical to the 'full' TDS ramps. They only start to deviate above 500 K were the oven is either retracted or the temperature is held constant.

For the sample with the natural oxide (Fig. 5.12 a)), the D_2 desorption flux (red) shows a maximum, when the temperature of 500 K is reached and afterwards decays exponentially. This is expected, as the D release is governed by thermal de-trapping from material defects in the self-damaged W and thus only a limited amount of D can be accessed at a given temperature. The maximum of the D_2 desorption flux for the ramp-&-hold at 500 K nearly reaches the maximum desorption flux of the "full" TDS spectrum (gray). However, the total D amount, which degassed during the ramp-&-hold of the sample with natural oxide in the form of D_2, HD, HDO and D_2O was 9.4×10^{16} D atoms, which is about 36 % of the total D amount that was originally retained in the sample. This is the fraction of D that can be de-trapped at 500 K and serves as reference to quantify the D release through the oxide in the following. It is also clearly visible that the natural oxide sample emits almost no heavy water, as could be expected from the investigations of the previous sections.

The spectra of the samples with 100 nm thick oxide (Fig. 5.12 b)) show several differences compared with the ones of the natural oxide already during the first ramp to 500 K (dotted blue and red lines): 1) The absolute D_2 flux is significantly lower. This is in accordance with Fig. 5.3 a), which shows a direct comparison of the D_2 release from samples with 100 nm thick oxide and natural oxide. This can in part be explained by the reservoir effect of the oxide which takes up significant amounts of D during the ramping phase (see Fig. 5.11). 2) For the 100 nm oxide, heavy water formation plays a role and a small heavy water contribution arises already during the ramp; i.e. below 500 K. 3) The D_2 desorption flux shows a short dip at around 500 K that coincides with a strong rise of the heavy water production. The total D amount, which degassed during the ramp in the form of D_2, HD, D_2O and HDO until the oven was retracted is 4.2×10^{15} D atoms, which agrees well with the D loss measured by NRA after the ramp (self-damaged area on sample: 1.4 cm^2).

For the holding phase of the 100 nm thick sample (solid red and blue lines in Fig. 5.12 b)), the shapes of the D release spectra are also different compared with the reference ramp-&-hold spectra with natural oxide (Fig. 5.12 a). Firstly, the D_2 signal shows an initial peak after the second ramp reaches 500 K. This peak is most likely caused by D that was stored inside the oxide film after the first ramp (compare with the D depth profiles after the ramp in Fig. 5.11). More

importantly, during the holding phase, the desorption does not show the expected exponential decay of the D_2 signal, but a relatively constant plateau of about 1×10^{12} D/s. On the other hand, the deuterium released as HDO (blue), peaks about half an hour after the holding temperature of 500 K was reached and then decreases continuously by about 60 % until the end of the holding phase. The sum of both signals, which forms the majority of the outgassing D, decreases in a linear and not in an exponential fashion by about 55 % during the holding phase. This linear decrease shows that, in contrast to the natural oxide sample, not all D that is released from the low-energy D traps in the self-damaged W that are accessible in this temperature range has left the sample during the holding phase at 500 K. This shows that the oxide film acts as a bottleneck for the D release at this temperature. In addition to being a D reservoir, the oxide film also acts a transport barrier that reduces D outgassing even after the reservoir is filled.

According to the TDS measurement, additional 35×10^{15} D atoms (13 % of the initially retained amount) have desorbed during the holding period. Thus,together with the first ramp only 14 % of the initial D content was released during the ramp-&-hold experiment at 500 K according to TDS. This is significantly lower than the 36 % measured for a reference sample with only natural oxide, which shows that the oxide film significantly reduces D release at this temperatures.

However, the 13 % of additional D loss measured by TDS during the holding phase are lower than the 25±4 % measured by NRA (see section 5.4.1). This discrepancy between the two methods occurs only for this singular experiment and can be used to gain additional insight into the release behavior of D through the oxide. Assuming both methods yield correct results[3], there are two possible explanations why the results could differ: 1) The oxide film could acts as a barrier for D release and the thermally de-trapped D in the self-damaged zone could have diffused deeper into the bulk during TDS instead of being released. The two orders of magnitude lower trap density in the bulk could in principle be compensated by the much larger extent (800 µm bulk vs. 2.3 µm self-damaged zone). Due to the limited range of NRA (7.4 µm in W), D trapped deeper in the bulk would not be measured by this method and the values would differ. 2) Large amounts of D could be trapped in the oxide film and the "missing" D could be released from the oxide between the end of the TDS measurement and the NRA measurements.

The first option has been investigated by a simulation with the transport code TESSIM-X by K. Schmid (not shown) under the assumption that the oxide film completely prevents D release through the surface, which serves as an upper limit scenario. From the simulation, it follows that diffusion of D into the depth of the bulk could account for only 2 % of the initial D amount for the given conditions, even under these conservative assumptions. Consequently this effect alone cannot explain the discrepancy between NRA and TDS.

Thus, it seems possible that during TDS to 500 K, the amount of D that is retained in the oxide film is larger than measured later by NRA. Under the assumption that the difference in D amount between the TDS and NRA measurements is fully retained in the oxide film, the total retention in the oxide would be 51×10^{19} D/m^2 or 26 % of the initial D amount. This would correspond to a D concentration of 8 % in the oxide film during TDS. It seems possible that the D content in the oxide decreases before the NRA measurement as a) some D might desorb during re-oxidation upon contact with ambient air after the sample is removed from the TDS vacuum chamber and b) the NRA measurement for this particular experiment was delayed and conducted eleven days after the TDS measurement. It has been previously shown that D can desorb from the oxide at room temperature over the course of weeks or months (see section 4.2). The present results

[3]For the NRA measurement, this assumption is backed by the fact that the NRA depth profile of the reference sample with natural oxide that was held at 500 K during TDS (see Fig. 5.12 a) for TDS spectra), shows an identical, remaining D concentration of 0.9 % in the self-damaged zone. This indicates that in both cases the same amount of D is thermally released from the trapping sites in the self-damaged zone.

indicate that this process is faster for the amorphous, electro-chemically grown oxide, which also shows significantly higher D uptake than the thermally grown oxide film. These findings emphasize that the oxide film acts as a reservoir for D that takes up large amounts of D and thus delays the release from the sample.

On the other hand, the D_2 signal in Fig. 5.12 b) stays about constant during the holding phase, indicating that the ratio of D released as heavy water to D released as molecular hydrogen decreases during the holding phase. This indicates that over time less D reacts with the oxide to form heavy water. As the formation of HDO indicates that oxide is reduced and thus removed from the sample, one would expect that the bottleneck effect of the oxide decreases over time, which would cause an increase in the D_2 flux from the sample. As the overall D release from the sample declines over time by slow partial depletion of the available D reservoir, this relative increase of the D_2 signal results in the measured constant D_2 out-flux. A possible explanation for this relative increase in the D_2 out-flux is the formation of channels through the oxide film due to reduction by the outgassing D through which the D can be released from the sample without direct contact with the oxide. In other words, the bottleneck is expanding, which counteracts the decaying total D out-flux. This hypothesis of channel formation is supported by the SEM images of the sample after the ramp-&-hold experiment, which also shows pinholes/channels in the oxide film as discussed in the next section.

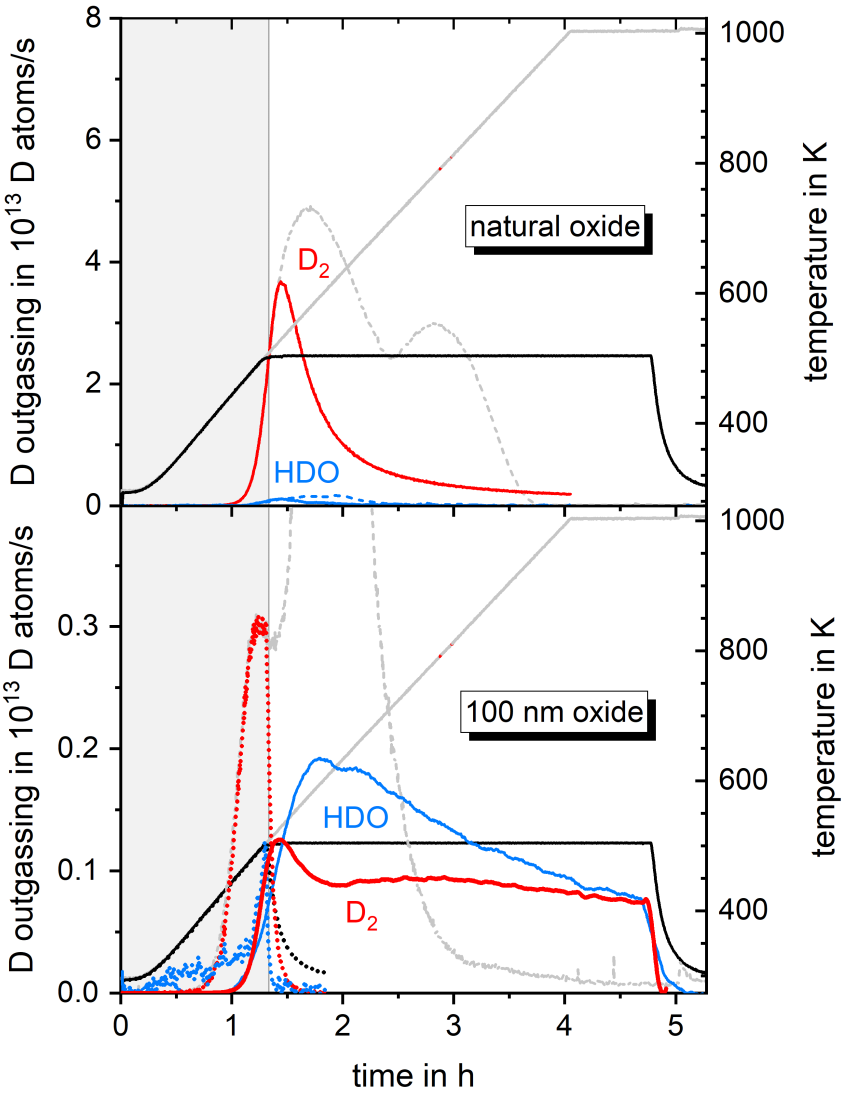

Figure 5.12 – D_2 (red) and HDO (blue) desorption from W during ramp-&-hold experiments to 500 K. a) shows a sample with natural oxide and b) shows a sample with 100 nm thick oxide (note the a factor of 20 different y-scale). The temperature ramp to 500 K is shown in black. In b) the D release of the first ramp and the quick cool-down is shown with thick dotted lines; the D release for the ramp-&-hold phase is shown as thick solid lines and the ramping phase is also indicated by the light gray background. For identical samples also a "full" D_2 TDS spectra (dashed gray lines) and their temperature ramps up to 1000 K (solid gray lines) are shown for comparison.

5.4.3 SEM images and FIB cuts

Fig. 5.13 shows SEM images of the surface of the 100 nm thick oxide film after the ramp-&-hold experiment to 500 K. The oxide film is still mostly intact, as can be expected from the NRA measurements and the TDS spectra that showed only comparatively little oxygen loss. However, across the surface many small "hole-" or "bubble-like" structures are visible (see Fig. 5.13 a)). They are distributed across the whole sample surface, but appear to be more frequent along grain boundaries. In Fig. 5.13 b) and c) a magnified image of these features is shown in SE and backscattered electron (BSE) mode, respectively. Here, the features appear to be small bubbles that are burst open towards the surface. Please note that these features are only observed after D release and not after D uptake experiments.

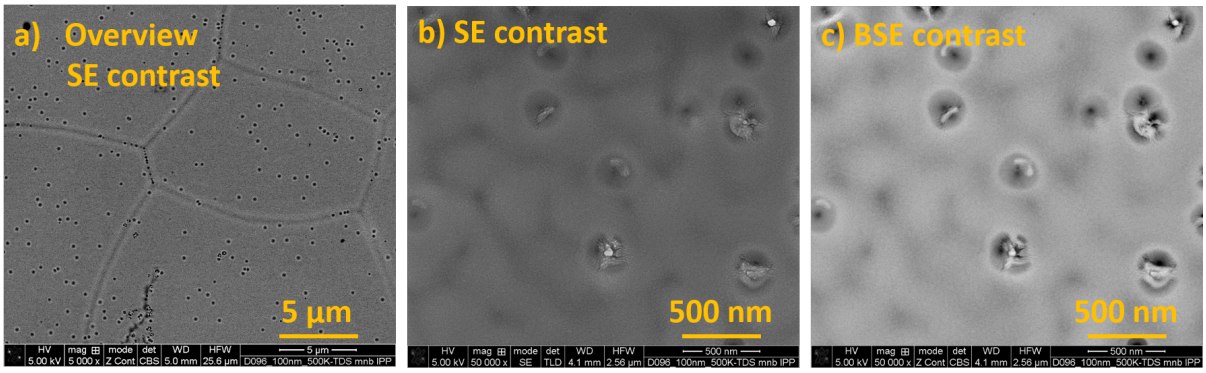

Figure 5.13 – SEM images of a 100 nm thick oxide film after the ramp-&-hold experiment to 500 K. In a) many small "hole-like" structures can been seen across the surface. They are more frequent along grain boundaries. In b) and c) enlarged views of these structures are shown in SE and BSE contrast, respectively. They appear to be burst bubbles, which are open towards the surface.

To study these features more closely a focused-ion-beam (FIB) cross section has been prepared through several of these bubbles. Fig. 5.14 a) shows an overview image of the region where the cut was applied. Besides the bubbles, some "worm-like" remnants of the electro-polishing or grinding process are visible. They cause an uneven, wave-like tungsten surface, but apart from that, it can be assumed that they are of no further consequence here. In Fig. 5.14 b), the cross section through the oxide film and some of the bubbles is shown. It becomes apparent that the oxide film is mostly intact and still has a thickness close to its original 100 nm. However, there are several holes or bubbles visible in the oxide film. For some of them channels are visible which reach towards the surface. It seems likely that the bubbles are formed during D outgassing in one of two ways: a) outgassing of D forms clusters inside the oxide, which leads to D_2 filled cavity or b) the outgassing D reacts with the oxide film and creates heavy water (D_2O or HDO) filled cavities. In any case, the bubbles seem to eventually burst and create an open release channel towards the surface.

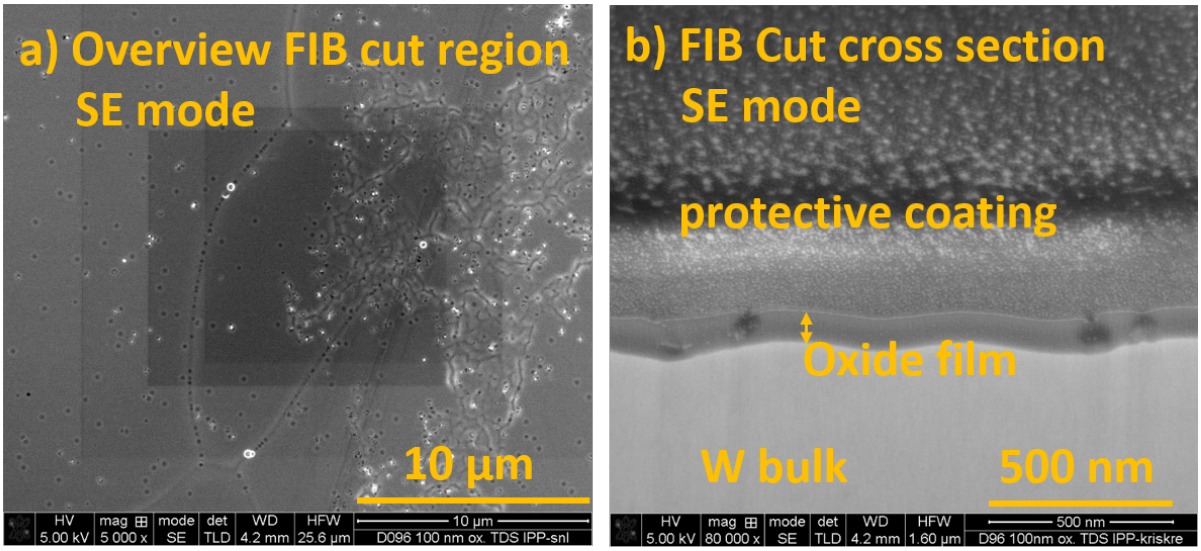

Figure 5.14 – SEM cross section image of the 100 nm thick sample after the ramp-&-hold experiment to 500 K. a) an overview image over the FIB cut region. Some artifacts of the electro-polishing are also visible. b) Cross section image of the FIB cut. The "bubble-like" features in the oxide film are clearly visible and appear to have burst and form open channels towards the surface in some cases.

5.5 Summary and conclusion of D release through surface oxide films on W

This chapter investigated which effects 5–100 nm thick surface oxide films have on D release from tungsten during thermal desorption spectroscopy (TDS). This question is addressed by a novel method that uses self-damaged W as a stable and well-quantifiable D reservoir underneath the oxide films. After all experimental steps, nuclear reaction analysis was applied to determine the oxygen amount on the sample and the depth-resolved D concentration in the oxide film and the self-damaged zone. Additionally changes of the morphology of the oxide film due to the outgassing of D were investigated with scanning electron microscopy (SEM).

It has been found that the thin oxide films significantly influence and alter the release behavior of D from W in two ways: 1) By changing the release species from D-containing, molecular gas (HD and D_2) to heavy water (HDO and D_2O) at elevated temperatures and 2) by shifting the position of the first D release peak to higher temperatures.

Already at 475 K, D starts to interact chemically with the oxide film and is released not only as molecular gas but also in the form of heavy water. Above 700 K, this becomes the dominant release channel and D is released only as heavy water as long as enough oxide is available. This shows that, if oxide films are present, the signals from heavy water (mass channels 19 and 20) have to be considered and quantified in order to obtain all information on release energies and the quantity of released D from W during TDS. However, heavy water quantification in TDS is very difficult and the D_2 and HD signals are often the only ones that can be evaluated quantitatively. Therefore, it is important to estimate at which thickness (or quantity of oxygen) surface oxide films significantly influence the release spectra of these two mass channels. From analysis of the D release spectra of very thin oxide films (5, 10 and 15 nm), it can be concluded that for O/D ratios of $>10\,\%$ (5 nm thick oxide), the oxide film already strongly affects the D release spectra. If the O/D ratio is $>30\,\%$ (15 nm thick oxide), the D release spectra is completely dominated by the oxide film in the sense that the second (high) temperature peak

vanishes completely in the $D_2 + HD$ signal and is only present in the heavy water signal. In case of the natural oxide, the O/D ratio is 4.2 % for the here used self-damaged W and the effects of the oxide should thus be negligible. However, it is important to keep in mind that the present study used self-damaged W, which has a D retention that is orders of magnitude higher than for un-damaged W. Thus, for experiments that use un-damaged W, even the small amounts of oxygen in the natural oxide film could significantly influence the D release.

SEM images show that the oxide film is strongly modified by the outgassing of D and forms a complex two-dimensional structure. The thickest oxide films (50 and 100 nm) still cover the sample completely but show an inhomogeneous crystalline structure and some pinholes. Thinner films (25 nm) are partially removed and the remaining oxide forms snowflake-like structures on the metallic W. For 15 nm thick films, only small oxide islands remain on an otherwise metallic W surface and for even lower oxide thicknesses, the oxide is fully reduced and the metallic W surface is recovered. Since D is released exclusively as heavy water at temperatures above 700 K as long as oxygen remains on the surface, one can conclude that the mobility of D atoms at the surface is very high. Even D atoms that surface far (several µm) from an oxide island apparently travel along the surface to form an O-D group at the W oxide before they recombine with another D atom to be desorbed as water.

Furthermore, the oxide film influences the release spectra also at low temperature: The first D release peak at about 560 K (and especially its left flank that marks the beginning of strong D release) is shifted to higher temperature with increasing oxide thickness. This indicates that the oxide film acts as a transport barrier that reduces D release at temperatures above 475 K. For lower temperatures, the D release from the self-damaged W is too small to draw any conclusions. In addition, the amount of D that is released in this low-temperature peak becomes smaller with increasing oxide thickness. This is compensated later by a larger D release at higher temperatures. This indicates that the oxide film also acts as a reservoir that retains D and delays its release from the sample. A qualitative understanding of this system can be gained by an analogy to a sponge in a water pipe. The sponge will both retain some water and limit the total flux of water through the pipe. At temperatures above 700 K, this effect is lost due to increasing reduction of the oxide and the release of D as heavy water.

The release behavior at moderate temperatures has been further studied by holding a sample with a 100 nm thick oxide film at 500 K during TDS. At this temperature, the chemical reaction between oxide and D just sets in and the oxide film is reduced only slowly by the outgassing D. According to TDS measurements, the total amount of D released during the ramp and the hold period at 500 K for 3.5 h was 14 % of the amount initially stored in the self-damaged zone. This is a factor of 2.6 lower than for a reference sample with only natural oxide, which released 36 % of its total D content during an identical treatment. The remaining not released D from the oxidized sample is most likely stored within the oxide film. According to NRA measurements, up to D 13 % of the total initial content are located within the oxide film itself after the hold experiment and D concentrations in the film reach up to 4 %. A discrepancy between the NRA measurements (eleven days after TDS) and the recorded D release during TDS indicates that this value could even be a factor of two higher and that D is released from the oxide after TDS upon contact with ambient air or during storage before the NRA measurement.

However, as a significant amount of D was released through the oxide during the holding period, it can be concluded that the reservoir is fully filled during the experiment. Nevertheless, the out-flux of D stays much lower than for a reference sample with only natural oxide during the course of the experiment. This confirms that the oxide film acts not only as a reservoir but also as a transport barrier for the D at a temperature of 500 K. This result is further supported by the fact that the total release of D (in form of HD, D_2, D_2O and HDO) from the sample with

a 100 nm thick oxide film decreased only linearly during the holding period. If the thermally triggered release of D from material defects would be the limiting factor for D outgassing from the sample, one would expect an exponential decay of the D signal at constant temperature, as was the case for the reference sample.

Furthermore, during the holding period (3.5 h), the slow reduction of the oxide leads to the formation of bubbles inside the oxide film, which have been observed by FIB cross sections after the holding phase. Eventually these bubbles burst open towards the surface and form channels through which D can be released in molecular form as D_2 or HD.

5.6 Consequences of tungsten oxide films on hydrogen isotope uptake, retention and release in a fusion reactor

It has been shown that thin surface oxide films on W with thicknesses in the range of 5–100 nm can have a surprisingly strong effect on the uptake and release of hydrogen isotopes such as deuterium and tritium from metallic W. In particular, it has been shown that W oxide films can completely prevent deuterium uptake into metallic W until they are sufficiently reduced by hydrogen isotopes from a plasma.

While this work is focused exclusively on ex-situ *laboratory* studies, the obtained results lead to the question whether hydrogen isotope uptake and release from W PFCs in a future fusion reactor such as ITER or the European DEMO could also be affected by the formation of oxide films. A rigorous investigation of this issue is beyond the scope of this thesis, as it would require detailed information on the rate of formation vs. the rate of reduction/removal of oxide from each PFC. This, in turn would require not only exact knowledge of the design and operational regime of the envisaged reactor but also of the temperature, oxygen or water partial pressure, energy-resolved particle in-flux and hydrogen isotope release flux at each PFC.

Nevertheless, such an estimate will be attempted here for the future European fusion reactor DEMO by using available data on expected wall temperatures, particle fluxes, oxygen and water partial pressures and operating scenarios. Current breeding blanked concepts for the European DEMO assume a wall temperature of 673 K for water-cooled lithium lead [89] or 793 K for a helium-cooled pebble bed [90], respectively.

An upper limit for the oxidation of PFCs in a fusion reactor can be estimated by calculating the impingement rate of oxygen containing impurities such as O_2 or H_2O on the PFCs, assuming a sticking coefficient of 100 % and further assuming that all adsorbed oxygen reacts to W oxide. Assuming an ideal gas distribution at the wall temperature, the impingement rate Z is given by:

$$Z = \sqrt{\frac{p^2}{2\pi m k_B T}}$$

where p is the pressure in Pa, m is the mass of the impinging particles in kg (when assuming H_2O, m=2.99×10^{-26} kg),k_B is Boltzmann's constant and $T = 693$ K is the temperature of the gas. According to [91] the base pressure of oxygen or water in the torus vacuum of ITER is below 10^{-7} Pa. With these values, Z is 2.4×10^{15} atoms/m^{2}s and the formation of a monolayer of oxide ($\approx10^{19}$ O atoms/m^2) would take about 1.2 h. The formation of an oxide in the range of the natural oxide film on W at room temperature in air (1.2 nm or 8.4×10^{19} atoms/m^2) would take

approximately 10 h, if no reduction by the plasma or the hydrogen partial pressure were taking place simultaneously. This conservative upper limit for the oxidation rate has to be compared with the reduction rate by the particle flux from the plasma.

Behrisch et al. [92] have performed substantial calculations of the expected wall fluxes for a future fusion device similar to the planned European DEMO[4] for a given burning plasma with the code B2-EIRENE. According to their work, the flux of neutral particles from charge exchange reactions onto the first wall is in the range of 10^{19} to 10^{21} particles/m^{2}s with average energies of 5 to 300 eV. The lowest energies correspond to the wall regions that receive the highest flux and vice versa. In addition, the flux of D^+ ions is in the range of 4×10^{19} to 2×10^{20} with plasma ion temperatures between 1 and 100 eV (again the lowest temperatures correspond to the highest flux). These particle fluxes to the first wall of the reactor are slightly higher than the D fluxes in the here used laboratory plasma device "PlaQ" (section 3.4), which are 5.6 and 9.0×10^{19} D/m^{2}s for floating potential (5 eV/D) and -100 V bias (38 eV/D), respectively. Thus, the oxide reduction rate in PlaQ can be assumed as a lower limit of the oxide reduction on the first wall of a fusion device.

It has been shown above that oxide reduction strongly increases with sample temperature and with the energy of the impinging particles (sections 4.4.1 and 4.4.2). For 5 eV/D at 370 K, the reduction rate is 5.4×10^{-4} O/D, for 5 eV/D at 500 K it is 14×10^{-4} O/D and for 38 eV/D at 370 K it is 23×10^{-4} O/D. Since the wall temperature in the European DEMO will be at least 693 K it can be assumed that the reduction rates in the reactor are significantly higher than the ones measured in this work even in the small regions of the first wall where the energy of the impinging particles is low (see [92] for spatially resolved energy distribution of impinging particles). In regions with a higher average energy of the impinging particles, which are most parts of the wall, the reduction rate is presumably higher. In order to make a conservative estimation a minimum reduction rate of 25×10^{-4} O per impinging D particle is assumed. For an impinging particle flux of $>5\times10^{19}$, this yields a minimum reduction rate of 1.25×10^{17} O/m^{2}s, which is more than 50 times higher than the maximum oxidation rate.

The fluxes in the divertor region of the fusion reactor are several orders of magnitude higher and accordingly the reduction rates will be higher. Consequently, during plasma operation no oxide can form and a 1 nm thick oxide film that might form during a plasma break of 10 h would be reduced within 11 minutes of plasma operation. It should be stressed again that this is a very conservative estimate, in which an upper limit for the oxidation rate and a low reduction rate were assumed.

Thus, it can be concluded that under the here used assumptions of the impurity base pressure and particle fluxes to the wall, surface oxide films will have none or only a very minor influence on the uptake, retention and release of hydrogen isotopes from the W PFCs in the first wall or divertor of a future fusion reactor. Any oxide that could potentially form would be quickly reduced by the fusion plasma.

[4] Calculations have been done for the "old" larger version of ITER that was originally planned

Chapter 6

Summary, Conclusion and Outlook

In this work extensive studies on the effects of surface oxide films on deuterium (D) uptake and release from tungsten (W) were conducted. These investigations are important to assure that conclusion from ex-situ laboratory studies (with natural oxide films) are also valid for the plasma facing components (PFCs) of future fusion reactors, where the oxide will most likely not be present (see section 5.6). It was observed, that 5–100 nm thick oxide films have a surprisingly strong effect on both D uptake and D release from W. The results have already been summarized in sections 4.6 (uptake) and 5.5 (release) and here only the main results will be repeated. After that, the implications of these results for laboratory ex-situ studies of D uptake and release are discussed and remaining open questions are addressed.

6.1 Summary of the results for D uptake and release:

Recrystallized W samples have been deliberately oxidized to film thicknesses of 5 to 100 nm by thermal or electro-chemical oxidation. The resulting oxide films were characterized with nuclear reaction analysis (NRA), Rutherford backscattering spectroscopy (RBS) and scanning electron microscopy (SEM) including focused ion beam (FIB) cross sections. It has been shown that the oxide films consist of stoichiometric WO_3 in nano-crystalline form (thermal oxidation) or amorphous form (electro-chemical oxidation) although small contributions of oxygen-deficient oxides cannot be fully excluded.

Underneath the oxide film, a so-called "self-damaged" W layer was created by bombardment with 20 MeV W ions. This irradiation introduces displacement damage in the material and creates a 2.3 µm thick zone of defect-rich material that can trap large quantities of D. For the experiments on D uptake through the oxide film, this self-damaged zone is used as a "getter-layer" that binds D that enters the metallic W. This is a crucial and novel experimental technique to determine the D concentration underneath the oxide in later ex-situ measurements. For the D release experiments, the self-damaged zone is filled with D prior to oxidation and serves as a D reservoir underneath the oxide. This reservoir provides sufficient D to quantify the effects the oxide film has on thermal release of D from W.

For the uptake experiments, the samples were exposed to D plasma at various D energies, sample temperatures and D fluence in the well-characterized plasma device "PlaQ" with a temperature-controlled sample holder. After each relevant experimental step, extensive analysis of the D content in the sample and of the state of the oxide film was undertaken. The depth-resolved D concentration in the oxide film and in the self-damaged zone was determined with NRA, which also yields information on the total areal density of oxygen on the sample surface. The depth-resolved concentration of oxygen in the oxide film was determined with RBS to gain information on the reduction state of the oxide. Furthermore, the oxide film was

investigated with SEM imaging and cross section through the films were prepared with FIB to image the changes in the oxide film directly.

To study the release of D from W through the surface oxide film, thermal desorption spectroscopy (TDS) up to 1000 K was performed in a well-quantified device with focus not only on D-containing species HD and D_2 but also on heavy water HDO and D_2O.

D uptake: It was shown in the present work, that surface oxide films on W completely block D uptake into metallic W at an exposure temperature of 370 K. It was concluded that this is due to the difference in the enthalpy of solution of D in WO_3 and W, as long as the interface of W oxide to metallic W is covered by intact WO_3. It was further shown that exposure to D plasma reduces the oxide film depending on D energy, sample temperature and D fluence. Once the reduction of the oxide has reached the interface, D can enter the metallic W. The ability to block D uptake decreases with the fraction of the interface area that is covered by intact WO_3. The oxide film itself can take up a significant amount of D up to a concentration of 1.5 at.%. In addition, it was observed that D is slowly released from the oxide film on a timescale of weeks to months, but no significant amount of D is lost in the period of up to 24 h after plasma exposure. However, an initial outgassing directly after plasma exposure or upon first contact with ambient air on the transit to the ion beam facility cannot be excluded with the present ex-situ experiment.

It was shown that the reduction of the oxide is not governed by the availability of D, which diffuses through the full extent of the oxide film within minutes and form a so called deuterium-tungsten-bronze (D_xWO_3), but by the diffusion of O-containing molecules (most likely DO or D_2O) to the surface. The oxygen loss is fastest at the beginning of the plasma exposure and decreases as a W enrichment zone grows at the surface of the oxide film and slows down further out-diffusion of O-containing species. For exposure of initially 33 and 55 nm thick oxide films to gentle D plasma (<5 eV/D, 370 K), the W-enrichment zone reaches a stable state and prevents further reduction. Thus, the oxide films would prevent D uptake into metallic W in principle indefinitely for these conditions. However, at a very high fluence of 1.6×10^{25} D/m^2, cracks in the oxide film reach the interface to the metallic W and minuscule amounts of D can enter the metal at these spots. At higher D energies (15 and 38 eV/D) or sample temperatures (500 K), the oxide reduction progresses significantly faster and laterally more inhomogeneous. Under these conditions, the reduction eventually reaches the interface to the metallic W and D can enter the metal.

In addition, it was shown that during plasma exposure at gentle conditions (< 5 eV/D) no W but only O is removed from the sample. For a higher D energy of 38 eV, it was shown that also W atoms are sputtered by D from the W oxide, although the D energies are too low to sputter W from a metallic lattice. The lower sputter threshold of W in W oxide can thus lead to a full removal of the oxide film by the plasma.

In conclusion, WO_3 blocks D uptake into metallic W but shows significant reduction by D plasma depending on D energy and sample temperature. Once the oxide at the interface is sufficiently reduced, D can enter the metallic W, which indicates that the difference in the enthalpy of solution between the reduced oxide and the metallic W is small enough to be overcome by thermalized D at 370 K.

D release: The goal of the D release studies in this work was to clarify which effects thin surface oxide films have on the D release from tungsten during thermal desorption spectroscopy (TDS). This question is addressed by a novel method that is based on a stable and

well-quantifiable reservoir of D ($>200\times10^{19}$ D/m^2) in self-damaged W underneath electro-chemically grown W oxide films with thicknesses of 5–100 nm.

It has been found that the thin oxide films significantly influence the release behavior of D from W in two ways: 1) By changing the release species from D-containing, molecular gas (HD and D_2) to heavy water (HDO and D_2O) at elevated temperatures and 2) by shifting the position of the first D release peak to higher temperatures.

It was shown that the oxide film acts as a transport barrier that reduces D release at temperatures above 475 K proportional to its thickness. Additionally, the oxide film acts also as a reservoir that retains significant amounts of D and delays its release from the sample. A qualitative understanding of this system can be gained by an analogy to a sponge in a water pipe. The sponge will both retain some water and limit the total flux of water through the pipe. At 500 K, a 100 nm thick oxide film reduces the D release by a factor of 2.6 compared to a sample with natural oxide. The D concentrations in the electro-chemically grown oxide film reach at least up to 4 % after D release at 500 K and there is indication that this value could even be a factor of two higher. At temperatures above 700 K, both effects are lost due to increasing reduction of the oxide and the release of D as heavy water.

Since heavy water quantification in TDS is difficult and the D_2 and HD signals are often the only ones that can be evaluated quantitatively, it is important to estimate at when surface oxide films influence the release spectra of these two mass channels. It was concluded that for O/D ratios of >10 %, the oxide film already strongly affects the D release spectra. If the O/D ratio is >30 % (15 nm thick oxide), the D release spectra is completely dominated by the oxide film in the sense that the second (high) temperature peak vanishes completely in the $D_2 + HD$ signal and is only present in the heavy water signal. In case of the natural oxide, the O/D ratio is 4.2 % for the here used self-damaged W and the effects of the oxide should be negligible. However, the present study used self-damaged W, which has a two orders of magnitude higher D retention than un-damaged W. Thus, for experiments that use un-damaged W, even the small amounts of oxygen in the natural oxide film could significantly influence the D release.

Tungsten oxides in fusion reactors: Based on these results, a conservative estimate was made of the role that W oxide films play in a fusion reactor. It was found that during plasma operation no oxide can form and the about 1 nm thick oxide film that might form during a plasma break of 10 h would be reduced within 11 minutes of plasma operation. Consequently, it was concluded that oxides will have none or only a very minor influence on the hydrogen isotope uptake, retention and release from W PFCs in a fusion reactor.

6.2 Conclusions and implication for ex-situ studies of D uptake, retention and release from W

This section discusses which conclusions can be drawn for the influence of natural oxide films on D uptake and D release from W in ex-situ laboratory studies.

D uptake: It was shown above that a) the permeation barrier effect of W oxide breaks down when the oxide at the interface to the metallic W is reduced and b) that even for the shortest gentle plasma exposure a reduction zone with an extent of 13.5 nm is formed. This suggests that the thin natural oxide film of 1.2 nm will lose its permeation barrier effect already at a low

fluence in ex-situ laboratory studies of D uptake into W. Assuming a constant rate of oxygen loss of $5.4\pm0.7\times10^{-4}$ O atoms per incident D and a constant growth of the W-enrichment zone during this first gentle plasma exposure, the required D fluence to reduce the natural oxide would be $1.6\pm0.4\times10^{23}$ D/m^2.

Furthermore, as it has been shown in section 4.3, the oxygen loss rate is largest at the beginning of a plasma exposure (where the natural oxide will be reduced) and decreases for higher D fluence, as the W-enrichment zone grows and slows down further reduction. Consequently, it can be assumed that the oxygen loss rate that was determined from the 7 h long first gentle exposure is only a lower limit and the fluence that would be required to reduce the natural oxide is even smaller than 1.6×10^{23} D/m^2.

It should, however, be kept in mind that the thickness of the natural oxide film can change depending on ambient conditions [34] such as storage temperature and air humidity. Furthermore, the final film thickness also depends on the grain orientation and surface modification of the W substrate [53]. Thus, the areal density of a natural oxide film may also be greater than in the present case. If one assumes a thickness of 2 nm (15×10^{19} atoms/m^2), the upper limit of the required D fluence to reduce it would be 2.8×10^{23} D/m^2.

Those values show that even the natural oxide films on W can have a significant influence on the D uptake into W if the applied D fluence is in the range of several 10^{23} D/m^2 or if fluence series experiments are conducted and the sample is exposed to ambient air (and re-oxidation) in-between exposures.

However, as indicated above, some oxide may remain on the sample surface even for "harsh" plasma conditions (38 eV/D, fluence $> 10^{25}$ D/m^2) and it may be possible that also for a natural oxide film, some oxygen in the range of a few monolayers remains on the surface. It has been reported in literature that even such a small oxygen coverage may affect the D release from W [9, 19]. This is relevant for D uptake because the total D uptake into metallic W by plasma implantation into the subsurface region is governed by an equilibrium of D diffusion back to the surface were it can be released and D diffusing deeper into the self-damaged zone or the bulk. Consequently, a lower probability for D release at the surface (due to oxygen contamination) could potentially increase the D equilibrium concentration in the subsurface region and thus also the overall D uptake from the plasma. The effects that oxygen contamination on the surface has on this process are still under active investigation [19] and are currently not fully understood.

A systematic investigation of this question would require an in-situ experiment, which combines the use of a self-damaged W as a "getter-layer" with the capacity to a) remove all oxygen, e.g., by Ar sputtering, b) introduce D via a plasma source and c) determine the D uptake and oxygen surface coverage in real time by, e.g., ion beam analysis. Such a device is currently under construction at the tandem accelerator laboratory at the Max-Planck-Institute for Plasma Physics in Garching bei München, Germany. The device is called IBIS for "ion beam in-situ experiment" and could potentially shine light on this remaining open question concerning the effect of natural W oxide films on D uptake (and release) from W.

D release: As discussed in section 6.1, oxide films have a strong effect on the release behavior of D from tungsten during TDS studies, if the ratio of O atoms at the surface to D atoms in the sample is larger than 5–10 %. This indicates that previous TDS studies on D release from W with higher ratios of O to D (such as, e.g., [9]) may have been influenced by natural surface oxide films. Thus, also the predictions for D and tritium retention and release for PFCs of a future fusion reactor that are drawn from such studies may have been influenced in two ways. Firstly, the temperature of the D release peaks in TDS studies is relevant for calculating the

binding energies of D in neutron- or ion-induced material defects in W. Any shift of these peaks due to the influence of surface oxide films represents a systematic error in the determination of these binding energies and thus leads to a distortion of the obtained retention and release values for hydrogen isotopes in the PFCs. Secondly, surface oxide films can lead to a significant part of the total D release being in form of heavy water due to chemical reaction of outgassing D with the oxide. Since heavy water signals are commonly not quantified in TDS studies, the total D release and thus also the retention in W may have been systematically underestimated in the past.

The effect of surface oxide films will be especially pronounced for experiments with low D content, i.e., without self-damaged W to enhance the D retention, or for studies with repeated air exposure in-between measurement steps. There even the natural oxide film (1–2 nm), that forms on W upon contact with ambient atmosphere, may already influence the D release spectra. In these cases, a careful re-examination of the experimental conditions is advisable. For future TDS studies, the O/D ratio should be monitored and ideally kept low in order to make reliable predictions on hydrogen isotope retention and release from W for a future fusion reactor.

However, even for O/D ratios $<< 10\,\%$, where the natural oxide film is reduced early during TDS by the outgassing D, it cannot be excluded that minuscule amounts of oxygen in the order of one monolayer remain on the surface (identical to the case described above for D uptake). If this is the case, the remaining oxygen on the surface may influence the release behavior and play a role for TDS even at elevated temperatures.

To investigate this effect it would be necessary to remove the oxide in-situ by, e.g., Ar sputtering prior to the TDS experiment to assure an oxide-free surface and compare the results to an identical reference sample were the oxide is not removed. It is currently planned to add the capability for in-situ TDS to the above-described “IBIS” device via a heated sample holder and an attached quadrupole mass spectrometer. Detailed knowledge of the effect of natural oxide for early D release in TDS and the effect of possibly remaining surface oxygen on D release from W also at higher temperatures would be valuable input parameters for modeling of the D release from W and would complete the understanding of the interaction between W oxide and D release.

Bibliography

[1] W.R. Wampler and R.P. Doerner. "The influence of displacement damage on deuterium retention in tungsten exposed to plasma". In: *Nuclear Fusion* 49.11 (Nov. 2009), p. 115023. DOI: 10.1088/0029-5515/49/11/115023.

[2] G. De Temmerman, T. Hirai, and R. A. Pitts. "The influence of plasma-surface interaction on the performance of tungsten at the ITER divertor vertical targets". In: *Plasma Physics and Controlled Fusion* 60.4 (Apr. 1, 2018), p. 044018. DOI: 10.1088/1361-6587/aaaf62.

[3] D. Stork et al. "Materials R&D for a timely DEMO: Key findings and recommendations of the EU Roadmap Materials Assessment Group". In: *Fusion Engineering and Design* 89.7 (Oct. 2014), pp. 1586–1594. DOI: 10.1016/j.fusengdes.2013.11.007.

[4] J. Roth and K. Schmid. "Hydrogen in tungsten as plasma-facing material". In: *Physica Scripta* T145 (Dec. 1, 2011), p. 014031. DOI: 10.1088/0031-8949/2011/T145/014031.

[5] O.V. Ogorodnikova and V. Gann. "Simulation of neutron-induced damage in tungsten by irradiation with energetic self-ions". In: *Journal of Nuclear Materials* 460 (May 2015), pp. 60–71. DOI: 10.1016/j.jnucmat.2015.02.004.

[6] T. Schwarz-Selinger et al. "Influence of the presence of deuterium on displacement damage in tungsten". In: *Nuclear Materials and Energy* 17 (Dec. 2018), pp. 228–234. DOI: 10.1016/j.nme.2018.10.005.

[7] K. Schmid et al. "Recent progress in the understanding of H transport and trapping in W". In: *Physica Scripta* T170 (Dec. 1, 2017), p. 014037. DOI: 10.1088/1402-4896/aa8de0.

[8] M.J. Simmonds et al. "Isolating the detrapping of deuterium in heavy ion damaged tungsten via partial thermal desorption". In: *Journal of Nuclear Materials* 522 (Aug. 2019), pp. 158–167. DOI: 10.1016/j.jnucmat.2019.05.016.

[9] E.A. Hodille et al. "Retention and release of hydrogen isotopes in tungsten plasma-facing components: the role of grain boundaries and the native oxide layer from a joint experiment-simulation integrated approach". In: *Nuclear Fusion* 57.7 (July 1, 2017), p. 076019. DOI: 10.1088/1741-4326/aa6d24.

[10] R. Bisson et al. "Dynamic fuel retention in tokamak wall materials: An in situ laboratory study of deuterium release from polycrystalline tungsten at room temperature". In: *Journal of Nuclear Materials* 467 (Dec. 2015), pp. 432–438. DOI: 10.1016/j.jnucmat.2015.07.028.

[11] S. Markelj et al. "Deuterium retention in tungsten simultaneously damaged by high energy W ions and loaded by D atoms". In: *Nuclear Materials and Energy* 12 (Aug. 2017), pp. 169–174. DOI: 10.1016/j.nme.2016.11.010.

[12] B. Wielunska et al. "Deuterium retention in tungsten irradiated by different ions". In: *Nuclear Fusion* 60.9 (Sept. 1, 2020), p. 096002. DOI: 10.1088/1741-4326/ab9a65.

[13] E.A. Hodille et al. “Macroscopic rate equation modeling of trapping/detrapping of hydrogen isotopes in tungsten materials”. In: *Journal of Nuclear Materials* 467 (Dec. 2015), pp. 424–431. DOI: 10.1016/j.jnucmat.2015.06.041.

[14] M. Zibrov et al. “Experimental determination of the deuterium binding energy with vacancies in tungsten”. In: *Journal of Nuclear Materials* 477 (Aug. 2016), pp. 292–297. DOI: 10.1016/j.jnucmat.2016.04.052.

[15] M. Pečovnik et al. “New rate equation model to describe the stabilization of displacement damage by hydrogen atoms during ion irradiation in tungsten”. In: *Nuclear Fusion* 60.3 (Mar. 1, 2020), p. 036024. DOI: 10.1088/1741-4326/ab680f.

[16] H. Jehn. *Gmelin-Handbuch der anorganischen Chemie System-Nr. 54. Erg.-Bd. Teil B. 1. Die Systeme mit Edelgasen, Wasserstoff und Sauerstoff*. OCLC: 722327227. 1978.

[17] C.H. Skinner et al. “Recent Advances on Hydrogen Retention in ITER Plasma-Facing Materials: Beryllium, Carbon, and Tungsten”. In: *Fusion Science and Technology* 54.4 (Nov. 2008), pp. 891–945. DOI: 10.13182/FST54-891.

[18] R.A. Causey. “Hydrogen isotope retention and recycling in fusion reactor plasma-facing components”. In: *Journal of Nuclear Materials* 300.2 (Feb. 2002), pp. 91–117. DOI: 10.1016/S0022-3115(01)00732-2.

[19] A. Dunand et al. “Surface oxygen versus native oxide on tungsten: contrasting effects on deuterium retention and release”. In: *Nuclear Fusion* 62.5 (May 1, 2022), p. 054002. DOI: 10.1088/1741-4326/ac583a.

[20] C. Hopf, W. Jacob, and V. Rohde. “Oxygen glow discharge cleaning in nuclear fusion devices”. In: *Journal of Nuclear Materials* 374.3 (Mar. 2008), pp. 413–421. DOI: 10.1016/j.jnucmat.2007.10.001.

[21] V.Kh. Alimov et al. “Surface morphology and deuterium retention in tungsten oxide layers exposed to low-energy, high flux D plasma”. In: *Journal of Nuclear Materials* 409.1 (Feb. 2011), pp. 27–32. DOI: 10.1016/j.jnucmat.2010.12.028.

[22] S.K. Deb. “Opportunities and challenges in science and technology of WO_3 for electrochromic and related applications”. In: *Solar Energy Materials and Solar Cells* 92.2 (Feb. 2008), pp. 245–258. DOI: 10.1016/j.solmat.2007.01.026.

[23] M.H. Yaacob et al. “Absorption spectral response of nanotextured WO_3 thin films with Pt catalyst towards H2”. In: *Sensors and Actuators B: Chemical* 137.1 (Mar. 2009), pp. 115–120. DOI: 10.1016/j.snb.2008.12.035.

[24] O.V. Ogorodnikova, J. Roth, and M. Mayer. “Deuterium retention in tungsten in dependence of the surface conditions”. In: *Journal of Nuclear Materials* 313-316 (Mar. 2003), pp. 469–477. DOI: 10.1016/S0022-3115(02)01375-2.

[25] Y. Addab et al. “Formation of thin tungsten oxide layers: characterization and exposure to deuterium”. In: *Physica Scripta* T167 (Feb. 20, 2016), p. 014036. DOI: 10.1088/0031-8949/T167/1/014036.

[26] J.W. Davis and A.A. Haasz. “Reemission of deuterium atoms from Mo, Ta and W during D+-irradiation”. In: *Journal of Nuclear Materials* 223.3 (June 1995), pp. 312–315. DOI: 10.1016/0022-3115(95)00041-0.

[27] A. Manhard et al. “Influence of the microstructure on the deuterium retention in tungsten”. In: *Journal of Nuclear Materials* 415.1 (Aug. 2011), S632–S635. DOI: 10.1016/j.jnucmat.2010.10.045.

[28] J. Roth et al. “Hydrogen isotope exchange in tungsten: Discussion as removal method for tritium”. In: *Journal of Nuclear Materials* 432.1 (Jan. 2013), pp. 341–347. DOI: 10.1016/j.jnucmat.2012.08.004.

[29] G. Holzner. “Determining fundamental transport parameters of hydrogen isotopes in tungsten”. PhD Thesis, Technische Universität München. 2020.

[30] G. Holzner et al. “Solute diffusion of hydrogen isotopes in tungsten - a gas loading experiment”. In: *Physica Scripta* T171 (Jan. 1, 2020), p. 014034. DOI: 10.1088/1402-4896/ab4b42.

[31] S. Kapser et al. “Influence of sub-surface damage evolution on low-energy-plasma-driven deuterium permeation through tungsten”. In: *Nuclear Fusion* 58.5 (May 1, 2018), p. 056027. DOI: 10.1088/1741-4326/aab571.

[32] A. Manhard. “Deuterium inventory in tungsten after plasma exposure - A microstructural survey”. doctoral thesis. Universitaet Augsburg, 2013.

[33] E.A. Hodille et al. “Stabilization of defects by the presence of hydrogen in tungsten: simultaneous W-ion damaging and D-atom exposure”. In: *Nuclear Fusion* 59.1 (Jan. 1, 2019), p. 016011. DOI: 10.1088/1741-4326/aaec97.

[34] E. Lassner and W. Schubert. *Tungsten: Properties, Chemistry, Technology of the Element, Alloys, and Chemical Compounds*. Boston, MA: Springer US, 1999. DOI: 10.1007/978-1-4615-4907-9.

[35] B. Erich. *Gmelin-Handbuch der anorganischen Chemie: System-Nummer 54. Erg.-Bd. B 2: Wolfram Oxide*. Berlin Heidelberg New York: Springer, 1979. 225 pp.

[36] D. Schneider et al. *W Wolfram: Ergänzungsband Teil B 1. Die Systeme mit Edelgasen, Wasserstoff und Sauerstoff*. 1978.

[37] P.G. Dickens, J.H. Moore, and D.J. Neild. “Thermochemistry of Hydrogen Tungsten Bronze Phases H,WO”. In: *Journal of Solid State Chemistry* 7.2 (1972), pp. 241–244. DOI: https://doi.org/10.1016/0022-4596(73)90160-6.

[38] H. Lin et al. “Non-Grotthuss proton diffusion mechanism in tungsten oxide dihydrate from first-principles calculations”. In: *Journal of Materials Chemistry A* 2.31 (June 19, 2014), p. 12280. DOI: 10.1039/C4TA02465F.

[39] J. Randin and R. Viennet. “Proton Diffusion in Tungsten Trioxide Thin Films”. In: *Journal of The Electrochemical Society* 129.10 (Oct. 1, 1982), pp. 2349–2354. DOI: 10.1149/1.2123510.

[40] S. Burkhardt et al. “In Situ Monitoring of Lateral Hydrogen Diffusion in Amorphous and Polycrystalline WO_3 Thin Films”. In: *Advanced Materials Interfaces* 5.6 (Mar. 2018), p. 1701587. DOI: 10.1002/admi.201701587.

[41] *Plansee High Performance Materials GMBH in Plansee, A-6600 Reutte, Austria*. http: //www.plansee.com.

[42] A. Manhard, G. Matern, and M. Balden. “A Step-By-Step Analysis of the Polishing Process for Tungsten Specimens”. In: *Practical Metallography* 50.1 (Jan. 2013), pp. 5–16. DOI: 10.3139/147.110215.

[43] J.F. Ziegler. *www.srim.org*.

[44] T. Schwarz-Selinger. “Deuterium retention in MeV self-implanted tungsten: Influence of damaging dose rate”. In: *Nuclear Materials and Energy* 12 (Aug. 2017), pp. 683–688. DOI: 10.1016/j.nme.2017.02.003.

[45] A. Manhard, T. Schwarz-Selinger, and W. Jacob. "Quantification of the deuterium ion fluxes from a plasma source". In: *Plasma Sources Science and Technology* 20.1 (Feb. 1, 2011), p. 015010. DOI: 10.1088/0963-0252/20/1/015010.

[46] A. Manhard, M. Balden, and U. von Toussaint. "Blister formation on rough and technical tungsten surfaces exposed to deuterium plasma". In: *Nuclear Fusion* 57.12 (Dec. 1, 2017), p. 126012. DOI: 10.1088/1741-4326/aa82c8.

[47] S. Möller et al. "Dynamic outgassing of deuterium, helium and nitrogen from plasma-facing materials under DEMO relevant conditions". In: *Nuclear Fusion* 57.1 (Jan. 1, 2017), p. 016020. DOI: 10.1088/0029-5515/57/1/016020.

[48] E. Markina et al. "Recovery temperatures of defects in tungsten created by self-implantation". In: *Journal of Nuclear Materials* 463 (Aug. 2015), pp. 329–332. DOI: 10.1016/j.jnucmat.2014.12.005.

[49] M. Zibrov et al. "High temperature recovery of radiation defects in tungsten and its effect on deuterium retention". In: *Nuclear Materials and Energy* 23 (May 2020), p. 100747. DOI: 10.1016/j.nme.2020.100747.

[50] F.Y. Xie. "XPS studies on surface reduction of tungsten oxide nanowire film by Ar^+ bombardment". In: *Journal of Electron Spectroscopy and Related Phenomena* (2012), p. 7.

[51] G. Fulton and A. Lunev. "Probing the correlation between phase evolution and growth kinetics in the oxide layers of tungsten using Raman spectroscopy and EBSD". In: *Corrosion Science* 162 (Jan. 2020), p. 108221. DOI: 10.1016/j.corsci.2019.108221. arXiv: 1904.04392.

[52] K. Schlüter and M. Balden. "Dependence of oxidation on the surface orientation of tungsten grains". In: *International Journal of Refractory Metals and Hard Materials* 79 (Feb. 2019), pp. 102–107. DOI: 10.1016/j.ijrmhm.2018.11.012.

[53] K. Schlüter. "Tungsten Properties Correlated with the Orientation of its Crystals". PhD thesis. Technische Universität München, 2021. 173 pp.

[54] M. McCargo, J.A. Davies, and F. Brown. "Range of Xe^{133} and Ar^{41} ions of keV energies in tungsten". In: *Canadian Journal of Physics* 41.8 (Aug. 1, 1963), pp. 1231–1244. DOI: 10.1139/p63-120.

[55] J. Zavasnik and V. Shvalya. *Private communication*. Josef-Stefan-Institute, Jamova cesta 39, 1000 Ljubljana, Slovenia, 2021.

[56] V. Nemanič et al. "Hydrogen permeability of non-stoichiometric tungsten oxides". In: *Journal of Nuclear Materials* 548 (May 2021), p. 152860. DOI: 10.1016/j.jnucmat.2021.152860.

[57] M. Mayer et al. "Quantitative depth profiling of deuterium up to very large depths". In: *Nuclear Instruments and Methods in Physics Research Section B: Beam Interactions with Materials and Atoms* 267.3 (Feb. 2009), pp. 506–512. DOI: 10.1016/j.nimb.2008.11.033.

[58] M. Mayer. "RESOLNRA: A new program for optimizing the achievable depth resolution of ion beam analysis methods". In: *Nuclear Instruments and Methods in Physics Research Section B: Beam Interactions with Materials and Atoms* 266.8 (Apr. 2008), pp. 1852–1857. DOI: 10.1016/j.nimb.2007.11.071.

[59] K. Schmid and U. von Toussaint. "Statistically sound evaluation of trace element depth profiles by ion beam analysis". In: *Nuclear Instruments and Methods in Physics Research Section B: Beam Interactions with Materials and Atoms* 281 (June 2012), pp. 64–71. DOI: 10.1016/j.nimb.2012.03.024.

[60] M. Guitart Corominas and T. Schwarz-Selinger. "Experimental determination of the $^{16}O(^{3}He,p_0)^{18}F$ differential cross section". In: *Nuclear Instruments and Methods in Physics Research Section B: Beam Interactions with Materials and Atoms* 450 (July 2019), pp. 13–18. DOI: 10.1016/j.nimb.2018.05.018.

[61] *https://materialsproject.org/materials/mp-19033/*. Nov. 19, 2020.

[62] *GESTIS-Stoffdatenbank*. URL: https://gestis.dguv.de/data?name=005920 (visited on 04/19/2022).

[63] Mayer M. *SIMNRA User Guide, IPP Report 9/113, Max-Planck-Institut fuer Plasmaphysik, Garching, Germany, April 1997. URL http://hdl.handle.net/11858/00-001M-0000-0027-6157-F*.

[64] M. Mayer. "Improved physics in SIMNRA 7". In: *Nuclear Instruments and Methods in Physics Research Section B: Beam Interactions with Materials and Atoms* 332 (Aug. 2014), pp. 176–180. DOI: 10.1016/j.nimb.2014.02.056.

[65] F. Besenbacher and W. Möller. "A note on the ^{3}He + D nuclear-reaction cross section". In: *Nuclear Instruments and Methods 168* (1980), pp. 111–114.

[66] B. Wielunska et al. "Cross section data for the $D(^{3}He,p)^{4}He$ nuclear reaction from 0.25 to 6 MeV". In: *Nuclear Instruments and Methods in Physics Research Section B: Beam Interactions with Materials and Atoms* 371 (Mar. 2016), pp. 41–45. DOI: 10.1016/j.nimb.2015.09.049.

[67] M. Zibrov et al. "Deuterium trapping by deformation-induced defects in tungsten". In: *Nuclear Fusion* 59.10 (Oct. 1, 2019), p. 106056. DOI: 10.1088/1741-4326/ab3c7e.

[68] T.F. Silva et al. "MultiSIMNRA: A computational tool for self-consistent ion beam analysis using SIMNRA". In: *Nuclear Instruments and Methods in Physics Research Section B: Beam Interactions with Materials and Atoms* 371 (Mar. 2016), pp. 86–89. DOI: 10.1016/j.nimb.2015.10.038.

[69] Wikimedia Commnos. *Skaningowy mikroskop elektronowy*. Page Vers. ID: 66648904. Mar. 22, 2022. URL: https://pl.wikipedia.org/w/index.php?title=Skaningowy_mikroskop_elektronowy&oldid=66648904 (visited on 04/17/2022).

[70] H.G. Tompkins and E.A. Irene, eds. *Handbook of ellipsometry*. Norwich, NY : Heidelberg, Germany: William Andrew Pub. ; Springer, 2005. 870 pp.

[71] A. Paliwal et al. "Optical properties of WO_3 thin films using surface plasmon resonance technique". In: *Journal of Applied Physics* 115.4 (Jan. 28, 2014), p. 043104. DOI: 10.1063/1.4862962.

[72] W. Jacob et al. "Bonding States of Hydrogen in Plasma-Deposited Hydrocarbon Films". In: *Journal of Carbon Research* 6.1 (Jan. 9, 2020), p. 3. DOI: 10.3390/c6010003.

[73] E. Salançon et al. "Redeposition of amorphous hydrogenated carbon films during thermal decomposition". In: *Journal of Nuclear Materials* 376.2 (May 2008), pp. 160–168. DOI: 10.1016/j.jnucmat.2008.02.070.

[74] M. Brucker et al. "To be published". In: ().

[75] K. Kremer, T. Schwarz-Selinger, and W. Jacob. "Influence of thin tungsten oxide films on hydrogen isotope uptake and retention in tungsten - Evidence for permeation barrier effect". In: *Nuclear Materials and Energy* 27 (June 2021), p. 100991. DOI: 10.1016/j.nme.2021.100991.

[76] K. Ito, T. Ohgami, and T. Nakazawa. "Effect of water on hydrogen-sensitive tungsten oxide films". In: *Sensors and Actuators B: Chemical* 12.3 (Apr. 1993), pp. 161–167. DOI: 10.1016/0925-4005(93)80014-3.

[77] C. Martin et al. "Tungsten oxide thin film bombarded with a low energy He ion beam: evidence for a reduced erosion and W enrichment". In: *Physica Scripta* T170 (Dec. 1, 2017), p. 014019. DOI: 10.1088/1402-4896/aa89c1.

[78] W. Möller, W. Eckstein, and J.P. Biersack. "Tridyn-binary collision simulation of atomic collisions and dynamic composition changes in solids". In: *Computer Physics Communications* 51.3 (Nov. 1988), pp. 355–368. DOI: 10.1016/0010-4655(88)90148-8.

[79] J. Bauer et al. "Influence of near-surface blisters on deuterium transport in tungsten". In: *Nuclear Fusion* 57.8 (Aug. 1, 2017), p. 086015. DOI: 10.1088/1741-4326/aa7212.

[80] S.J. Ippolito et al. "Hydrogen sensing characteristics of WO_3 thin film conductometric sensors activated by Pt and Au catalysts". In: *Sensors and Actuators B: Chemical* 108.1 (July 2005), pp. 154–158. DOI: 10.1016/j.snb.2004.11.092.

[81] M.I. Guseva et al. "Sputtering of beryllium, tungsten, tungsten oxide and mixed W C layers by deuterium ions in the near-threshold energy range". In: *Journal of Nuclear Materials* 266-269 (Mar. 1999), pp. 222–227. DOI: 10.1016/S0022-3115(98)00819-8.

[82] J. Roth, J. Bohdansky, and W. Ottenberger. *Data on low energy light ion sputtering*. Report IPP 9/26, Max-Planck-Institut für Plasmaphysik.

[83] M. Pecovnik et al. "Effect of D on the evolution of radiation damage in W during high temperature annealing". In: *Nuclear Fusion* 60.10 (Oct. 1, 2020), p. 106028. DOI: 10.1088/1741-4326/abaff6.

[84] R. Behrisch and W. Eckstein, eds. *Sputtering by particle bombardment: experiments and computer calculations from threshold to MeV energies*. Topics in applied physics 110. OCLC: ocn144222189. Berlin ; New York: Springer, 2007. 507 pp.

[85] H. Tu et al. "The erosion and retention properties of tungsten trioxide films exposed to low energy deuterium ions: Temperature dependence". In: *Journal of Nuclear Materials* 562 (Apr. 2022), p. 153590. DOI: 10.1016/j.jnucmat.2022.153590.

[86] K. Kremer et al. "Influence of thin surface oxide films on hydrogen isotope release from ion-irradiated tungsten". In: *Nuclear Materials and Energy* 30 (2022), p. 15. DOI: https://doi.org/10.1016/j.nme.2022.101137.

[87] E. Ozkan et al. "Comparison of electrochromic amorphous and crystalline tungsten oxide films". In: *Solar Energy Materials and Solar Cells* 79.4 (Sept. 2003), pp. 439–448. DOI: 10.1016/S0927-0248(03)00019-9.

[88] J.A. Basford. "Analysis of offgassed water: Calibration and techniques". In: *Journal of Vacuum Science & Technology A: Vacuum, Surfaces, and Films* 12.4 (July 1994), pp. 1778–1781. DOI: 10.1116/1.579005.

[89] E. Martelli et al. “Advancements in DEMO WCLL breeding blanket design and integration: Advancements in DEMO WCLL breeding blanket design and integration”. In: *International Journal of Energy Research* 42.1 (Jan. 2018), pp. 27–52. DOI: 10.1002/er.3750.

[90] F. Hernández et al. “A new HCPB breeding blanket for the EU DEMO: Evolution, rationale and preliminary performances”. In: *Fusion Engineering and Design* 124 (Nov. 2017), pp. 882–886. DOI: 10.1016/j.fusengdes.2017.02.008.

[91] C. Day and D. Murdoch. “The ITER vacuum systems”. In: *Journal of Physics: Conference Series* 114 (May 1, 2008), p. 012013. DOI: 10.1088/1742-6596/114/1/012013.

[92] R. Behrisch et al. “Material erosion at the vessel walls of future fusion devices”. In: *Journal of Nuclear Materials* 313-316 (Mar. 2003), pp. 388–392. DOI: 10.1016/S0022-3115(02)01580-5.

Appendix A

Appendix

A.1 Instructive example of ^{4}He RBS on thin WO_3 films on W

In Fig. A.1, SIMNRA calculations [63, 64] of thin W and WO_3 films with identical W areal density on silicon (Si) are shown, as an instructive example of how to determine the oxygen concentration within thin oxide films on W with RBS. Additionally, also the spectrum of an identical WO_3 film on bulk W is shown. These examples complement the measured RBS spectrum for WO_3 on W that is shown in Fig. 3.8

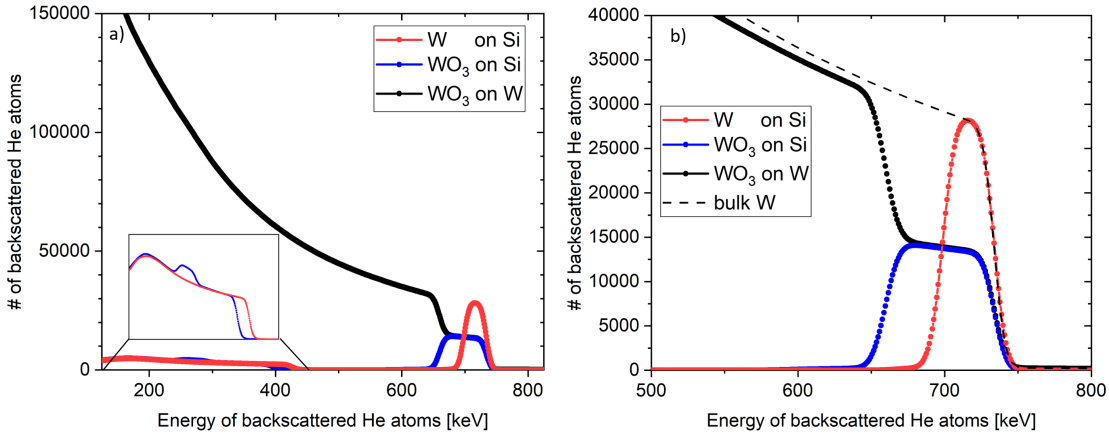

Figure A.1 – Simulated RBS spectra (^{3}He with 800 keV, incident angle 70.5°) showing a thin layer of pure W on a Si substrate and thin layers of WO_3 on a Si or W substrate, respectively. All surface layers contain 50×10^{19} W atoms/m^2 and in case of WO_3 additionally 150×10^{19} O atoms/m^2. The inset in a) shows the small oxygen peak visible for WO_3 on Si; for WO_3 on W the oxygen peak is not visible in the W background. Image b) shows an enlarged view of the backscattering signal from W at the surface.

Fig. A.1 a) depicts the backscattering spectra of ^{3}He ions from different substrates over the energy range (from 100 to 800 keV). For the given experimental conditions, ^{3}He backscattered from W at the surface has an energy of about 734 keV. A realistic detector resolution of 15 keV was assumed in the simulations. The RBS signal for the silicon underneath the W or WO_3 surface film appears for energies lower than 454 keV. An enlarged view of the Si signal region is shown in the inset in Fig. A.1 a). In this inset, the small RBS signal for O is clearly visible in the energy range from about 220 to 240 keV. In the original scale it is barely visible and on the huge W background (black spectrum in Fig. A.1 a)) it is invisible even on the simulated spectrum. From this comparison, it becomes evident that in the measured spectra which carry additional

experimental noise, the O contribution cannot be separated from the huge W background. A direct measurement of the O signal is thus not feasible for bulk W samples with RBS.

Fig. A.1 b) shows an enlarged view of the backscattering signal from W at the surface. The thin W or WO_3 layer on Si substrate (red and blue) both contain the same amount of W (50×10^{19} W atoms/m^2). The integral over the counts in both peaks in the energy interval from 600 to 800 keV is almost the same: 1.007×10^6 for pure W on Si and 1.034×10^6 for WO3 on Si. The almost identical integrals show that backscattering of He atoms at O atoms in the WO_3 layer does not reduce the W signal that is measured. This is because the cross section for RBS is proportional to Z^2. Therefore, the low-Z material O can scatter only a negligible amount of He atoms compared with the high Z material W. Please note that the reason that the integral counts are not identical is that the cross section for He scattering on W is slightly energy dependent and thus affected by the additional stopping of the oxide.

However, the W peak of the WO_3 surface film (blue) is stretched over a wider energy interval, although both layers contain the identical amount of W. This effect is caused by the additional electronic stopping experienced by the ^{3}He projectiles due to the presence of the O atoms in the WO_3 layer. It decreases the energy of He atoms as they move through the WO_3 before and after they are backscattered at W atoms. With other words, it increases the energy loss in the oxide film such that the same amount of He atoms backscattered from W is spread over a wider energy interval. This is the dominant mechanism causing the lower intensity of the W RBS signal in case of a W oxide layer compared with a pure W layer. The additional stopping is proportional to the relative fraction of O in the oxide film. Thus, it is possible to determine the concentration of O atoms in the W oxide at a given depth from the height of the RBS signal by adequate fitting of the experimental data. Of course, the determination of the O concentration by this method is only possible, if no other impurities that would contribute to additional electronic stopping are present in the layer.

A.2 Numerical Data to Fig. 4.5

sample	areal density in 10^{19} O/m^2					
	NRA			RBS		
	before plasma exposure	after plasma exposure	oxygen loss	before plasma exposure	after plasma exposure	oxygen loss
thick oxide	305±5	233±5	72±8	300±9	240±8	59±12
thin oxide	185±3	106±4	79±5	189±12	121±8	67±15
natural oxide (reference)	8.4±1.1	5.4±1.2	3.0±1.7	10.5±10	10.1±10	0.4±15

Table A.1 – Table with numerical values of the data presented in Fig. 4.5. Oxygen loss and oxygen areal density as measured with NRA and RBS before and after plasma exposure with a D fluence of 1.4×10^{24} D/m^2 at 370 K with an energy of <5 eV/D. In case of NRA, the uncertainty of the oxygen areal density is derived from the statistical uncertainty of the integral over the oxygen peak and the uncertainty of the background subtraction. In case of RBS, the uncertainty is derived by manually varying the oxygen amount until obvious mismatch between the simulation and the data was visible. The uncertainty of the oxygen loss (difference) is calculated with Gaussian error propagation.

A.3 Video analysis of the color change of WO_3 surface oxide films during D plasma exposure

The video was taken in-situ during plasma loading with a high-resolution camera system. In Fig. A.2 several single frames of the video are presented at decisive moments during the plasma loading. The depicted area measures 2 mm×1 mm on the sample. The full video can be found in the supplementary material to [75].

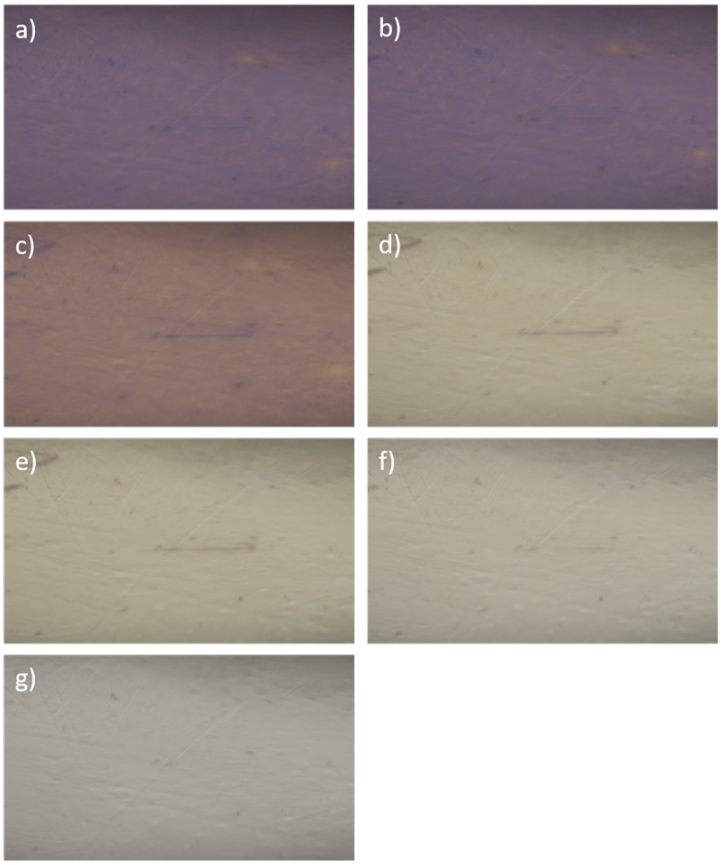

Figure A.2 – Single frames at decisive moments of a video analysis of thick oxide (55 nm) during "burn-in" phase and plasma exposure in PlaQ: a) Initial conditions before D plasma exposure. Area size: 2 mm×1 mm. b) After heat up but before D exposure. No color change visible. c) After 1 minute of "burn in phase". In this phase, the plasma is started but a shutter between the sample and the plasma is closed so that only atomic D can reach the sample. A quick color change within this 1 minute is visible. d) After 30 minutes of „burn in". The color has significantly changed during this first 30 minutes of burn in phase. e) End of "burn in" phase after 36 minutes. Only very little color change during the last 6 minutes of burn in. Assumption: "Quick color change" due to atomic D now saturated. No further change during prolonged "burn in phase" expected. f) After 1 minute of plasma exposure. Slight color change visible compared with end of burn in phase. Influence of plasma visible. g) After 3 hours of plasma exposure. Some further (slow) color change visible, but far less pronounced than color change due to D intercalation. This slow color change during plasma operation is attributed to the thinning of the oxide film due to oxygen removal during D plasma exposure.

A.4 Part 4: Details to the static SDTRIMSP simulation that was used to determine the implantation depth of D into the WO_3 film

5 eV D -> WO3 &TRI_INP

text=’---elemements---’ ncp = 3 symbol = "D", "W", "O"

text=’---beam---’ case_e0=0 e0 = 5, 0.00, 0.00 case_alpha=0 alpha0 = 0.000, 0.000, 0.000 qubeam = 1.000, 0.000, 0.000 text=’---control---’ flc = 20 nh = 2000 nr_pproj = 4 idout = 2000 idrel =1 iintegral=3 ipivot =8

text=’---target---’ nm = 4 i_two_comp=3 two_comp ="WO3" ttarget = 2000 nqx = 400 qu = 0.000, 0.25, 0.75 qumax = 1.000, 1.000, 1.0 inel0 = 3, 3, 3 ipot = 1 isbv = 7 e_cutoff= 0.9 ,0.9 ,0.9 text=’ e_surfb=0.0, 4.72, 2.58’ e_surfb = 0.0, 4.72, 1.00 irc0=1

text=’---output parameter’ qu_int = .true. case_layer_thick=2 loutgas = .true. diff_koeff1 =1.6e5, 0.0, 0.0 diff_koeff2 = 5, 0.0, 0.0 /

Used parameters for WO3 (in compound table): Molar mass [g/mol]: 231.84 Density [g/cm^3]: 7.16 Enthalpy of formation deltaH_F [kJ/mol]: 83

0 Density [atoms/A^3]: 0.07439 Enthalpy of formation deltaH_F [eV]: 8.6853 [2] Nr.comp: 4 1 3 tungsten oxide

A.5 SEM images for thermally (33 nm) and electro-chemically (20 nm) grown tungsten oxide films

The already nano-crystalline thermally grown oxide in Fig. A.3 a) and b)), does not undergo further transformation during the heating and remains unaffected for most of the surface area. However, some small snowflake-like structures of cracks in the oxide appear randomly distributed at the surface. These may be formed by thermal stress on the oxide during the 1000 K temperature ramp, which is significantly higher than the oxidation temperature of 600 K. The electro-chemically grown oxide (Fig. A.3 c) and d) undergoes recrystallization and behaves very similar to the 40 nm thick electro-chemical oxide that is discussed in section 5.1. In Fig. A.3 d) the oxide is visible as a dark film on top of the gray metallic W. The white elements are protruding columns of W oxide, which appear brighter due to the edge effect in secondary electron mode, which highlights small protruding volumes.

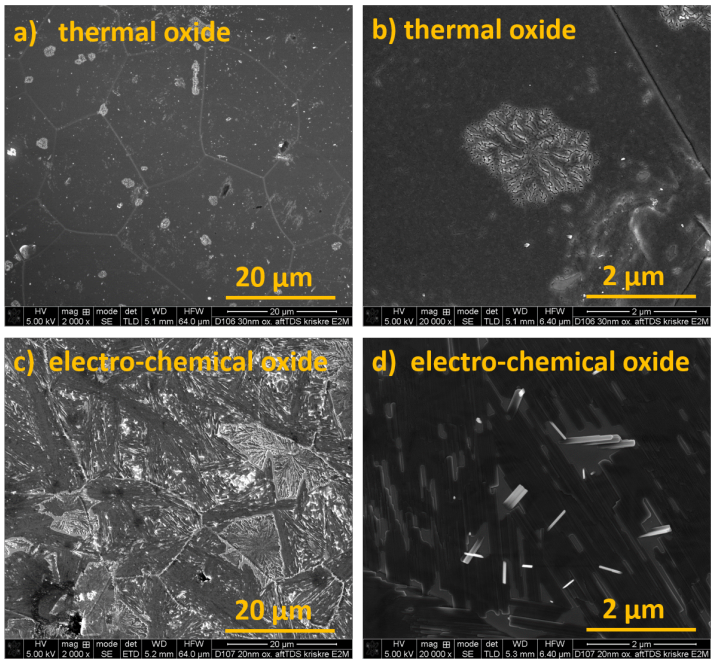

Figure A.3 – SEM images of oxide films after exposure to 1000 K: a) and b) thermally grown oxide film of originally 30 nm thickness in two different magnifications; c) and d) electro-chemically grown oxide film of originally 20 nm thickness in two magnifications.

Acknowledgment

First of all I want to thank my direct supervisor Thomas Schwarz-Selinger for his continuous support and advice throughout the last three years. Next I want to give special thanks to my former group leader Wolfgang Jacob, who took continuous interest in my work and was always willing to share his considerable experience and provide detailed and constructive feedback on my work. The guidance and mentoring by both of you is greatly appreciated! Special thank goes also to Maximilian Brucker for the fruitful cooperation during his time as a master student at IPP and for his help in conducting the experiments and the data analysis for the D release studies.

I also want to thank my doctoral supervisor Prof. Dr. Ulrich Stroth for his continuous interest in my work and regular meetings with guidance and support throughout the PhD project.

Furthermore I would like to thank K. Hunger for her assistance in grinding and polishing the samples and Martin Balden and Stefan Elgeti for training me on how to use the electron microscopes and for their assistance with operating them. I further want to thank Thomas Dürbeck for his support with the TDS setup and Klaus Schmid for providing the deconvolution program NRADC and his efficient support in using it. I also thank Armin Manhard for his help in operating PlaQ. Special thanks goes also to Michael Fusseder and Joachim Dorner for operating the accelerator for the tungsten irradiation and the ion beam analysis. Finally I want to thank all other colleagues at IPP and the E2M department who were always ready to lend a helping hand when needed.